

Engineering Journal



American Institute of Steel Construction

First Quarter 2010 Volume 47, No. 1

- 1 Critical Evaluation of Equivalent Moment Factor Procedures for Laterally Unsupported Beams
Edgar Wong and Robert G. Driver
- 21 Impact of Diaphragm Behavior on the Seismic Design of Low-Rise Steel Buildings
Colin A. Rogers and Robert Tremblay
- 37 Notes on the Impact of Hole Reduction on the Flexural Strength of Rolled Beams
Louis F. Geschwindner
- 41 A Case for a Single Stiffness Reduction Factor in the 2010 AISC Specification
Louis F. Geschwindner
- 47 Bolt Shear Design Considerations
Raymond H.R. Tide
- 65 Current Steel Structures Research
Reidar Bjorhovde

ENGINEERING JOURNAL

AMERICAN INSTITUTE OF STEEL CONSTRUCTION

*Dedicated to the development and improvement of steel construction,
through the interchange of ideas, experiences and data.*

Editorial Staff

Editor: KEITH GRUBB, P.E., S.E.

Research Editor: REIDAR BJORHOVDE, PH.D.

Production Editor: ARETI CARTER

Officers

DAVID HARWELL, *Chairman*

Central Texas Iron Works, Inc., Waco, TX

WILLIAM B. BOURNE, III, *Vice Chairman*

Universal Steel, Inc., Atlanta, GA

STEPHEN E. PORTER, *Treasurer*

Indiana Steel Fabricating, Inc., Indianapolis, IN

ROGER E. FERCH, P.E., *President*

American Institute of Steel Construction, Chicago

DAVID B. RATTERMAN, *Secretary & General Counsel*

American Institute of Steel Construction, Chicago

CHARLES J. CARTER, S.E., P.E., PH.D., *Vice President and
Chief Structural Engineer*

American Institute of Steel Construction, Chicago

JOHN P. CROSS, P.E., *Vice President*

American Institute of Steel Construction, Chicago

LOUIS F. GESCHWINDNER, P.E., PH.D., *Vice President, Special Projects*

American Institute of Steel Construction, University Park, PA

SCOTT L. MELNICK, *Vice President*

American Institute of Steel Construction, Chicago

The articles contained herein are not intended to represent official attitudes, recommendations or policies of the Institute. The Institute is not responsible for any statements made or opinions expressed by contributors to this Journal.

The opinions of the authors herein do not represent an official position of the Institute, and in every case the officially adopted publications of the Institute will control and supersede any suggestions or modifications contained in any articles herein.

The information presented herein is based on recognized engineering principles and is for general information only. While it is believed to be accurate, this information should not be applied to any specific application without competent professional examination and verification by a licensed professional engineer. Anyone making use of this information assumes all liability arising from such use.

Manuscripts are welcomed, but publication cannot be guaranteed. All manuscripts should be submitted in duplicate. Authors do not receive a remuneration. A "Guide for Authors" is printed on the inside back cover.

ENGINEERING JOURNAL (ISSN 0013-8029) is published quarterly. Subscriptions: Members: one subscription, \$20 per year, included in dues; Additional Member Subscriptions: \$15 per year. Non-Members U.S., Canada, and Mexico: \$40 per year, \$110 for three years, single copy \$15. International Members and Non-Members: \$90 per year; \$250 for three years; single copy \$25. Published by the American Institute of Steel Construction at One East Wacker Drive, Suite 700, Chicago, IL 60601.

Periodicals postage paid at Chicago, IL and additional mailing offices. **Postmaster:** Send address changes to ENGINEERING JOURNAL in care of the American Institute of Steel Construction, One East Wacker Drive, Suite 700, Chicago, IL 60601.

Copyright 2010 by the American Institute of Steel Construction. All rights reserved. No part of this publication may be reproduced without written permission. The AISC logo is a registered trademark of AISC.

Subscribe to *Engineering Journal* by visiting our web site www.aisc.org/ej or by calling 312.670.5444.

Copies of current and past *Engineering Journal* articles are available free to members online at www.aisc.org/ej.

Non-members may purchase *Engineering Journal* article downloads at the AISC Bookstore at www.aisc.org/ej for \$10 each.

Critical Evaluation of Equivalent Moment Factor Procedures for Laterally Unsupported Beams

EDGAR WONG and ROBERT G. DRIVER

ABSTRACT

This paper compares the numerous approaches to determining equivalent moment factors used in evaluating the elastic critical moment of laterally unsupported beams for a wide variety of moment distributions. The investigation revealed that the procedure used currently in the Canadian design standard produces unacceptable results for the majority of the common bending moment distributions considered. Large abrupt changes in C_b values with only slight changes in the shape of the moment diagram were observed in 6 out of the 12 moment distribution comparisons, which contributes to the overall poor performance of the procedure.

The study also revealed drawbacks inherent in other methods. Overall, the quarter-point moment equations developed for general moment distributions capture the trends of the numerical data reasonably well. However, for example, the evaluations show that the 2005 AISC equation produces non-conservative results in some situations, while the British equation, although generally conservative, produces comparatively less accurate results. Other equations examined capture the trends of the numerical data more consistently by implementing a square root format in the quarter-point moment method. However, they produce results that exceed the numerical data in several cases, implying that they are too aggressive for design purposes.

To capture the best features of the various methods investigated, yet improve the overall suitability for general design purposes, a modified quarter-point moment equation using the square root format is proposed. Not only does it simulate the trends of the numerical solutions closely, but it also produces reasonable and conservative equivalent moment factors, even in cases where other methods do not. Like all quarter-point moment methods, the proposed equation does not produce good results in some situations where concentrated moments are applied. Nevertheless, it is believed to be appropriate for the vast majority of typical design cases.

Keywords: lateral support, equivalent moment factors, C_b , beams.

INTRODUCTION

The elastic lateral-torsional buckling moment capacity of a doubly-symmetric steel beam is governed primarily by the member's weak-axis moment of inertia, I_y , and the torsion parameter. The latter factor can be expressed as

$$\frac{\pi}{L} \sqrt{\frac{EC_w}{GJ}}$$

where L is the laterally (and torsionally) unbraced length of the beam, E is the elastic modulus, G is the shear modulus, C_w is the warping constant, and J is the torsional constant. Previous research has shown that the following factors can also influence the critical moment capacity significantly (Clark and Hill, 1960; Nethercot and Rockey, 1972; Nethercot and Trahair, 1976):

1. The internal moment distribution between brace points;
2. The elevation of the applied load with respect to the shear center;
3. The degree of lateral, rotational, and warping restraint at the brace points; and
4. The potential for less critical adjacent unbraced segments to restrain buckling (i.e., interaction buckling).

Although methods that consider all of these factors in the computation of the elastic critical moment are available, most steel design specifications simplify the analytical process by accounting only for the moment distribution effect among the four factors. That is, loads are assumed to be applied at the shear center (unless, perhaps, they are applied significantly above the shear center (for downward loads) by a means that does not also serve as a brace), lateral braces are assumed to prevent both lateral displacement and twist of the beam's cross section, while restraining neither weak-axis rotation nor warping, and the potential for interaction buckling is neglected. For these reasons, this paper addresses the effect of the moment distribution only.

Edgar Wong, M.Eng., P.Eng., structural engineer, Walters Chambers and Associates Ltd., 501, 10709 Jasper Ave., Edmonton, AB, T5J 3N3, Canada. E-mail: edgar.wong@walterschambers.com

Robert G. Driver, Ph.D., P.Eng., Professor, Department of Civil and Environmental Engineering, University of Alberta, Edmonton, AB, T6G 2W2, Canada (corresponding author). E-mail: rdriver@ualberta.ca

For a doubly-symmetric beam subject to a uniform (constant) moment about the strong axis along its length, the critical lateral-torsional buckling capacity, M_{cr} , can be expressed as:

$$M_{cr} = \frac{\pi}{L} \sqrt{EI_y GJ + \left(\frac{\pi E}{L}\right)^2 I_y C_w} \quad (1)$$

The boundary conditions assumed in this equation are such that both ends of the unbraced segment are restrained as described in the previous paragraph. The value determined from Equation 1 is commonly referred to as the “basic” lateral-torsional buckling moment capacity, not only because it is the simplest to derive theoretically, but, more importantly, it gives the lowest possible capacity of a beam segment between properly designed brace points when loads are applied at the shear center (Kirby and Nethercot, 1979). It is widely accepted that the effect of a non-uniform moment distribution can be approximated simply by multiplying Equation 1 by an equivalent (uniform) moment factor, C_b . Since a non-uniform moment distribution is less severe than a uniform one, the value of this factor is always greater than or equal to 1.0.

In general, non-uniform moment distributions between brace points can conveniently be categorized into three groups: (1) linear moment distributions arising when there are no loads or moments applied between brace points; (2) non-linear moment distributions with multiple constant moment gradient regions; and (3) non-linear moment distributions with continuously varying moment gradients. The primary difference between the last two groups is that beams within group 2 are not subjected to any distributed load and their moment distributions can be transformed into group 1 distributions by adding braces at points where the moment gradient changes. It is important to realize that some existing equivalent moment factor equations have been derived for group 1 moment distributions only, whereas others purport to be applicable for all groups. Misusing the equations may lead to significant errors in critical moment predictions.

It should be noted for clarity that in many cases the means of delivering loads to a beam will also provide effective lateral bracing to that beam, apparently making group 1 moment distributions the only case that will occur in practice. However, circumstances where loads are applied to a beam with little, or perhaps uncertain, resulting bracing effectiveness are relatively common. One example of this is where two parallel primary beams have loads delivered to them by simply supported transverse secondary framing members (i.e., the two primary beams “lean on” each other with respect to the intermediate lateral support points at the ends of the secondary members). If the two primary beams become unstable at a similar time in the loading regime, they cannot be considered to support each other laterally (Galambos, 1998). Another common example is where a secondary

member delivers its reaction load to the primary beam away from its compression flange without providing significant rotational restraint to the beam and the designer deems this to be inadequate as a bracing mechanism. Other typical examples of loads that are not associated with the provision of effective bracing include suspended loads, supported column reaction loads and loads where the connection of the tributary beam to the primary beam is bolted and employs horizontally slotted holes. Considering the multitude of conditions that a structural designer may face, group 1, 2 and 3 moment distributions must all be included in any evaluation of equivalent moment factors.

There are many equations and methods published in the general literature and design specifications for determining equivalent moment factors. In this paper, comparisons of equivalent moment factors determined using various methods for 12 different moment distribution types, described in Table 1, are presented. In order to generalize the moment distribution types, three factors are introduced in Table 1: (1) for Type 1, the factor κ is the ratio of the absolute value of the smaller to larger end moment of the unbraced segment, and it is taken as positive for double curvature bending and negative for single curvature; (2) for Types 2 to 5, 8, 9, 11 and 12, the factor β is the ratio of the actual end moment to the fixed end moment; and (3) for Types 6, 7 and 10, the factor a is the distance from a concentrated load to the nearest vertical support (see Table 1). The moment distribution types selected are believed to be common enough to correspond with typical design loading cases and cover a broad enough range to lead to general conclusions.

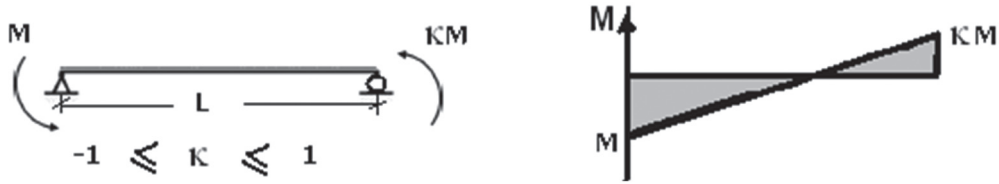
The original objective of this study was to examine the adequacy of the equivalent moment factor specified in Canadian standard CAN/CSA-S16-01. During the course of this examination, a critical evaluation of other published methods was also conducted. Not only are the shortcomings of the CAN/CSA-S16-01 procedure clarified, but a broad collection of solutions determined by other methods is also presented herein to illustrate their performance and limitations. Although relevant physical test data are scarce, numerical data are included as reference values where available. Finally, a new equivalent moment factor equation is proposed based on the findings of the investigation that incorporates the best features observed in the various existing methods. It is demonstrated that the proposed equation effectively rectifies current CAN/CSA-S16-01 deficiencies and produces accurate, yet conservative, approximations to the numerical solutions over a wide range of moment distribution types.

PROCEDURES PUBLISHED IN THE GENERAL LITERATURE

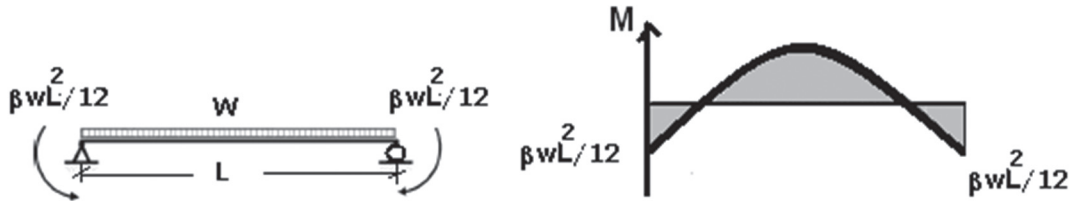
The fundamental aspects that characterize the non-uniform moment effect are the rate of change of the moment along the beam length, the number of curvature reversals between

Table 1. Types of Moment Distributions Considered in the Study*

Type 1—End Moments Only



Type 2—Uniformly Distributed Load with Equal End Moments



Type 3—Uniformly Distributed Load with One End Moment



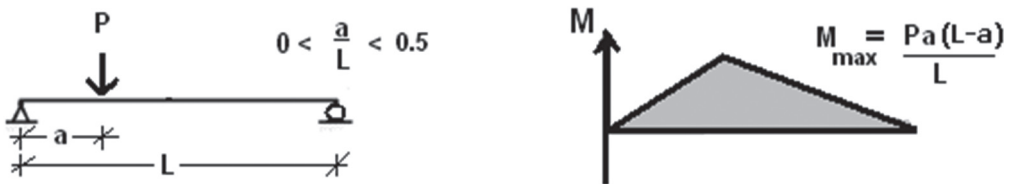
Type 4—Mid-span Concentrated Load with Equal End Moments



Type 5—Mid-span Concentrated Load with One End Moment



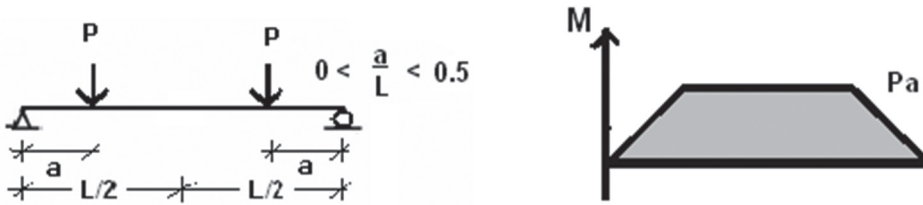
Type 6—Concentrated Load with Pinned Ends



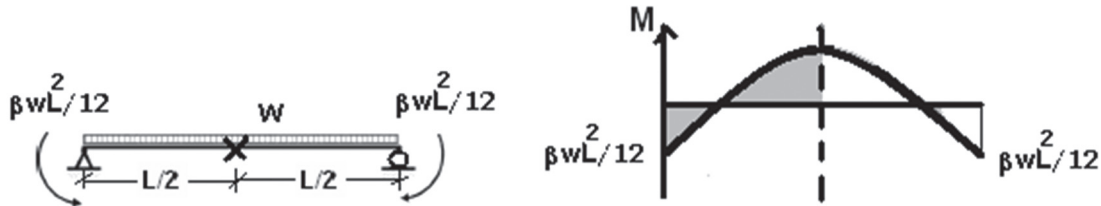
* The ends of the members depicted are brace points, as well as points denoted by the symbol x .

Table 1 (cont.). Types of Moment Distributions Considered in the Study*

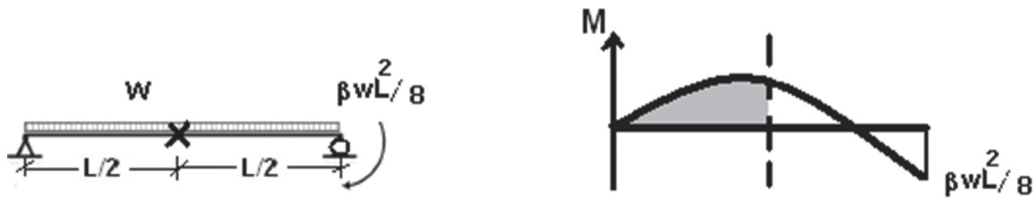
Type 7—Two Equal Concentrated Loads Symmetrically Placed with Pinned End



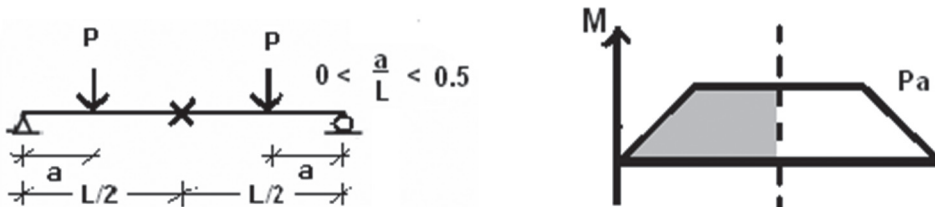
Type 8—Uniformly Distributed Load with Equal End Moments, Brace at Mid-span



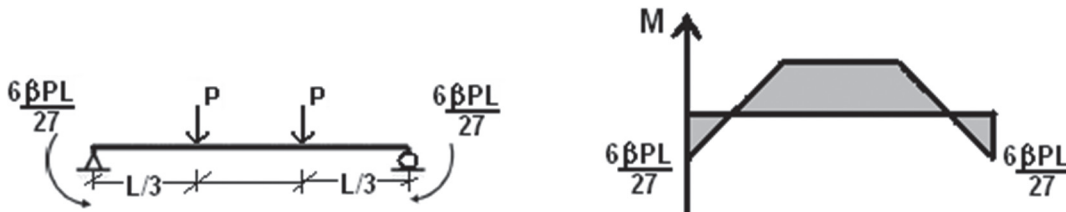
Type 9—Uniformly Distributed Load with One End Moment, Brace at Mid-span



Type 10—Two Equal Concentrated Loads Symmetrically Placed, Brace at Mid-span



Type 11—Two Equal Concentrated Loads at Third Points with Equal End Moments



Type 12—Two Equal Concentrated Loads at Third Points with One End Moment



* The ends of the members depicted are brace points, as well as points denoted by the symbol x.

brace points, and the distance between the maximum moment and the brace locations. Due to the challenge of developing a simple procedure for determining equivalent moment factors that can capture all three aspects concurrently for all kinds of moment distributions, not all published methods are applicable to all moment distribution types. Available methods for determining equivalent moment factors can be divided into three categories:

1. Methods developed for unequal end moments only (e.g., Salvadori, 1955; Austin, 1961).
2. Methods developed for a general moment distribution (e.g., Kirby and Nethercot, 1979; Serna et al., 2006)
3. Methods developed to address numerous specific moment distributions individually (e.g., Trahair, 1993; Clark and Hill, 1960; Suryoatmono and Ho, 2002).

Methods Developed for Unequal End Moments Only

Two equations that are commonly used to approximate the effect of a constant moment gradient between brace points on the critical elastic moment are Equations 2 and 3 shown in Table 2. The parameter κ quantifies the influence of the flange force variation between the two ends. That is, if a beam flange is subjected to a bending-induced compression that varies between lateral supports, the degree of variation dictates the tendency of the beam to buckle elastically (Zuraski, 1992). Furthermore, if the flange force varies between tension and compression (i.e., when the unbraced segment of the beam is in double curvature), the beam is even less susceptible to lateral-torsional buckling. Equation 2 represents a lower bound to the original solutions developed by Salvadori (1955) using the Rayleigh-Ritz method, and Equation 3 is from the work of Austin (1961) for in-plane bending of beam-columns. Equation 3 is considered inappropriate for assessing out-of-plane buckling due to flexure alone because it is derived for members subjected to both axial load and bending simultaneously (AISC, 2005b), and, as such, it is not considered further.

Methods Developed for a General Moment Distribution—Quarter-Point Moment Methods

Equation 4, shown in Table 2, was developed to be applicable to all types of moment distributions (Kirby and Nethercot, 1979). It utilizes the magnitudes of the bending moments at four specific locations along the unbraced segment: the quarter point, M_a , centerline, M_b , third-quarter point, M_c , and maximum, M_{max} , moments. Equations with this format are referred to as the “quarter-point moment methods” in this paper. The main function of these four moments is to describe the degree of non-uniformity of the moment along the unbraced length, thus approximating its influence on the critical moment. Although not specified explicitly in the

original publication, it has been indicated in numerous subsequent publications that using the absolute values of these moments in the equation is appropriate. Unlike Equations 2 and 3, the quarter-point moment methods are independent of the magnitudes of the end moments, unless one or both are also the maximum moment in the unbraced segment.

Another quarter-point moment method was developed by Serna et al. (2006) by curve fitting their numerical analysis results that account not only for the effect of a non-uniform moment distribution, but also the lateral, rotational and warping restraints at the brace points. Since the latter influences are not within the scope of this paper, the equation is written in a simplified form for laterally and torsionally simple end conditions as Equation 5 in Table 2. The main distinction of this equation as compared to Equation 4 is that the individual moment terms are squared and a square root format is assigned.

Methods Developed for Specific Moment Distributions

Clark and Hill (1960) and Nethercot and Trahair (1976) each published a list of equivalent moment factor values based on numerical analyses for specific non-uniform moment distributions, as shown in Table 3. Although not applicable to all typical design loading cases, they provide a good database from which designers can approximate equivalent moment factors for other distributions. The two sets are nearly identical, except for the value in the Type 2 distribution when β equals 1.0. For this case, the value of 1.30 from Clark and Hill (1960) appears to be incorrect, and if it is recalculated using the original source of data, a value of 2.52 is obtained, as reflected in Table 3.

Instead of discrete values, Trahair (1993) published individual equations (see Table 3) for several moment distribution types based on curve fitting of numerical data. These equations apply to a much wider range of moment distributions than do the lists of discrete values because the designer can adjust the point load location along a beam or the magnitude of the end moments. Nethercot and Rockey (1972) also proposed a C_b equation for moment Type 7 that is a function of the distance between the point load and the closer support. Analogous equations presented by Suryoatmono and Ho (2002) are relatively complex as compared to those of Trahair (1993), and they address moment Types 1 through 3 only; therefore, they are not included in the comparisons in this paper.

PROCEDURES IN DESIGN SPECIFICATIONS

Because the methodologies discussed in the previous section have various degrees of practicality, accuracy, consistency and computational complexity, different steel design specifications have adopted different procedures for determining the equivalent moment factor to be used for the design of laterally unsupported beams. Nevertheless, the majority use a single method that is intended to be applicable to all types of moment distributions.

Table 2. Equivalent Moment Factor Equations Evaluated in This Study		
Equation ^a	Publication	Equivalent Moment Factor Equation
2	Salvadori (1955) ^{b, c}	$C_b = 1.75 + 1.05\kappa + 0.3\kappa^2 \leq 2.3$
3	Austin (1961)	$C_b = (0.6 - 0.4\kappa)^{-1} \leq 2.5$
4	Kirby and Nethercot (1979)	$C_b = \frac{12M_{max}}{2M_{max} + 3M_a + 4M_b + 3M_c}$
5	Serna et al. (2006)	$C_b = \sqrt{\frac{35M_{max}^2}{M_{max}^2 + 9M_a^2 + 16M_b^2 + 9M_c^2}}$
6	AISC Specification	$C_b = \frac{12.5M_{max}}{2.5M_{max} + 3M_a + 4M_b + 3M_c} \leq 3.0$
7	British Standard BS 5950-1	$C_b = \frac{M_{max}}{0.2M_{max} + 0.15M_a + 0.5M_b + 0.15M_c} \leq 2.273$
8	Australian Standard AS4100	$C_b = \frac{1.7M_{max}}{\sqrt{M_a^2 + M_b^2 + M_c^2}} \leq 2.5$
9	Proposed Equation	$C_b = \frac{4M_{max}}{\sqrt{M_{max}^2 + 4M_a^2 + 7M_b^2 + 4M_c^2}} \leq 2.5$
^a Equation 1, specified in the body text, is the general lateral-torsional buckling equation to which these C_b equations are applied. ^b Adopted by CAN/CSA-S16-01 and CAN/CSA-S6-06, but with an upper limit of 2.5. ^c Adopted by AASHTO with additional requirements.		

CAN/CSA-S16-01—Limit States Design of Steel Structures (CSA, 2001)

This Canadian design standard specifies Equation 2 in Table 2 for determining the equivalent moment factor for unbraced beam segments subjected to end moments, except that an upper limit of 2.5 is used instead of 2.3. It is not clearly stated in the standard whether or not this is intended to apply to beams that are also subjected to transverse loads within this length. Although the sign of κ is assigned as described previously, no indication is given of how to account for triple curvature (e.g., Moment Type 2 in Table 1). The standard also specifies that for non-linear moment distributions where “the bending moment at any point within the unbraced length is larger than the larger end moment” (CSA, 2001), the equivalent moment factor be taken as 1.0. This additional clause effectively requires the designer to ignore the beneficial effect of a non-uniform moment distribution under this common circumstance. Moreover, if the standard is interpreted to mean that Equation 2 applies just for cases of end moments

only (without any transverse loads), then it is silent on how to account for non-uniform moment distributions that are not captured by this additional clause.

CAN/CSA-S6-06—Canadian Highway Bridge Design Code (CSA, 2006)

This standard has adopted the same procedure as CAN/CSA-S16-01; however, the commentary to the standard refers users to the procedures of Clark and Hill (1960) as an alternative approach.

ANSI/AISC 360-05—Specification for Structural Steel Buildings (AISC, 2005a)

The American steel design specification for buildings stipulates that Equation 6 in Table 2 be used to determine the equivalent moment factor. As shown in the table, the only differences between Equations 4 and 6 are the coefficients for the terms M_{max} . This adjustment was made in an attempt

Table 3. Discrete Equivalent Moment Factors and Equations from the Literature ^a

Moment Type	Clark & Hill (1960)	Nethercot & Trahair (1976)	Trahair (1993)	Eurocode 3 (ECS, 1992)
1	$\kappa = -0.5$ $C_b = 1.31$ $\kappa = 0$ $C_b = 1.77$ $\kappa = 0.5$ $C_b = 2.33$ $\kappa = 1.0$ $C_b = 2.56$	$\kappa = 0$ $C_b = 1.75$ $\kappa = 1.0$ $C_b = 2.56$	Equation 2 (Table 2)	$\kappa = -0.75$ $C_b = 1.141$ $\kappa = -0.5$ $C_b = 1.323$ $\kappa = -0.25$ $C_b = 1.563$ $\kappa = 0$ $C_b = 1.879$ $\kappa = 0.25$ $C_b = 2.281$ $\kappa = 0.5$ $C_b = 2.7$ $\kappa = 0.75$ $C_b = 2.927$ $\kappa = 1.0$ $C_b = 2.752$
2 ^b	$\beta = 0$ $C_b = 1.13$ $\beta = 1.0$ $C_b = 1.30$ $\beta = 1.0$ $C_b = 2.52$	$\beta = 0$ $C_b = 1.13$ $\beta = 1.0$ $C_b = 2.58$	Numerical result: $\beta = 0$ $C_b = 1.09$ Equations: For $0 \leq \beta < 0.75$, $C_b = 1.13 + 0.12\beta$ For $0.75 \leq \beta \leq 1.0$, $C_b = -2.38 + 4.8\beta$	$\beta = 0$ $C_b = 1.13$ $\beta = 1.0$ $C_b = 1.285$ $\beta = 1.0$ $C_b = 2.52$
3	same as Type 2 for $\beta = 0$	same as Type 2 for $\beta = 0$	Numerical result: $\beta = 0$ $C_b = 1.09$ Equations: For $0 \leq \beta < 0.7$, $C_b = 1.13 + 0.1\beta$ For $0.7 \leq \beta \leq 1.0$, $C_b = -1.25 + 3.5\beta$	same as Type 2 for $\beta = 0$
4	$\beta = 0$ $C_b = 1.35$ $\beta = 1.0$ $C_b = 1.70$	$\beta = 0$ $C_b = 1.35$ $\beta = 1.0$ $C_b = 1.70$	Numerical result: $\beta = 0$ $C_b = 1.31$ Equation: For $0 \leq \beta \leq 1.0$, $C_b = 1.35 + 0.36\beta$	$\beta = 0$ $C_b = 1.365$ $\beta = 1.0$ $C_b = 1.565$
5	same as Type 4 for $\beta = 0$	same as Type 4 for $\beta = 0$	Numerical result: $\beta = 0$ $C_b = 1.31$ Equations: For $0 \leq \beta < 0.89$, $C_b = 1.35 + 0.15\beta$ For $0.89 \leq \beta \leq 1.0$, $C_b = -1.2 + 3.0\beta$	same as Type 4 for $\beta = 0$
6	$a = L/2$ same as Type 4 for $\beta = 0$	$a = L/4$ $C_b = 1.44$ $a = L/2$ $C_b = 1.35$	Numerical result: $a = L/2$ $C_b = 1.31$ Equation: For $0 \leq a/L \leq 0.5$, $C_b = 1.35 + 0.4(1-2a/L)^2$	$a = L/2$ same as Type 4 for $\beta = 0$
7 ^c	$a = L/4$ $C_b = 1.04$ $a = L/2$ same as Type 4 for $\beta = 0$	$a = L/4$ $C_b = 1.04$ $a = L/2$ same as Type 4 for $\beta = 0$	Numerical result: $a = L/2$ $C_b = 1.31$ Equation: For $0 \leq a/L \leq 0.5$, $C_b = 1.0 + 0.35(2a/L)^2$	$a = L/4$ $C_b = 1.046$ $a = L/2$ same as Type 4 for $\beta = 0$

^a No C_b values or equations were published for moment Types 8 to 12.
^b Strikethrough indicates error in original reference; refer to text for clarification.
^c For moment Type 7 only, Nethercot and Rockey (1972) propose $C_b = 1.0 + (a/L)^2$.

to give better results for cases of fixed end supports (AISC, 2005b). For design purposes, this specification sets an upper limit to the equivalent moment factor of 3.0, which is the highest among all specifications discussed here. The commentary to the specification indicates that Equation 2 is also appropriate for cases where the moment distribution is linear between brace points.

AASHTO—LRFD Bridge Design Specifications (AASHTO, 2007)

Similar to the current CAN/CSA-S16-01 procedure, this specification uses Equation 2 as the primary equivalent moment factor equation and also specifies that the value be taken as 1.0 whenever the larger end moment is not the largest moment throughout the unbraced segment. However,

the main difference between the two specifications is that in order to avoid the non-conservative results obtained when Equation 2 is used for certain non-uniform moment distributions, AASHTO (2007) introduces an equivalent linear moment distribution. The larger end moment and the mid-span moment are projected back linearly to obtain an imaginary smaller end moment, and then the larger value of the actual and imaginary smaller end moment is used to determine κ in Equation 2. Figure 1 illustrates an example for which a more appropriate solution is obtained if the magnitude of the mid-span moment is taken into consideration. The AASHTO (2007) procedure requires the calculation of two different equivalent moment factors—one for each of the top and bottom flanges—if both flanges experience compression due to reversing curvatures.

BS 5950-1—Structural Use of Steelwork in Building: Code of Practice for Design (BSI, 2000)

The British standard specifies Equation 7 in Table 2 for determining the equivalent moment factor. Among all specifications discussed in this study, BS 5950-1 has the lowest upper limit (2.273).

Eurocode 3 EN-1993-1-1—Design of Steel Structures (ECS, 1992)

In Annex F of the European design code, tabulated discrete equivalent moment factors are provided for moment Types 1, 2, 4 and 7 (see Table 1). These values are similar to those published by Clark and Hill (1960), as shown in Table 3. As in the original publication, the value for moment Type 2 when β equals 1.0 appears to be in error, and it has been corrected accordingly in Table 3.

AS 4100—Australian Standard: Steel Structures (SAA, 1998)

The Australian design standard specifies Equation 8 in Table 2 for determining the equivalent moment factor. Similar to Equation 5, it employs a square root format.

ASSESSMENT APPROACH

Equivalent moment factors for 12 diverse selections of bending moment distribution types have been determined from the various equations discussed in this paper. These solutions are compared against each other, as well as with numerical results presented in the literature. Although White and Kim (2008) included the results of hundreds of physical test results collected from numerous sources in a comprehensive statistical study on the flexural resistance of beams, the majority of these do not fall within the scope of the current study because the experiments either involved transverse loading applied above or below the shear center, were conducted on beams with mono-symmetric or hybrid cross-sections, were influenced by interaction buckling, or resulted in inelastic global or local buckling. Nonetheless, they included four experimental results from simply supported beams tested with a mid-span concentrated load applied through the shear center (i.e., moment Type 6, $a/L = 0.5$) that failed by elastic lateral-torsional buckling. Since there are so few suitable test results available, and because this particular moment distribution is associated with a relatively well-established equivalent moment factor, their inclusion would add little to the discussion presented herein. Therefore, these four tests are excluded from the comparisons in this paper.

Representative Moment Distributions

As shown in Table 1, the bending moment types considered in this study have been selected to cover a broad variety of potential situations. Moreover, each moment type envelopes a wide range of moment diagrams by varying either the magnitude of the end moments or the concentrated load locations.

The value of κ for Type 1 (linear) moment distributions reflects the ratio of the end moments and can therefore vary only from -1.0 to 1.0 . The variable β , used for moment Types 2 to 5, 8, 9, 11 and 12, was assigned to alter the magnitude of the end moments. When β is set to 0, it represents a pinned (in plane) boundary condition, whereas when it is equal to 1.0, it represents a fixed boundary condition. The

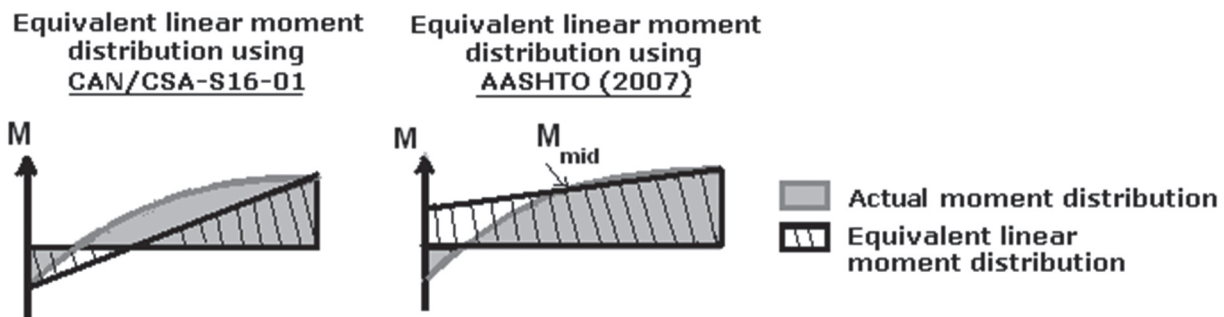


Fig. 1. Simplified moment diagrams according to CAN/CSA-S16-01 and AASHTO.

factor β was considered over a range from negative to a large enough positive value so that the scenarios of single, double and triple flexural curvature, combined with either a maximum moment at the end or away from the braces, were all covered and examined. Moment diagrams with negative values of β or values greater than 1.0 provide useful insight for evaluating continuous span structures. The variable a , used for moment Types 6, 7 and 10, was assigned to provide a means for altering the point load location along an unbraced beam segment. As the location of the concentrated load coincides with the maximum moment for these moment distribution types, this variation helps to develop trends of solutions that depict the influence of a varying distance between the point of maximum moment and the brace points.

Moment Types 2, 4 and 11 were selected, in part, because they include moment distributions that correspond to triple curvature. Due to the ambiguous instruction provided in standard CAN/CSA-S16-01 regarding the sign of κ for segments in triple curvature, solutions calculated by setting κ to both negative and positive are compared.

Moment Types 8, 9 and 10 are transformations of Types 2, 3 and 7, respectively, that simulate situations in which an extra brace is placed in the middle of the original unbraced segment. Moment Types 8 and 10 are included in the analysis to create circumstances where the moment is relatively uniform over much of the length, but no moment within the unbraced segment exceeds the larger end moment. As noted previously, this situation is not covered explicitly in CAN/CSA-S16-01. Unlike Types 8 and 10, the moment distributions of the left and right segments for moment Type 9 are different; thus, two sets of equivalent moment factor results are evaluated.

Numerical Simulation Data

Numerical analysis results from six different research programs are included in the comparisons as reference solutions. No numerical simulations were found in the literature for moment Types 8 to 12.

A total of 1500 critical bending stresses calculated using numerical analysis were tabulated by Austin et al., (1955). This extensive set of results was created by determining the critical moment of wide-flange sections with 10 different levels of flexural slenderness. Two loading cases—a uniformly distributed load and a mid-span point load—and 25 discrete levels of in-plane and out-of-plane end rotational restraint combinations were used. Moreover, three discrete levels of load application (i.e., load applied at the top flange, shear center, and bottom flange) were evaluated for each combination of the loading and boundary conditions. Because the effects of the height of load application and the out-of-plane rotational end restraint are not considered in the current study, only 10 out of the 1,500 solutions are used in the comparisons. Half of these solutions are selected from numerical models subjected to a uniformly distributed load

(Type 2) and the other half are from models subjected to a mid-span point load (Type 4). The solutions selected are based on cross-sectional properties similar to the two distinct numerical models used in the analyses of Serna et al. (2006).

Suryoatmono and Ho (2002) published a suite of finite difference solutions for a 10-m-long (32.8 ft) doubly-symmetric wide-flange section with several different moment types: Type 1 with κ varying from -1.0 to 1.0 ; Types 2 and 3 with β varying from 0 to 2.0; and Type 6 with $a = L/2$ (same as Types 4 and 5 with $\beta = 0$). A total of 38 data points are used in the comparisons.

Serna et al. (2006) published an extensive set of equivalent moment factors based on numerical results for moment Types 1 to 5, with various end support conditions. Only data associated with no end lateral rotational restraint and no warping restraint are used in the evaluation. These researchers analyzed two models with different flexural slenderness values to ensure that the effect of the flexural slenderness on the equivalent moment factors was observed. Only the lower value of C_b from the two models is utilized for each loading condition in this study. As such, a total of 67 data points are used.

Other numerical results used in the comparisons were published by Clark and Hill (1960), Nethercot and Trahair (1976), and Trahair (1993). They are summarized in Table 3.

RESULTS AND IMPORTANT OBSERVATIONS

Comparisons Among Methods

The equivalent moment factor values determined by the methods discussed previously for all 12 moment distribution types are graphically presented alongside available numerical results in Figures 2 to 14. The purposes of these comparisons are to identify deficiencies and strengths of the various methods and to propose a method that optimizes the trade-off between computational effort and accuracy over a broad range of moment distribution types.

Due to the large quantity of data assembled, for clarity of the graphs in Figures 2 through 14 not all results from the various methods and equations could be included. Therefore, methods that are deemed not to provide any particular insight are sometimes omitted. To further alleviate difficulties in interpreting the graphs due to congestion of the data, all numerical results use filled symbols so as to distinguish them from the open and unfilled symbols used for design specifications and other published equations. Where the solutions for Equations 6 through 9 are controlled by the prescribed upper limit in the relevant design specification, the curves above the limit are shown dashed to reflect the accuracy of the equations in the event that the limit should be modified or eliminated.

Figure 2 demonstrates that all methods provide satisfactory approximations to the numerical results for Type 1 (linear) moment distributions for κ values up to about 0.5. As expected, results calculated using the CAN/CSA-S16-01 equation closely match the numerical results over the full range. Among all the quarter-point moment equations, the AISC equation gives the most conservative results within the region $0.5 < \kappa < 1.0$, with differences up to 18% compared to the numerical results.

For moment Type 2, the beam segment is under triple curvature bending when β is greater than 0. Since CAN/CSA-S16-01 does not specify whether the sign of κ in the C_b

equation should be positive or negative for such a case, both positive and negative values were used to develop two different sets of solutions for comparison. Nonetheless, both sets fail to follow the trend of the numerical solutions. As illustrated in Figure 3, all other methods produce reasonable approximations to the numerical data, with several utilizing a maximum permissible value to prevent the use of very large values in design. One exception is that the value suggested by Eurocode 3 for the fixed end moment case ($\beta = 1.0$) is very low. Although it provides an excellent representation of general trends, the equation proposed by Serna et al. (2006) appears to be too aggressive for design purposes in the

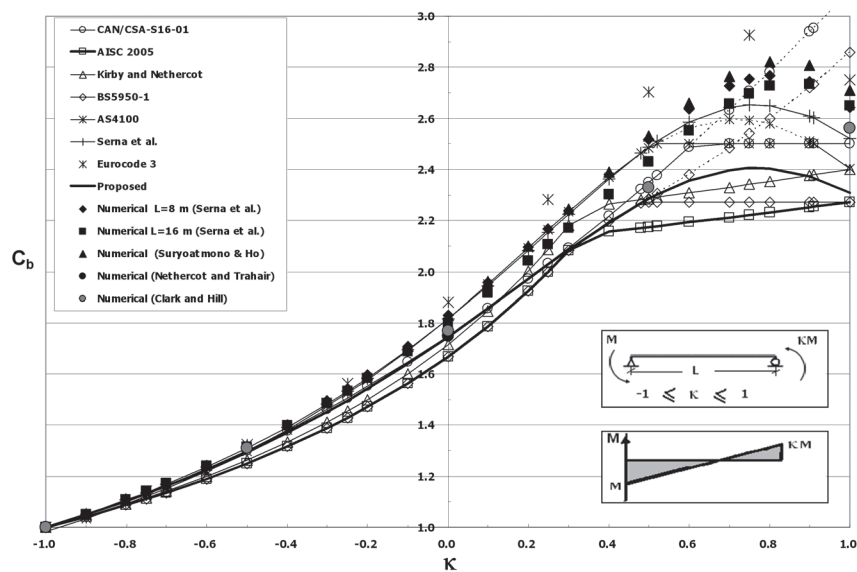


Fig. 2. C_b Results for Moment Type 1.

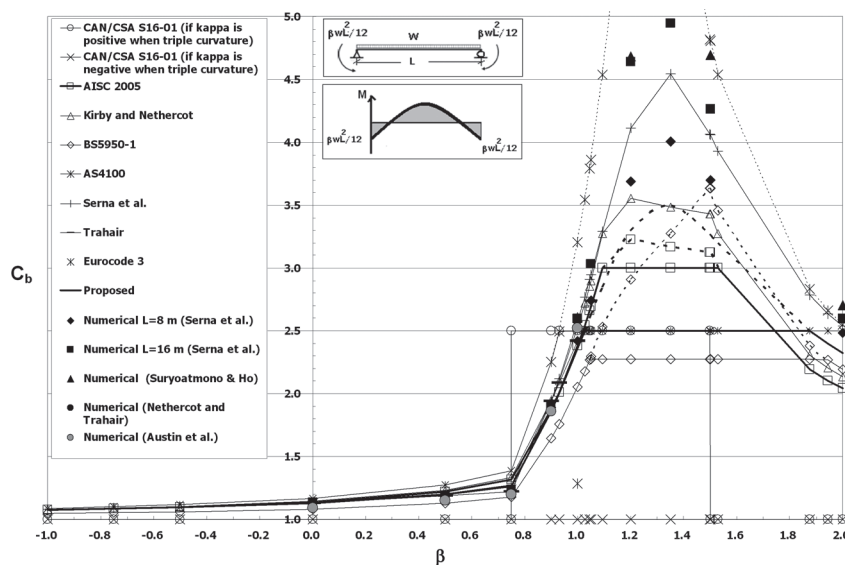


Fig. 3. C_b Results for Moment Type 2.

region $1.0 < \beta < 1.8$ because the values obtained exceed many of their own numerical results.

The CAN/CSA-S16-01 results also fail to follow the trend of the numerical data for moment Type 3. Since there is no moment at the left end of the unbraced segment, the C_b equation in this standard always gives results equal to 1.75 unless the opposite end moment is not the maximum moment in the segment, in which case the value is 1.0. The abrupt transition between these two cases is at $\beta = 0.69$. As shown in Figure 4, non-conservative results exist where $0.69 < \beta < 0.85$. Most other methods perform relatively well for this moment

distribution type over the majority of the range of common β values. If the upper limits of the design equations are not considered, AS 4100 and Serna et al. (2006) seem to approximate the upper and lower bounds, respectively, of the numerical data in the upper range of β , while the AISC equation is the most conservative method in the same region.

As seen in Figure 5 for moment Type 4, results obtained from the Kirby and Nethercot (1979) and AISC formulae differ significantly from the numerical results on the non-conservative side in the region of $0.6 < \beta < 1.1$ (restraint approaching a fixed end condition). Although the BS 5950-1

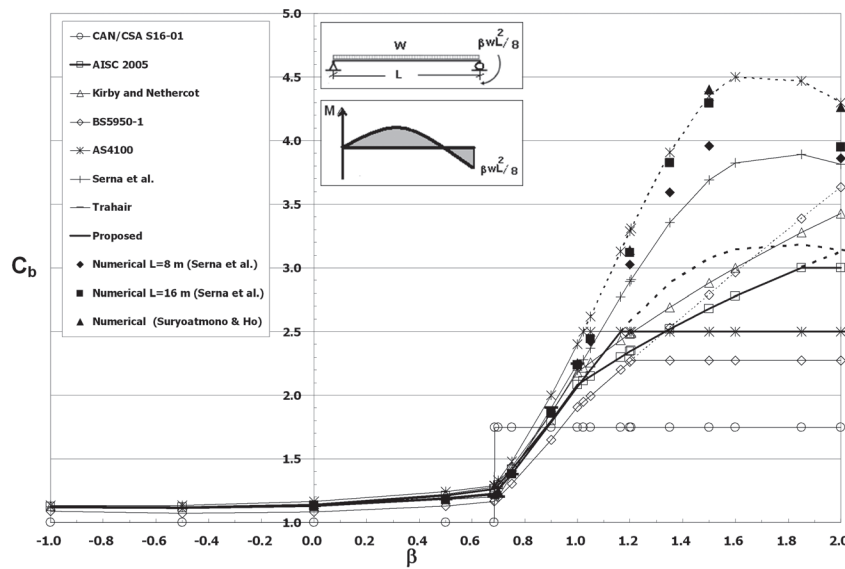


Fig. 4. C_b Results for Moment Type 3.

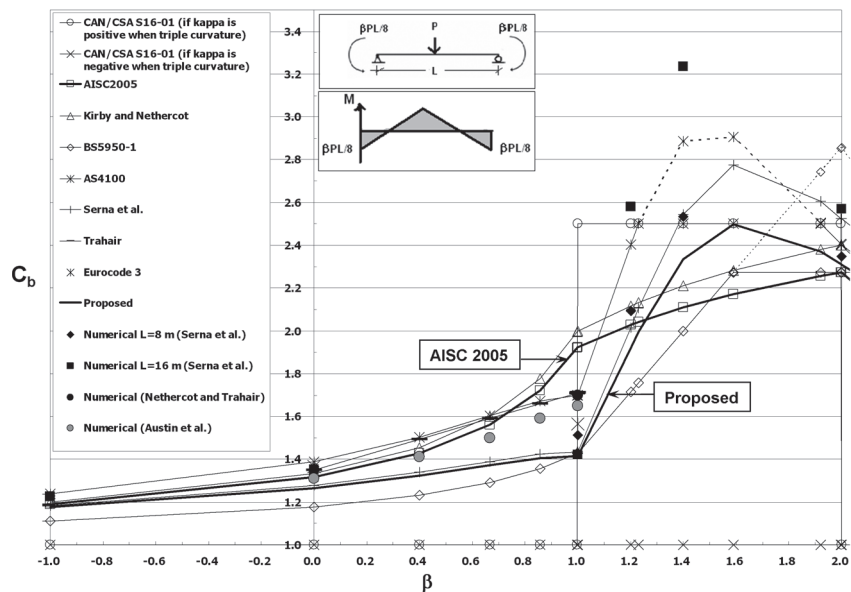


Fig. 5. C_b Results for Moment Type 4

equation is conservative in this region, it fails to capture the relatively abrupt change observed in the numerical data trends at about $\beta = 1.0$. Conversely, the AS 4100 and Serna et al. (2006) equations, which both use the square root format in the C_b equation, produce accurate approximations for this region and also capture the abrupt change in slope. The equation of Serna et al. (2006) is the more conservative of the two in this region. Similar to moment Type 2, two sets of solutions calculated using the CAN/CSA-S16-01 procedures are plotted for this moment type. Significantly non-conservative values are observed within the region $1.0 < \beta < 1.4$ if κ is

taken positive for triple curvature. Otherwise, grossly conservative values are obtained throughout.

The C_b values obtained using CAN/CSA-S16-01 for moment Type 5 change abruptly from 1.0 to 1.75 when $\beta = 0.89$. Figure 6 shows that these results are dissimilar to all other methods. Other methods generally give reasonable results, with the BS5950-1 equation being the most conservative.

Since there are no end moments in moment Type 6, CAN/CSA-S16-01 sets C_b equal to 1.0, regardless of the location of the point load. Figure 7 shows that this solution is highly conservative in all situations. Although numerical results are

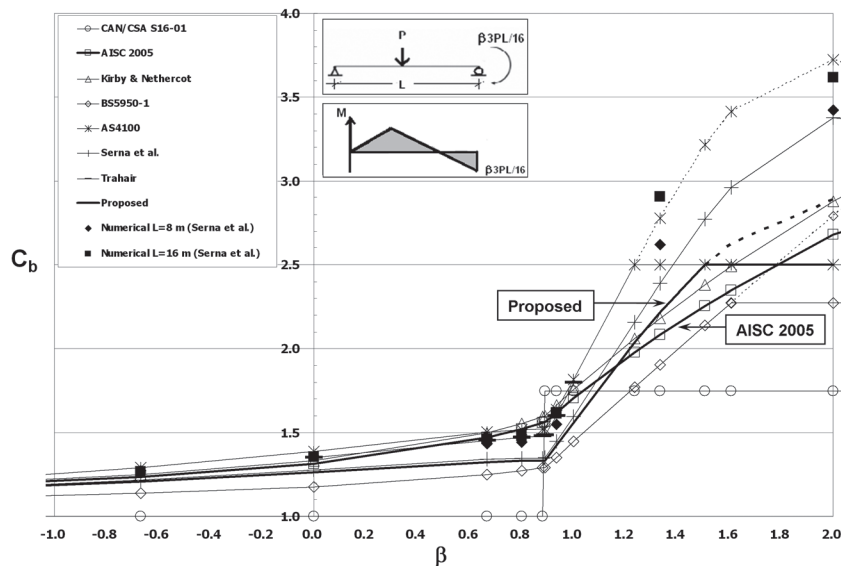


Fig. 6. C_b Results for Moment Type 5.

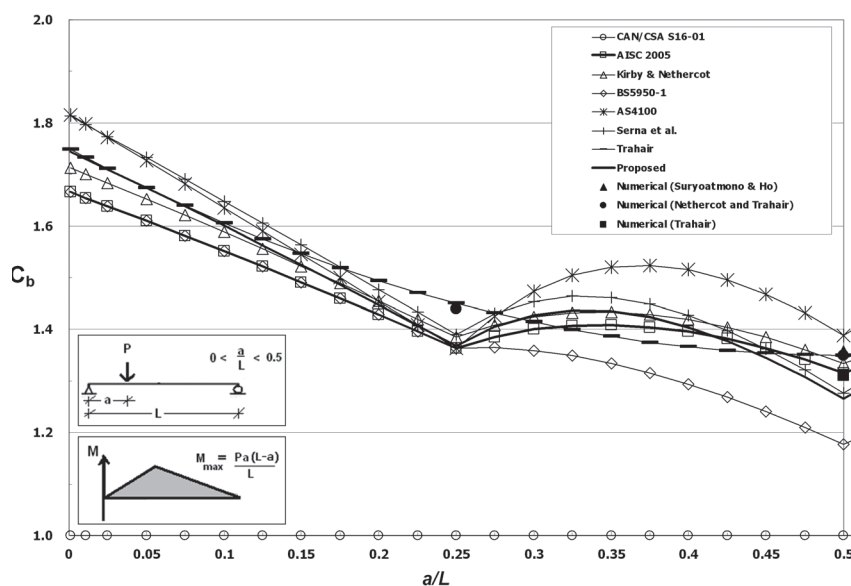


Fig. 7. C_b Results for Moment Type 6.

unavailable over the entire range of a/L , the actual trend of the solution can be reasonably predicted. The correct C_b solutions should decrease gradually from about 1.75 to 1.35 as the point load moves from one end of the unbraced segment toward mid-span. It is believed that the Trahair (1993) equation provides the closest approximation to the true solutions, although it is intended for use with this load case only. The local maxima in the curves predicted by most quarter-point moment methods at about $a/L = 0.35$ appear unreasonable, and in the case of the AS 4100 equation the C_b values around the peak are likely significantly non-conservative. Of all the

quarter-point moment methods, BS5950-1 gives the most conservative results in this region.

Similar to moment Type 6, the CAN/CSA-S16-01 equation gives C_b values equal to 1.0 for the full range of a/L for moment Type 7 because no end moment is present. In this case, it is apparent that the correct solutions should increase gradually from 1.0 to about 1.35 as the point loads move from the ends of the unbraced segment toward mid-span, as obtained from the equations by Trahair (1993) and Nethercot and Rockey (1972) that were derived for this load case only. Figure 8 shows that all quarter-point moment methods

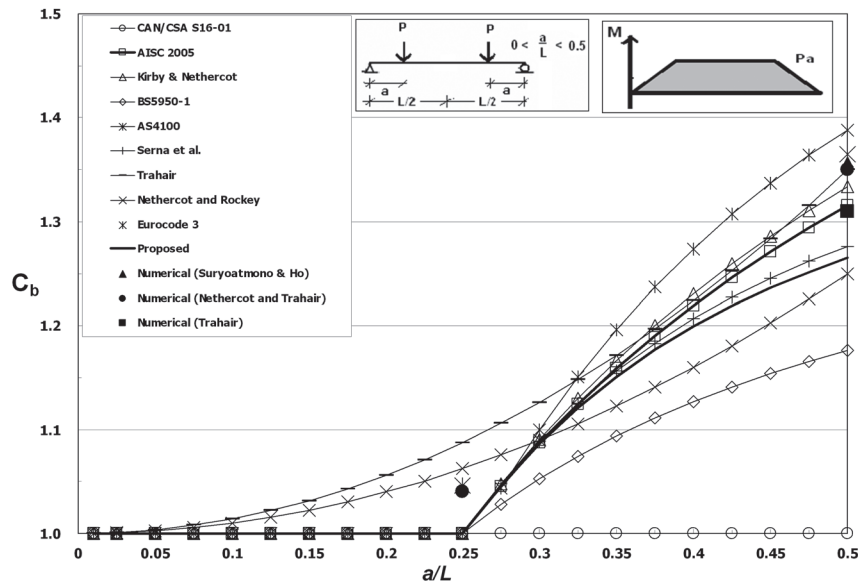


Fig. 8. C_b Results for Moment Type 7.

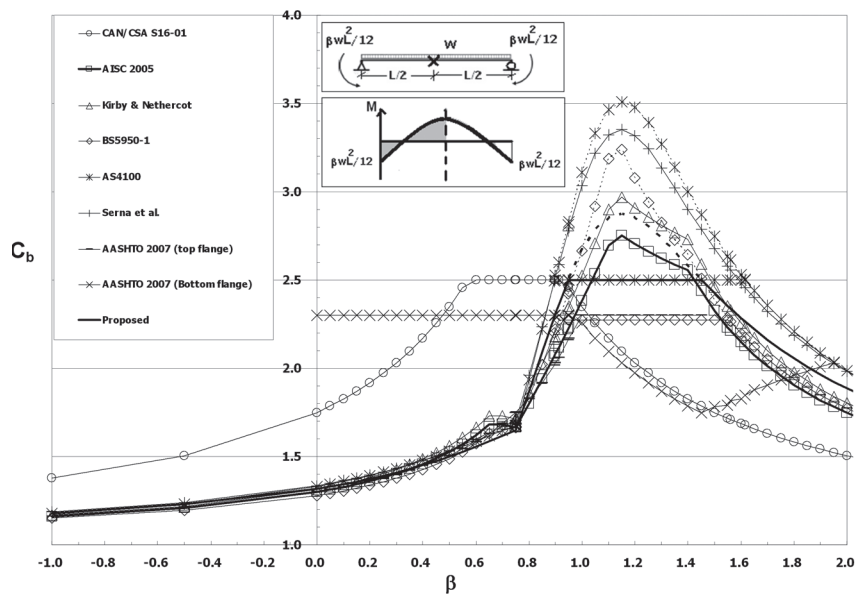


Fig. 9. C_b Results for Moment Type 8.

fail to reflect the effect of the non-uniform moment distribution when the point loads are between the end and the first quarter-point of the unbraced segment, although all methods appear to provide conservative solutions over the full range with the exception of AS 4100.

No numerical results are available for moment Types 8 to 12. However, evaluation of the performance of the various methods can be based on judgment and the knowledge obtained from the results observed for moment Types 1 to 7. Figure 9 (Type 8) and Figure 11 (Type 9, right unbraced segment) show that the C_b results obtained by CAN/CSA-S16-01 are much higher than the results of other methods

for the ranges of $-1.0 < \beta < 0.85$ and $0 < \beta < 0.75$, respectively, and are considered to be highly non-conservative over most of these ranges. On the other hand, Figure 10 (Type 9, left unbraced segment) shows that it produces highly conservative results as compared to other methods. Solutions by other methods are, in general, consistent and appear to be reasonable approximations to the true solutions. The equation in BS5950-1 tends to be the most conservative of the quarter-point moment methods over much of the ranges, and especially when the maximum value is invoked.

As illustrated in Figure 12, the CAN/CSA-S16-01 equation gives a solution of 1.75 for moment Type 10, regardless

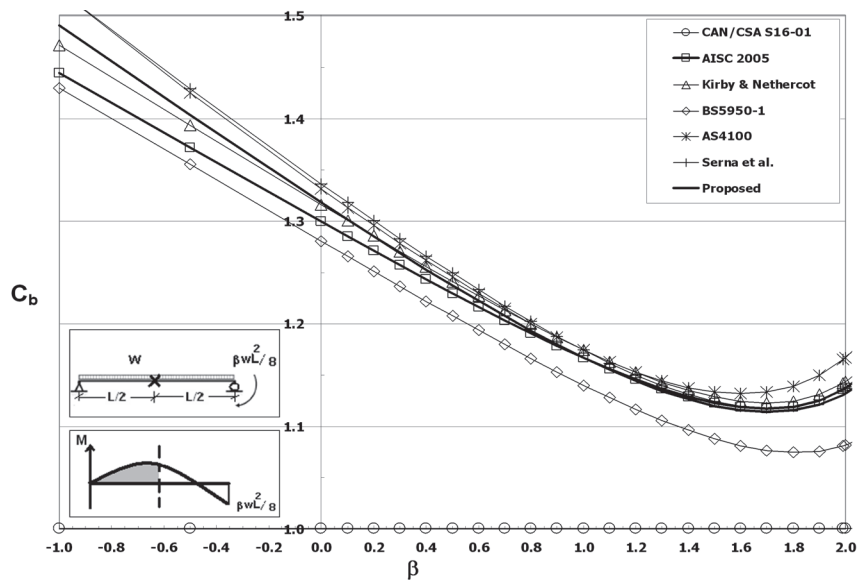


Fig. 10. C_b Results for Moment Type 9, left unbraced segment.

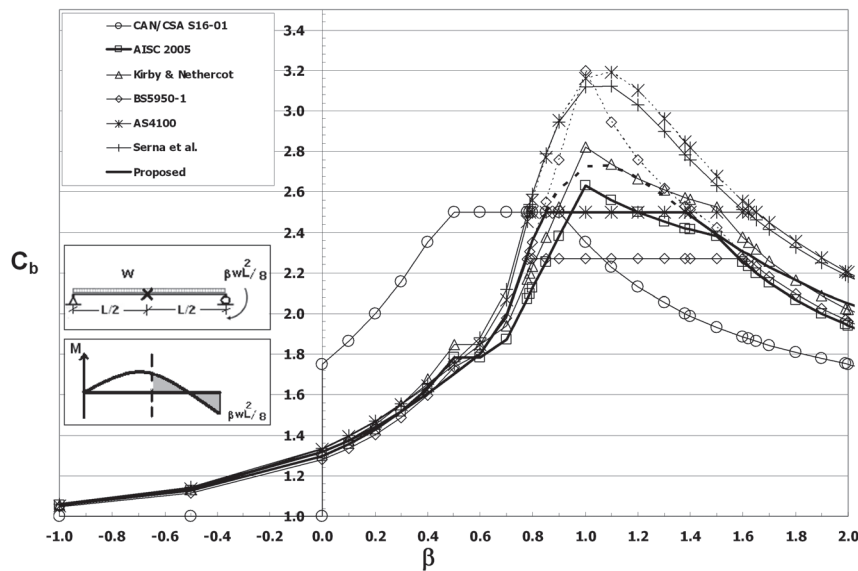


Fig. 11. C_b Results for Moment Type 9, right unbraced segment.

of the point load location. However, solutions determined by all other methods are much lower than 1.75 for the great majority of the range. It is evident in this case that the correct solutions should increase gradually from 1.0 to about 1.75 as the point loads move from the ends of the beam toward the braced mid-span. Although there are no numerical results to verify the correct solutions directly, it is clear that the solutions obtained using CAN/CSA-S16-01 are highly non-conservative. Conversely, the solutions of the AASHTO procedure, which uses the same equation as CAN/CSA-S16-01 but is based on an imaginary smaller end moment determined using the moment at the center of the unbraced

segment, as described previously, are in better agreement with other methods. Again, BS5950-1 provides the most conservative solutions among the quarter-point moment methods, although all such methods provide similar results over the full range of a/L .

Solutions developed for moment Types 11 and 12 are illustrated in Figure 13 and Figure 14, respectively. Findings and observations are similar to those discussed previously for moment Types 2 and 3.

Although a broad investigation is presented herein that includes many procedures from the literature and design specifications, it is instructive to clarify the deficiencies of the

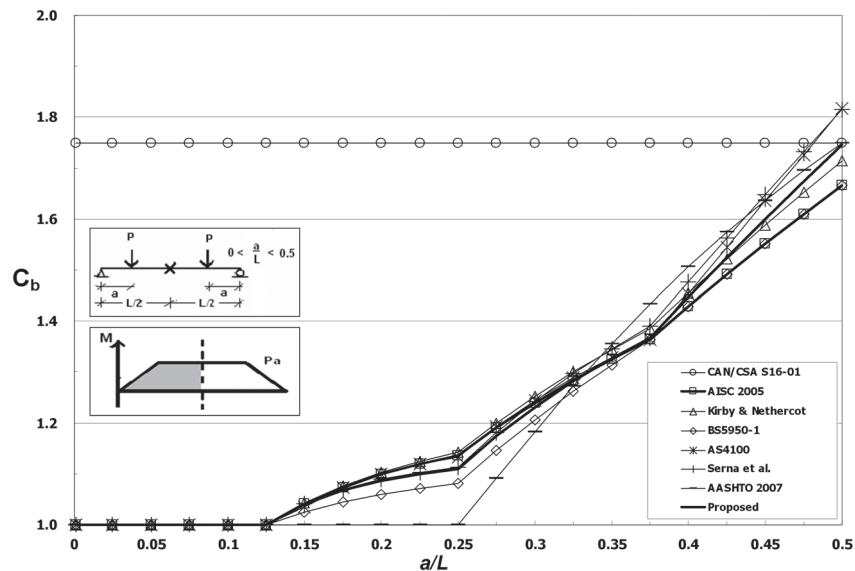


Fig. 12. C_b Results for Moment Type 10.

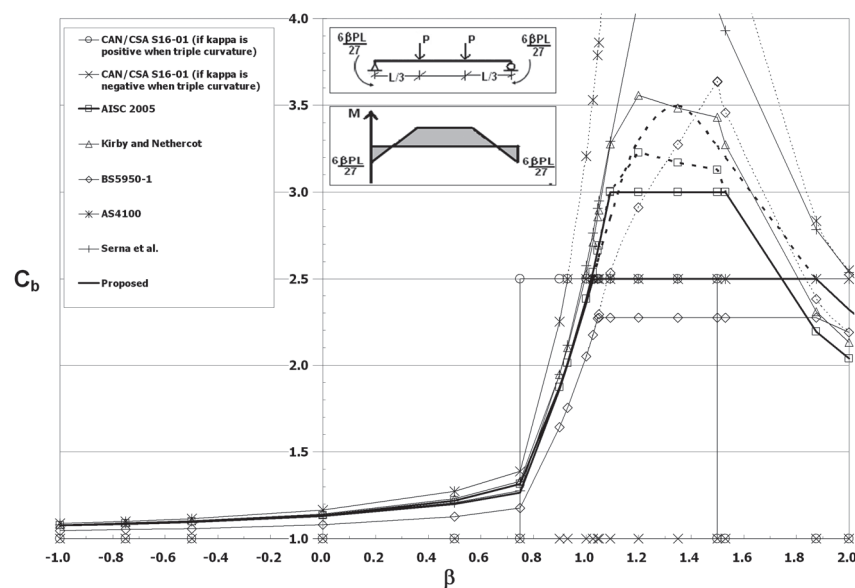


Fig. 13. C_b Results for Moment Type 11.

CAN/CSA-S16-01 method for determining equivalent moment factors. This design standard gives inconsistent results for all moment types evaluated in this study except for the linear moment distribution (Type 1), for which the procedure was originally derived. Driver and Wong (2007) summarize the ranges where this method produces acceptable results for each moment type presented here and conclude that the procedure is unsatisfactory over the full range in two out of the 12 types (Types 6 and 10) and over a significant part of the range in nine others. In all, they identified four general types of deficiencies in the CAN/CSA-S16-01 approach. First, its provisions tend to produce highly conservative results for simply supported beams that are unbraced between their ends because C_b always defaults to 1.0. Figure 7 indicates that C_b can be underestimated by more than 40% for moment Type 6, for example. Significantly conservative results can also occur in transversely loaded unbraced segments that experience either zero moment at one end of the segment ($C_b = 1.75$) or equal and opposite end moments ($C_b = 1.0$). Second, this method potentially overestimates C_b when a transversely loaded segment experiences a maximum moment at either end. For moment Type 10 (Figure 12), for example, the overestimation can be as high as 75%. Third, in 10 out of the 12 moment types discussed in this paper, C_b either remains unchanged over the entire range of a/L or β , or it experiences abrupt changes at particular β values, whereas for a gradually transforming moment distribution a gradually changing C_b function would appear more appropriate. This suggests that the CAN/CSA-S16-01 provisions, although not always producing non-conservative results, inconsistently accounts for the non-uniform moment

distribution effect. Finally, CAN/CSA-S16-01 is ambiguous in some common design circumstances because it does not clearly state whether or not its provisions are applicable to an unbraced segment that is subjected to end moments in combination with other loading, or whether the sign of κ should be positive or negative for the case of triple curvature. The latter ambiguity in some cases creates a situation where the choice of sign results in either a highly conservative or a highly non-conservative solution. Driver and Wong (2007) provide a more detailed discussion of the CAN/CSA-S16-01 provisions.

Important Observations Concerning Quarter-Point Moment Methods

As shown in all 12 comparisons, the quarter-point moment methods, which are purported to be applicable for any moment distribution, tend to give reasonable results for different moment types even though their levels of accuracy and conservatism vary. The coefficients for the four discrete moments used in these equations are selected deliberately to weight the influence of each quarter-point moment magnitude relative to the maximum moment, and the coefficients selected are highly influential to the accuracy of the results. A few common characteristics of these coefficients are observed by examining Equations 4 to 8. For example, the sum of all coefficients in the denominator is always equal to the coefficient in the numerator. This condition ensures that $C_b = 1.0$ for a uniform moment distribution (i.e., when $M_a = M_b = M_c = M_{max}$). Also, the coefficient of M_a is identical to the coefficient of M_c to ensure that the C_b value is the same

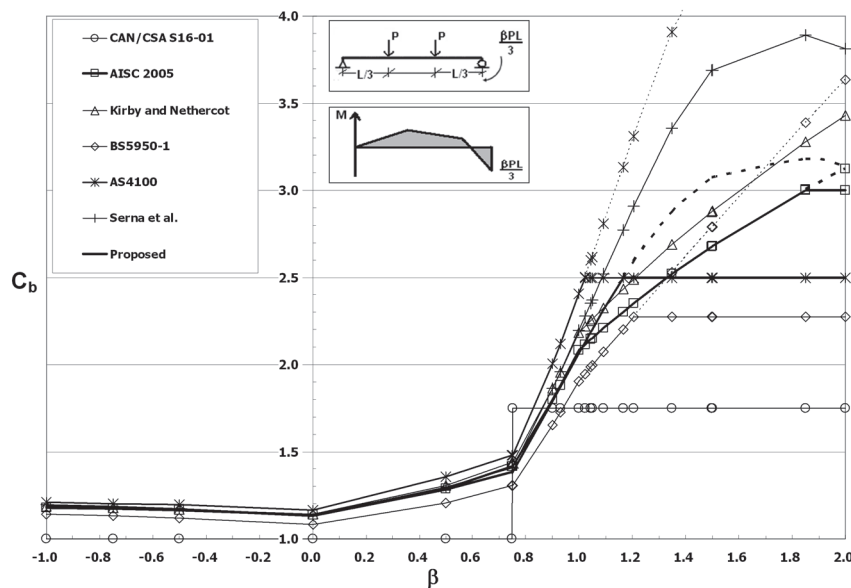


Fig. 14. C_b Results for Moment Type 12.

for any two mirrored moment distributions about the centerline of the unbraced segment. The last common characteristic is that the coefficient of M_b is always at least equal to that of M_a and M_c . This represents the fact that beams with moment distributions where the point of maximum moment is close to the centerline of the unbraced segment (i.e., $M_b \approx M_{max}$) are more prone to lateral-torsional buckling than those where it is close to the quarter points.

All quarter-point moment methods may fail to provide conservative approximations of the actual equivalent moment factor under the presence of abrupt changes in the moment diagram, i.e., for segments loaded with concentrated moments. Arguably, this condition is rare in typical design problems, but it can occur, for example, when a vertical cantilever post affixed to the beam flange is loaded parallel to the beam axis. Figure 15 demonstrates one situation where the accuracy of the quarter-point moment equations is questionable because they fail to capture the uniformity of the moment distribution between the quarter points. Using any of Equations 4 through 8 for the two different moment distributions shown in this example results in the same C_b value, although one case is clearly more critical than the other. If a designer were simply to set M_a and M_c equal to M_{max} instead

of using the actual quarter-point values, Equations 4 to 8 produce the result $C_b = 1.0$, which may be highly conservative, depending on the actual locations of the concentrated moments. One way to address this deficiency would be to increase the number of moment parameters in the equation to better represent the actual moment distribution, but it would also increase the complexity of the equation as well as the concomitant computational effort required for design. Due to the relative rarity of these cases, this increase in complexity is likely unwarranted if designers are simply aware of cases where the quarter-point moment equations should be applied with due caution.

Another concern with the quarter-point moment equations arises because the resulting equivalent moment factor is independent of the sign of the internal moments. It is unclear how these equations can account for the effect of an abrupt reversal of curvature in a beam, such as the one illustrated in Figure 16, Case 2. Although it is apparent that Case 2 loading should result in a more favorable equivalent moment factor than Case 1 due to the presence of double curvature, all quarter-point moment equations incorrectly give the same C_b value for both diagrams because the absolute values of the moment parameters fail to distinguish between the two

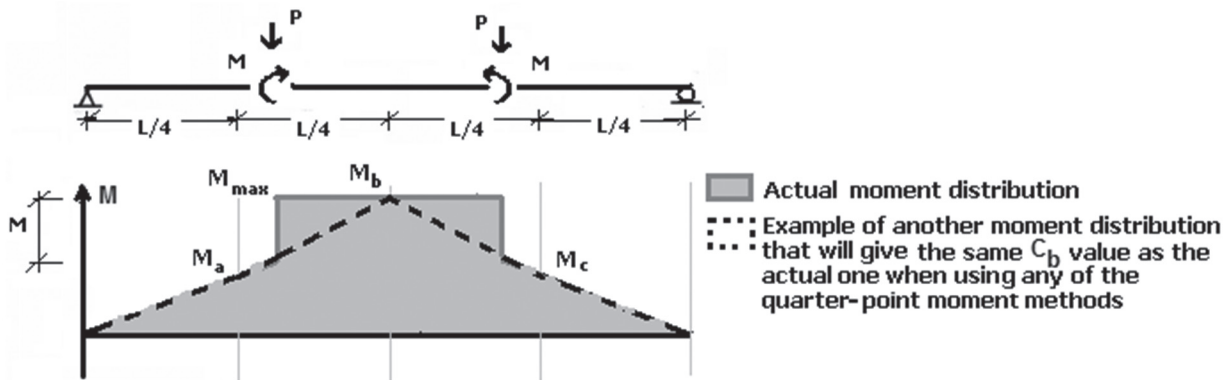


Fig. 15. Inaccuracy of quarter-point moment methods for case of abrupt change in moment.

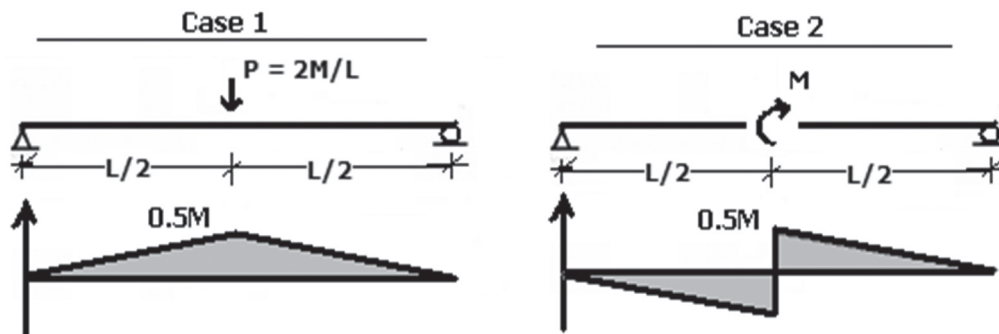


Fig. 16. Inaccuracy of quarter-point moment methods for case of abrupt curvature reversal.

cases. As a result, the solution for Case 2 is highly conservative. Again, refining the equations to rectify this shortcoming is likely unnecessary because this scenario is also relatively uncommon, but designers need to be aware of the limitations of the procedure.

PROPOSED EQUATION

It is evident from the foregoing discussion that modifications are required to improve the accuracy of the CAN/CSA-S16-01 equivalent moment factor procedures. All other methods considered in this investigation are more versatile; however, these methods have their own drawbacks. The method proposed by Trahair (1993) tends to provide very good results, but it relies on several independent equations, each having a limited scope of application, and therefore becomes somewhat cumbersome for general design purposes. The use of a table of individual C_b values for specific cases, similar to those of Clark and Hill (1960), Nethercot and Trahair (1976) and Eurocode 3, is considered undesirable for design specifications due to the innumerable common cases for which no guidance would be provided. Although the AASHTO procedure effectively eliminates many of the non-conservative results obtained from Equation 2 by using an equivalent linear moment diagram, it still gives highly conservative results for simply supported beams braced only at the ends and subjected to transverse loading. Despite their shortcomings for certain rare cases, as discussed in the previous section, the quarter-point moment approach shows the most promise of wide applicability, combined with simplicity, and for the most part these equations capture the trends observed in the numerical data well in the cases considered. Their accuracy, however, depends largely on the coefficients of the moment terms. The equation in the British standard tends to give very conservative results for several moment types. The Kirby and Nethercot (1979) and AISC equations are nearly equivalent and generally give good results. However, they are unable to capture the trends of the numerical data for the common case of moment Type 4 and give non-conservative results (up to about 32%) in the region of $0.6 < \beta < 1.1$.

Equations 5 and 8 (Table 2), by Serna et al. (2006) and specified in the Australian design standard, respectively, generally capture the C_b trends very well. Their ability to provide better results for moment Type 4 than the Kirby and Nethercot (1979) and AISC equations is attributed to the square root format that makes Equations 5 and 8 unique among the quarter-point moment equations considered in this investigation. However, both Equations 5 and 8 produce C_b values in some situations that exceed the numerical data significantly, thereby producing non-conservative results. Equation 8 gives results that exceed the numerical data for moment Types 2, 4 and 6, and in cases where no numerical data are available, it often produces the highest C_b val-

ues of all methods considered. Similar drawbacks exist for Equation 5, although many of the cases where the numerical data are exceeded are for the larger values of C_b that could be eliminated by using an upper bound on the permissible values. In light of the rather sparse set of corroborating numerical and experimental data available, both equations are judged to be too aggressive for design use. Therefore, a modified quarter-point moment equation utilizing the superior square root format is proposed for design in order to provide accurate C_b values and properly represent the data trends, while at the same time minimizing the chance of obtaining non-conservative beam capacities. This equation takes the following form:

$$C_b = \frac{4M_{max}}{\sqrt{M_{max}^2 + 4M_a^2 + 7M_b^2 + 4M_c^2}} \leq 2.5 \quad (9)$$

where the moment parameters are defined in the same way as for the other quarter-point moment equations discussed herein. The upper limit of 2.5 is selected to prohibit the use of very high C_b values in design, although a different upper limit could be selected and justified based on reliability considerations. Nevertheless, it must be noted that the proposed equation appears to produce good results even without this limit. Therefore, if the limit were to be increased or removed, the better performance of the proposed equation, as compared to the other quarter-point moment methods that use the square root format, becomes even more important.

As shown in Figures 2 through 14, the proposed equivalent moment factor equation (Equation 9) provides far better approximations to the numerical data (and to estimated correct solutions where no such data exist) than does the equation in CAN/CSA-S16-01, and it also addresses shortcomings of the other methods, while producing appropriately conservative C_b values for design. For instance, it effectively avoids producing the non-conservative results obtained by the AISC equation for moment Type 4 in the range $0.6 < \beta < 1.1$ (the AISC and proposed equation curves are plotted with a heavier line weight to facilitate comparison). The proposed equation also gives very good results for loading that produces a linear moment distribution between brace points (Type 1), as shown in Figure 2.

SUMMARY AND CONCLUSIONS

Numerous published methods and equations for determining equivalent moment factors used in evaluating the elastic critical moment of laterally unsupported beams have been compared for a wide variety of moment distribution types. The investigation revealed that the procedure used currently in the Canadian design standard produces unacceptable results for the majority of the common bending moment distributions considered. Not only does this method give

grossly conservative results for many common cases, it also frequently gives unconservative results. Large abrupt changes in C_b values with only slight changes in the shape of the moment diagram were observed in 6 out of the 12 moment distribution comparisons, which contributes to the overall poor performance of the procedure. Moreover, it does not give clear direction as to the sign of κ when the beam is under triple curvature.

The study also revealed drawbacks inherent in other methods. Overall, the quarter-point moment equations developed for general moment distributions capture the trends of the numerical data reasonably well. However, the evaluations show that the Kirby and Nethercot (1979) and AISC (2005) equations produce non-conservative results in some situations, while the BS 5950-1 (BSI, 2000) equation, although generally conservative, produces comparatively less accurate results. The Serna et al. (2006) and AS 4100 (SAA, 1998) equations capture the trends of the numerical data more consistently by implementing a square root format in the quarter-point moment method. However, they produce results that exceed the numerical data in several cases, implying that both equations are too aggressive for design purposes.

To capture the best features of the various methods investigated, yet improve the overall suitability for general design purposes, a modified quarter-point moment equation using the square root format (Equation 9) is proposed. Not only does it simulate the trends of the numerical solutions closely, but it also produces reasonable and conservative equivalent moment factors, even in cases where other methods do not. Moreover, it is simple and well-suited to design applications. Like all quarter-point moment methods, the proposed equation does not produce good results in some situations where concentrated moments are applied. Nevertheless, it is believed to be appropriate for the vast majority of typical design cases.

REFERENCES

- AASHTO (2007), *LRFD Bridge Design Specifications*, 4th edition, American Association of State Highway and Transportation Officials, Washington, DC.
- AISC (2005a), *Specification for Structural Steel Buildings*, ANSI/AISC 360-05, American Institution of Steel Construction, Chicago, IL.
- AISC (2005b), *Commentary on the Specification for Structural Steel Buildings*, American Institution of Steel Construction, Chicago, IL.
- Austin, W.J. (1961), "Strength and Design of Metal Beam-Columns," *Journal of the Structural Division*, American Society of Civil Engineers, Vol. 87, No. ST4, April, pp. 1–32.
- Austin, W.J., Yegian, S. and Tung, T.P. (1955), "Lateral Buckling of Elastically End-Restrained I-Beams," *Proceedings of the American Society of Civil Engineers*, Vol. 81, pp. 673–1–673–25.
- BSI (2000), *Structural Use of Steelwork in Building: Code of Practice for Design, Rolled and Welded Sections*, BS5950-1, British Standards Institution, London, United Kingdom.
- Clark, J.W. and Hill, H.N. (1960), "Lateral Buckling of Beams," *Journal of the Structural Division*, American Society of Civil Engineers, Vol. 86, No. ST7, pp. 175–196.
- CSA (2001), *Limit States Design of Steel Structures*, CAN/CSA-S16-01, Canadian Standards Association, Mississauga, ON.
- CSA (2006), *Canadian Highway Bridge Design Code*, CAN/CSA-S6-06, Canadian Standards Association, Mississauga, ON.
- Driver, R.G. and Wong, E. (2007), "Critical Evaluation of the CSA-S16-01 Equivalent Moment Factor for Laterally Unsupported Beams," *2007 Annual General Meeting and Conference*, Canadian Society for Civil Engineering, Paper GC-189.
- ECS (1992), *Eurocode 3: Design of Steel Structures, General Rules and Rules for Building*, EN-1993-1-1, European Committee for Standardization, Brussels, Belgium.
- Galambos, T.V., Ed. (1998), *Guide to Stability Design Criteria for Metal Structures*, Chapter 12 "Bracing," Structural Stability Research Council, John Wiley and Sons, Inc., New York, NY.
- Kirby, P.A. and Nethercot, D.A. (1979), *Design for Structural Stability*, Halsted Press, New York, NY.
- Nethercot, D.A. and Rockey, K.C. (1972), "A Unified Approach to the Elastic Lateral Buckling of Beams," *Engineering Journal*, American Institute of Steel Construction, July, pp. 96–107.
- Nethercot, D.A. and Trahair, N.S. (1976), "Lateral Buckling Approximations for Elastic Beams," *The Structural Engineer*, Vol. 54, No. 6, pp. 197–204.
- SAA (1998), *Australian Standard—Steel Structures*, AS4100, Standards Australia, Homebush, NSW, Australia.
- Salvadori, M.G. (1955), "Lateral Buckling of I-Beams," *ASCE Transactions*, American Society of Civil Engineers, Vol. 120, pp. 1165–1177.
- Serna, M.A., López, A., Puente, I. and Yong, D.J. (2006), "Equivalent Uniform Moment Factors for Lateral-Torsional Buckling of Steel Members," *Journal of Constructional Steel Research*, Vol. 62, pp. 566–580.

- Suryoatmono, B. and Ho, D. (2002), "The Moment-Gradient Factor in Lateral-Torsional Buckling on Wide Flange Steel Sections," *Journal of Constructional Steel Research*, Vol. 58, pp. 1247-1264.
- Trahair, N.S. (1993), *Flexural-Torsional Buckling of Structures*, CRC Press, Boca Raton, FL.
- White, D.W. and Kim, Y.D. (2008), "Unified Flexural Resistance Equations for Stability Design of Steel I-section Members: Moment Gradient Tests," *Journal of Structural Engineering*, American Society of Civil Engineers, Vol. 134, No. 9, pp. 1471-1486.
- Zuraski, P.D. (1992), "The Significance and Application of C_b in Beam Design," *Engineering Journal*, American Institute of Steel Construction, Vol. 39, No. 1, pp. 20-25.

Impact of Diaphragm Behavior on the Seismic Design of Low-Rise Steel Buildings

COLIN A. ROGERS and ROBERT TREMBLAY

ABSTRACT

Modern building codes allow engineers to use reduced seismic loads in design provided that the seismic load resisting system (SLRS) of the structure is adequately designed and detailed to withstand strong ground shaking through ductile inelastic response. This approach has been adopted by the North American model codes, which typically include special provisions to achieve satisfactory inelastic seismic performance. Single-story buildings often incorporate a steel roof deck diaphragm that is relied on to transfer lateral loads to the vertical bracing bents. The vertical braces are usually selected as the energy dissipating fuse element, while the diaphragm and other elements in the SLRS should be designed such that their capacity exceeds the nominal resistance of the braces. Steel bracing members designed for compression inherently possess significant reserve strength when loaded in tension, which means that large brace tension loads must be considered in the design of the surrounding protected structural components. Capacity design seismic provisions have led to the need for much thicker roof deck panels and more closely spaced diaphragm connection patterns compared with past practice in Canada. This paper describes the current U.S. seismic design approach and provides examples as it is applied to single-story buildings and their diaphragms. An overview of the related aspects of an ongoing research project on the flexibility and ductility of the roof diaphragm in low-rise steel buildings is also included.

Keywords: diaphragms, seismic performance, low-rise steel buildings.

INTRODUCTION

Single-story buildings often incorporate a steel roof deck diaphragm that is relied on to transfer lateral wind and seismic loads to the vertical bracing bents. Roof deck diaphragms in North America are commonly constructed of corrugated cold-formed steel panels that are connected to the underlying structure and to one another at side-laps. Standing seam roofs (SSRs) also incorporate a form of steel deck, although it is not rigidly attached to the supporting structure; therefore, SSRs do not provide the necessary diaphragm action for the purposes of this discussion. Design of roof deck diaphragms for in-plane shear forces can be carried out using the SDI *Diaphragm Design Manual* (Luttrell, 2004). The flexural capacity of the diaphragm can be developed through the use of continuous chord members (Figure 1a). Transfer of the horizontal forces to the vertical bracing bents relies on the action of the diaphragm collector elements (Figure 1a).

Diaphragms may also contribute to the overall dynamic properties and response of a building due to their in-plane flexural and shear flexibility.

North American model building codes (ASCE, 2005; NRCC, 2005) and steel design specifications (AISC, 2005a, 2005b; CSA, 2005) allow engineers to use reduced seismic loads in design provided that the seismic load resisting system (SLRS) of the structure is adequately designed and detailed to withstand strong ground shaking through ductile inelastic response. Building codes and standards include special provisions to achieve satisfactory inelastic seismic performance for the various SLRSs used in steel building construction (Tremblay, 2005). In particular, the design of the vertical structural system must be carried out with strict compliance to capacity design principles, i.e., the fuse elements of the SLRS are sized and detailed to dissipate seismic input energy through cyclic inelastic response, whereas the remaining elements should be provided with sufficient capacity to carry the maximum forces that are anticipated along the lateral load path.

The vertical braces of steel buildings are usually selected as the energy dissipating fuse element in the seismic load-resisting system, while the other elements in the SLRS are designed to have a capacity that is equal to or exceeds the expected strength of the braces. Figure 1b depicts the hierarchy of inelastic behavior in the elements located in the SLRS. When tension-compression bracing is used the steel bracing members designed for compression inherently

Colin A. Rogers, Associate Professor, Department of Civil Engineering and Applied Mechanics, McGill University, Montreal QC, H3A 2K6, Canada (corresponding author). E-mail: colin.rogers@mcgill.ca

Robert Tremblay, Professor, Group for Research in Structural Engineering, École Polytechnique, Montreal, QC, H3C 3A7, Canada. E-mail: robert.tremblay@polymtl.ca

possess significant reserve strength when loaded in tension, which means that large brace tension loads must be considered in the design of the surrounding protected structural components. In Canada the SLRS of single-story buildings includes the roof diaphragm as well as the other components in the vertical structural system. This design objective is clearly stated in the 2005 National Building Code of Canada (NBCC) (NRCC, 2005): “Diaphragms and their connections shall be designed so as not to yield.” (Article 4.1.8.15.1) and in CSA-S16 seismic provisions: “In capacity design ... diaphragms and collector elements are capable of transmitting the loads developed at each level to the vertical seismic-force-resisting system” (Clause 27.1.2). These seismic provisions have led to the need for much thicker roof deck panels and more closely spaced diaphragm connection patterns compared with past practice, especially in areas of high seismicity. Complying with these newly introduced design requirements has impacted significantly on the cost of steel building structures in Canada, making this system less attractive economically than in past years (Tremblay and Rogers, 2005). In contrast, no specific guidance is given by AISC (2005a, 2006) to prevent yielding or failure of roof diaphragms or beams acting as collectors or chords, and the designer must refer to ASCE 7 (2005) for the design forces. A capacity design requirement for the diaphragm to meet the expected yield strength of the braces in an ordinary or special concentrically braced frame (OCBF or SCBF) with $R > 3$, for example, does not exist.

This paper contains a description of the U.S. seismic design provisions for low-rise steel buildings, as well as a design example of a single-story building located in Boston, MA. The design is also performed assuming that the struc-

ture is located in Los Angeles, CA. In addition, the paper includes the interim findings of a study currently under way for which the objective is to develop seismic design strategies that account for the flexibility and ductility of the roof diaphragm in low-rise steel buildings. The scope of research includes quasi-static diaphragm shear tests (Tremblay et al., 2004; Essa et al., 2003), large-scale dynamic diaphragm tests (in progress), ambient vibration building measurements (Paultre et al., 2004; Lamarche, 2005; Tremblay et al. 2008a, 2008b), as well as dynamic analyses of representative buildings (in progress). At project end the aim is to make design recommendations on the following aspects: diaphragm stiffness under seismic loading, period of vibration for the building, seismic response modification factors, ductile detailing requirements and inelastic performance levels.

SEISMIC DESIGN OF LOW-RISE BUILDINGS ACCORDING TO U.S. PROVISIONS

Seismic Design Provisions

ASCE 7-05 provides the minimum seismic design loads for building structures in the U.S. Except for buildings with horizontal torsional irregularity, the equivalent lateral force procedure can be used for single-story steel buildings. This procedure comprises the application of an equivalent lateral seismic force that varies as function of the seismicity at the site, the soil type, the period of the buildings and the type of seismic load resisting system. The minimum lateral load, or seismic base shear, V , is given by:

$$V = C_s W \quad (1)$$

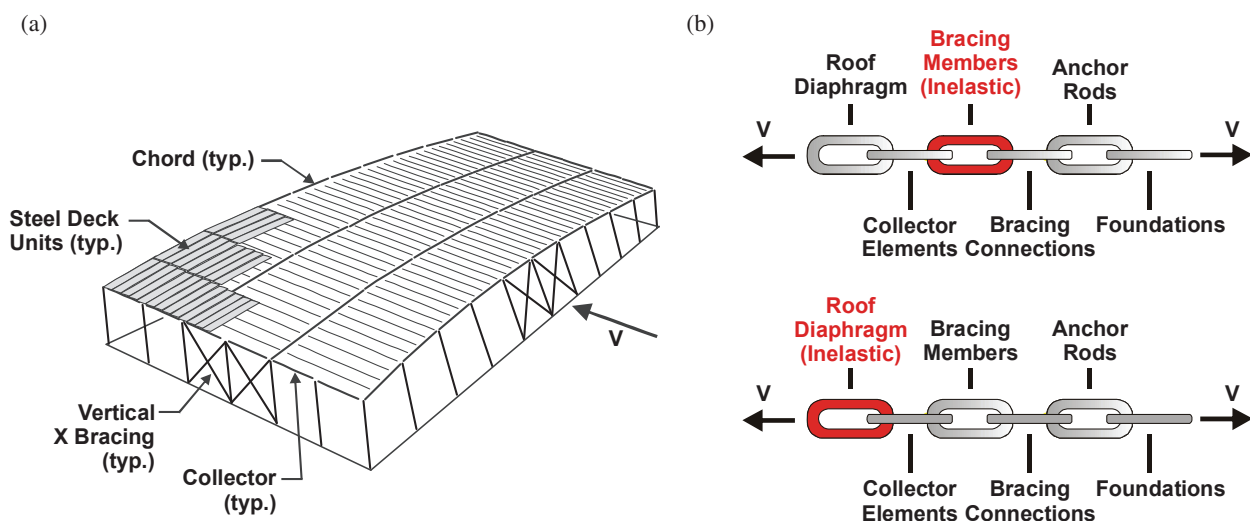


Fig. 1. Single-story buildings with capacity-based design concepts for SLRS.

where

$$\begin{aligned}
 C_s &= \frac{S_{DS}}{(R/I)} \\
 &\leq \frac{S_{D1}}{T(R/I)} \text{ for } T \leq T_L \\
 &\leq \frac{S_{D1}}{T^2(R/I)} \text{ for } T > T_L \\
 &\geq 0.044 S_{DS} I \\
 &\geq 0.01 \\
 &\geq \frac{0.5 S_1}{(R/I)} \text{ if } S_1 \geq 0.6g
 \end{aligned}$$

In these equations, W is the effective seismic weight, S_{DS} and S_{D1} are, respectively, the short-period and the one-second design spectral acceleration parameters, R is the response modification factor, I is the importance factor, T is the fundamental period of the building, and T_L is the long-period transition period at the site. For a single-story steel building, W includes the roof dead load, half the weight of the exterior walls, and 20% of the roof snow load when the snow load exceeds 30 psf. The spectral acceleration parameters are obtained from:

$$S_{DS} = \frac{2}{3} F_a S_s; S_{D1} = \frac{2}{3} F_v S_1 \quad (2)$$

where F_a and F_v are, respectively, the short-period and the long-period site coefficients that depend on the site class, and S_s and S_1 are, respectively, the mapped spectral accelerations at short-period and one second corresponding to the maximum credible earthquake (MCE) level. Values of F_a and F_v are specified in ASCE 7 for different site classes, while values of S_s and S_1 and T_L can be obtained from maps that are also included in ASCE 7. The period T for concentrically braced steel frames can be taken equal to the approximate period $T_a = 0.02h^{0.75}$, where h (ft) is the height of the building. Alternatively, the period obtained from dynamic analysis may be used, although the so-computed period cannot exceed the limit given by $T = C_u T_a$, where C_u is a coefficient that varies from 1.4 for high seismic zones to 1.7 for low seismic zones. The R factor depends on the type of lateral framing system. Single-story steel buildings typically rely on steel bracing for lateral resistance. Three categories of concentrically braced steel frames are described in ASCE 7: special concentrically braced steel frames (SCBFs); ordinary concentrically braced frames (OCBFs); and braced frames not specifically designed for seismic resistance. The main difference between the three systems is their expected inelastic deformation capacity under seismic ground motions. The AISC seismic design provisions (AISC, 2005a) provide detailing rules to ensure ductile inelastic response for the first two systems. More stringent requirements are prescribed for

SCBFs, which allow this framing system to qualify for an R factor of 6.0. An OCBF may be designed with less restrictive provisions; however, the seismic loads must be computed with $R = 3.25$. The third system, for which special ductility detailing requirements need not be considered, must be designed with $R = 3.0$ according to the AISC specification (AISC, 2005b). The importance factor varies from 1.0 to 1.5, depending upon the occupancy category.

Also of key importance in seismic design is the Seismic Design Category of the building. This parameter depends on the occupancy category and the spectral acceleration values at the site. Seismic Design Categories A and B typically apply to buildings that are located in low seismic areas or represent a low hazard to human life in the event of failure. Braced steel frames designed with an $R = 3.0$ are only permitted for seismic design categories A through C. Structures built in moderately or highly active seismic regions and/or buildings that represent a high hazard to human life or that are used for essential facilities generally are assigned to the more severe Seismic Design Category D. Where $S_1 \geq 0.75$, the structure is assigned to Seismic Design Category E, except that essential facilities are assigned to Seismic Design Category F. The OCBF system is limited to a height of 35 ft for Seismic Design Category D or E and is not permitted for Seismic Design Category F. The height limits for SCBFs—160 ft for Seismic Design Category D or E and 100 ft for Seismic Design Category F—typically would not apply to most single-story building applications. In ASCE 7, the seismic loads must be amplified by a redundancy factor, $\rho = 1.3$, for Seismic Design Category D, E or F. For braced steel frames, however, this factor can be taken equal to 1.0 if removal of one brace does not result in more than a 33% reduction in lateral strength nor result in an extreme torsional irregularity condition. The redundancy factor can also be ignored for rectangular buildings that are regular in plan provided that at least two bracing bays are constructed on each of the perimeter walls.

In view of their higher R factor, SCBFs are expected to develop significant inelastic response under the design earthquake. The aim of the AISC seismic provisions is to limit, for the most part, the inelastic demand to the bracing members so that the integrity of the gravity supporting system formed by the beams and columns will remain intact during a strong earthquake. Tension/compression bracing must be used for SCBFs. In addition, limits are imposed on the brace overall slenderness and width-to-thickness ratios to ensure ductile brace response and minimum energy dissipation without premature fracture under inelastic reversed cyclic loading. Brace connections must be designed to resist loads corresponding to the expected brace axial strength in tension, $T_{exp} = AR_y F_y$, and compression, $P_{exp} = 1.1R_y P_n$, where A is the brace cross-section, R_y is the ratio of the expected yield stress to the nominal yield stress, F_y , and P_n is the nominal brace

compressive strength. When the stress ratio, $P_u/\phi_c P_n$, under seismic load combinations exceeds 0.40, columns in bracing bents must be designed for the axial load obtained using the seismic load combinations, including system overstrength. Seismic load effects are amplified by the overstrength factor, Ω_0 , to approximate the maximum seismic induced force the columns will experience during strong ground shaking. In ASCE 7, $\Omega_0 = 2.0$ for braced steel frames. These amplified seismic loads need not exceed the forces arising from $1.1R_y$ times the nominal strengths of the connected braces nor the forces producing uplift of the foundation.

OCBFs are expected to undergo limited inelastic deformations under a design earthquake; thus fewer, less stringent ductility requirements apply. Both tension/compression and tension/only bracing designs are permitted in this category. The braces must still meet limits on their slenderness and width-to-thickness ratios. Brace connections must have a tensile strength equal to or greater than the expected brace yield tensile strength, $T_{exp} = AR_y F_y$, but need not exceed the load combination effects based upon the amplified seismic loads.

No specific guidance is given in AISC to prevent yielding or failure of roof diaphragms or beams acting as collectors or chords, and the designer must refer to ASCE 7 for the design forces for these components. For single-story structures, roof diaphragms are designed for the lateral force V , but this force must not be less than $0.2S_{DS}IW$ and need not exceed $0.4S_{DS}IW$. The redundancy factor, ρ , must be the same as that used for the vertical bracing bents. Collector beams must be capable of transferring the forces used in the design of the diaphragm to the supporting framework. For Seismic Design Category C, D, E or F, the collector elements must resist the load combinations including seismic loads amplified for overstrength. No specific requirement is given for beams acting as diaphragm chords and it is assumed that forces consistent with diaphragm design can be used.

In the analysis of a building's structure, the minimum accidental eccentricity corresponding to 5% of the dimension perpendicular to the loading direction must be considered if the diaphragm is anticipated to act as a rigid element. Resistance to the induced in-plane torsional moments can be assumed to be provided by all bracing bents if the roof diaphragm has sufficient in-plane stiffness to efficiently distribute the loads to the vertical system. If the diaphragm is flexible, the load becomes essentially resisted only by the bracing bents acting in the direction parallel to the applied load. Single-story buildings are said to have a flexible diaphragm when the maximum in-plane deformation of the roof diaphragm is more than twice the average of the building deflections computed along the two end walls parallel to the direction under consideration. ASCE 7 requires that in-plane deformations of the roof diaphragm be included in the determination of the building story drift. In this calcu-

lation, the deformations from elastic analysis, δ_{es} , must be multiplied by $C_d I$ to obtain the design story drift reflecting inelastic response, Δ . The factor C_d is, respectively, equal to 5.0 and 3.25 for SCBFs and OCBFs. For braced steel frames designed without ductile detailing, $C_d = 3.0$. When checking drift limits, it is noted that ASCE 7 allows the use of deflections due to seismic loads based on the building fundamental period obtained from dynamic analysis, without applying the upper limit $C_u T_a$.

Building Design Example (Boston)

The simple rectangular building located in Boston, MA, shown in Figure 2a is used to illustrate the seismic design provisions for single-story buildings with lateral seismic loads resisted by steel braced frames acting together with a metal roof deck diaphragm. The roof structure is made of open web steel joists supported on steel trusses spanning across the entire width of the building. Single-bay X-bracing is used on each of the four exterior walls. Only the design of the seismic load resisting system in the direction parallel to the short walls is considered in this example. In addition, the calculations are performed assuming that an SCBF system with $R = 6.0$ and $C_d = 5.0$ is adopted for the bracing bents. The main differences between this and an OCBF design are discussed at the end of the example.

The dead load of the roof and walls are given in the figure together with the roof snow load. The seismic weight, W , is equal to 593 kips. An Occupancy Category II is assumed for the building, the site class is D, and the importance factor $I = 1.0$. The seismic data S_s , S_1 and T_L for the chosen location are given in Figure 2a. For this site, $F_a = 1.56$ and $F_v = 2.4$, which gives design spectral accelerations $S_{DS} = 0.31g$ and $S_{D1} = 0.11g$. The building is 22 feet tall and the period $T_a = 0.02(22)^{0.75} = 0.20$ s. For this site ($S_{D1} = 0.11g$), the factor $C_u = 1.6$ and the amplified period $C_u T_a = 0.32$ s. This period estimate is used for the design and, hence, will need to be checked at the end of the design process. Using these parameters in Equation 1, it is found that $C_s = 0.052$ and $V = 30.8$ kips. Following ASCE 7 procedures, it is determined that the building can be assigned to Seismic Design Category B. Therefore, the redundancy factor, ρ , can be taken equal to 1.0.

The bracing bents are designed first. At this point, one cannot determine whether the roof diaphragm will be classified as flexible; as such it is conservatively assumed that the diaphragm is rigid and that in-plane torsional effects must be accounted for. The structure is symmetric and accidental torsion is included by moving the center of mass (CM) away from the center of rigidity (CR) by 5% of the length of the building (10 ft), as prescribed in ASCE 7 and illustrated in Figure 2b. Assuming that all four bracing bents are of equal stiffness, the load on the bracing bent on gridline A

is equal to 54% $V = 16.6$ kips. This load is resisted equally by the tension and compression acting braces (Figure 2c). Once the braces and columns are designed, analysis of the braced frame will be performed to assess gravity load effects on the braces. At this step, a first trial is made using the compression force of 11.0 kips; square tubing HSS $3 \times 3 \times \frac{3}{16}$ conforming to ASTM A500 Grade C ($F_y = 50$ ksi) is selected for the braces. The factored resistance of these braces $\phi P_n = 13.9$ kips, assuming a brace effective length $KL = (0.5)(400 \text{ in.}) = 200 \text{ in.}$ The braces have a design thickness $t_d = 0.174 \text{ in.}$, a cross sectional area $A = 1.89 \text{ in.}^2$, and they meet the AISC limits for overall slenderness ($KL/r = 175 < 200$) and width-to-thickness ratio ($b/t = 14.2 < 15.4$). For steel tubing, $R_y = 1.4$ in the AISC seismic provisions and the expected brace capacities can be determined: $T_{exp} = 132$ kips and $P_{exp} = 23.8$ kips.

W-shapes made of ASTM A992 steel ($F_y = 50$ ksi) are used for the columns. Axial compression due to gravity roof dead and snow loads are, respectively, equal to $P_D = 5.25$ kips and $P_S = 8.75$ kips. Since the brace $KL/r = 175$ exceeds $4(E/F_y)^{0.5} = 96$ (taking $E = 29,000$ ksi), the AISC *Seismic Provisions* require that the columns be designed to carry gravity load effects plus the brace force T_{exp} transferred to the column; $P_E = 132[\sin(41.3^\circ)] = 87.1$ kips. A W8x40 shape is found adequate to withstand the various load combination effects and meet the minimum width-to-thickness limits prescribed for columns in the AISC *Seismic Provisions*. The analysis of the braced frame under combined gravity and seismic loads shows that the brace compression force is increased to 11.8 kips, still lower than the brace factored resistance (13.9 kips). The elastic deflection, δ_B , of the bracing bent computed under half the seismic load (15.4 kips), is 0.11 in.

The roof diaphragm is formed of 1½-in.-deep, wide-rib (WR) Canam P3606 steel deck sheets having a trapezoidal cross-section. The sheets are 36 in. wide, with flutes spaced 6 in. on center, as illustrated in Figure 3a. The sheets are 25 ft long and span over four equal spans between the roof joists (see Figure 2a). No. 10 self-tapping screws are used for the side-lap connections whereas Hilti X-ENP-19 L15 pins are chosen to connect the steel deck to the supporting structure. The diaphragm design is performed according to the SDI method (Luttrell, 2004) together with the 2004 supplement to the 2001 specification for the design of cold-formed steel members (AISI, 2004). The resistance factor associated with fastener failure modes, ϕ_d , is equal to 0.65. In the direction studied the maximum shear flow in the diaphragm arises along gridline A with $S_u = 16.6 \text{ kips}/100 \text{ ft} = 0.166 \text{ kip}/\text{ft}$. A light diaphragm design consisting of 0.0295-in.-thick steel (22 ga.) panels is found adequate with two side-lap screws per joist span and pins installed on a 36/3 pattern (18 in. on center). Such a diaphragm has a factored shear resistance $\phi_d S_n = 0.281 \text{ kip}/\text{ft}$ and a shear stiffness, G' , of 12.9 kip/in.

The edge beams along the 200-ft-long walls act as the chord members resisting the axial loads induced by the in-plane bending moment, which is produced by the seismic load of 30.8 kips assumed to be uniformly distributed over the length $L = 200 \text{ ft}$, $w_E = 0.154 \text{ kip}/\text{ft}$. The maximum axial loads develop at the diaphragm mid-span, $P_u = (\pm 0.154)(200^2/8)/100 = \pm 7.7$ kips. This situation is illustrated in Figure 3b; W8x10 beams with a cross-sectional area, $A = 2.96 \text{ in.}^2$, are selected. It is noted that seismic loads acting parallel to the long walls also induce axial loads in the same beams and the worst scenario must be considered for the beam design. As illustrated in Figure 3c, when considering

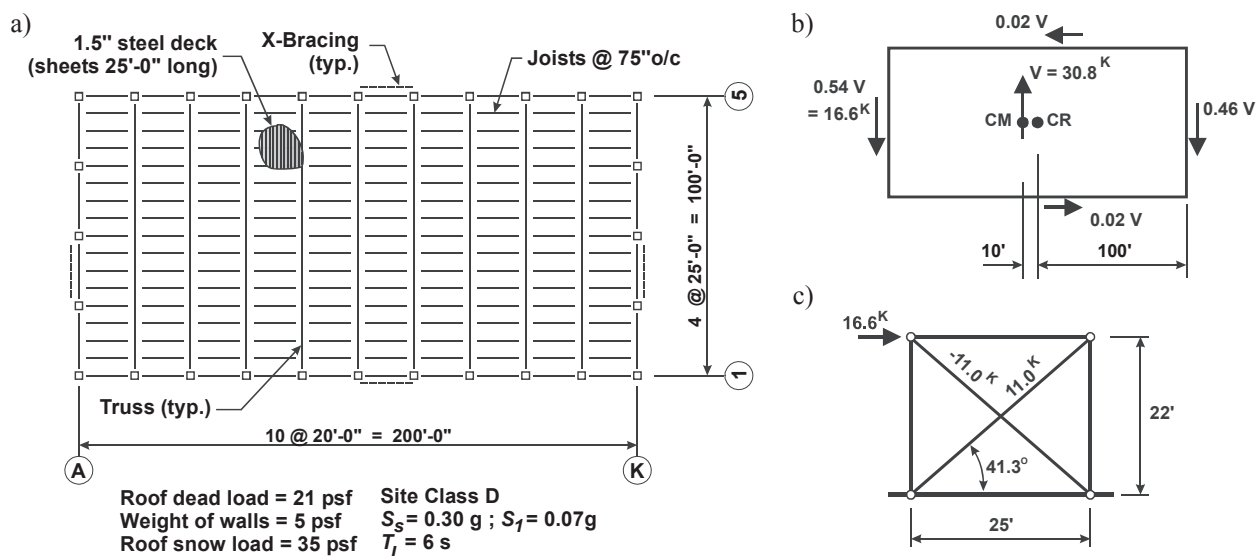


Fig. 2. (a) Plan view of the building studied, (b) in-plane torsion effects, and (c) bracing bent studied.

accidental eccentricity, a maximum force of 15.7 kips is transferred through the roof diaphragm to the bracing bent located along the long walls. The edge beams then act as collector elements transferring the shear flow from the diaphragm to the bracing bent (Figure 3d). In this particular case, the maximum compression axial load in the beams reaches 7.9 kips, which is more critical than the load induced when the same beams act as chord elements. It is noted that maximum forces in collector beams along braced column lines will be minimized if the bracing bents are located half-way along these grid lines. The designer must also provide proper connections between the steel deck and the perimeter members to allow the transfer of the shear flow from the diaphragm to the perimeter beams. In addition, attention must be paid to ensure the transfer of the computed beam axial loads through the beam-column joints. Once the diaphragm is designed and the chord members are selected, in-plane elastic deformations of the diaphragm due to flexure, δ_F , and shear, δ_w , can be determined. For this simple case, these two values can be calculated using:

$$\delta_D = \delta_F + \delta_w = \frac{5 w_E L^4}{384 E I_d} + \frac{w_E L^2}{8 G' b} \quad (3)$$

In this expression, I_d is the moment of inertia of the diaphragm in the direction considered ($I_d = 2.13 \times 10^6 \text{ in.}^4$). The deflections δ_F and δ_w are, respectively, equal to 0.09 in. and 0.60 in., giving $\delta_D = 0.69 \text{ in.}$ The ratio of the diaphragm

deflection to the bracing bent deflection (Figure 4a) is equal to $0.69/0.11 = 6.3$, which is much greater than 2.0, indicating that a flexible roof diaphragm could have been considered in design. The design should then be redone assuming that the diaphragm acts as a simply supported beam spanning between the bracing bents parallel to the load, thus neglecting the contribution of the bracing bents perpendicular to the load in the resistance to the in-plane torsion due to the accidental eccentricity of the seismic load. For regular rectangular buildings such as the one studied herein, a seismic force equal to $0.55V$ would then need to be considered along each of the perimeter bracing bents. This is slightly larger than the values obtained assuming in-plane torsional resistance provided by four equally stiff bracing bents on the perimeter: $0.54V$ and $0.51V$, in the short and long directions, respectively. For simplicity, however, the design obtained herein is kept unchanged in the example.

The design loads for earthquakes as calculated using ASCE 7 are based largely on the fundamental period of vibration of the vertical structure. It has, however, been shown through analytical means that the period of vibration of a single-story building with a flexible roof diaphragm may be longer than that predicted based on the stiffness of the vertical SLRS (Tremblay and Stiemer, 1996; Medhekar, 1997; Tremblay et al., 2000). In the determination of the equivalent-static lateral loads for single story-buildings ASCE 41 (2006) allows for the introduction of the flexibility of the roof diaphragm to estimate the fundamental period of vibration.

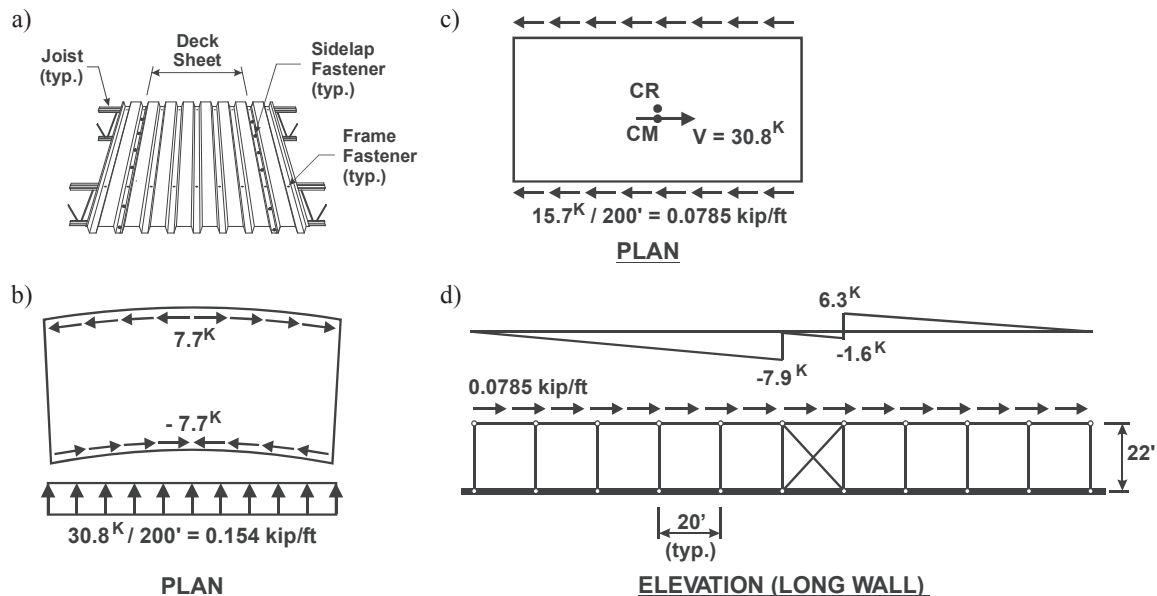


Fig. 3. (a) Steel deck panels, (b) axial loads in beams acting as diaphragm chord members, (c) force transfer from the diaphragm to the edge beam under seismic loads in the long direction, and (d) edge beams acting as collector elements under seismic loads acting in the long direction.

Similarly, an expression for the period was proposed by Medhekar (1997) and validated by shake table testing by Tremblay and Bérair (1999) and Tremblay et al. (2000). A longer building period can often provide for much lower seismic design forces based on the uniform hazard spectrum that is now required for design. Tremblay and Rogers (2005) illustrated that the use of this extended period of vibration can lead to significant savings in terms of the cost of the lateral load carrying system, mainly because of the lower design loads. Studies by Naman and Goodno (1986), Dubina et al. (1997), Tena-Colunga and Abrams (1996), Tremblay and Stierner (1996) and Tremblay et al. (2002), among others, also showed that the calculated seismic forces can be reduced by incorporating the diaphragm flexibility. Using the elastic deflections of the bracing bents and the diaphragm, δ_B and δ_D in Figure 4a, one can estimate the fundamental period of the structure with (ASCE 41, 2006):

$$T \approx \sqrt{\left(\frac{W}{V}\right)(0.10\delta_B + 0.078\delta_D)} \quad (4)$$

where δ_B and δ_D are in inches. When compared to the original equation found in ASCE 41, the ratio W/V has been incorporated in Equation 4 because the expression requires the use of deflections due to a horizontal load equal to the effective seismic weight, W . For the design presented herein, the computed fundamental period from Equation 4 is 1.12 s, which is much longer than the value assumed in design (0.32 s). For drift calculations, one uses the load obtained from

Equation 1 with this longer period, as permitted in ASCE 7-05. Figure 4b illustrates the significant reduction in design loads with $V(T=1.12 \text{ s}) = 0.0167W = 9.9$ kips, which is 32% of the seismic load determined using the period $T = C_u T_a$. Under this reduced lateral load, the elastic deflections δ_B and δ_D are respectively equal to 0.035 in. and 0.22 in. The design story drift can then be determined as $\Delta = (5.0)(0.035 + 0.22)/1.0 = 1.28$ in., giving an inter-story drift of 0.49%, which is less than the limit of 2% typically applicable to this type of building. One can check that for this structure P-delta effects are small and can be considered negligible.

In the structure as designed, the strength of the diaphragm is not related to the actual capacity of the vertical bracing system and there is no guarantee that the system will behave as intended under the design earthquake, i.e. with inelastic response developing in the bracing members that have been specially sized and detailed to undergo significant inelastic response without fracture. For instance, Figure 4c shows the diaphragm shear flow along the perimeter beams on the short exterior walls on grid lines A and F that was considered for the design of the roof diaphragm. The corresponding axial loads in the edge beams acting as collectors are also given in the figure (maximum = 8.30 kips). In Figure 4d, the same shear flow and beam axial loads are given when the braces reach their expected axial compression and tension strength P_{exp} and T_{exp} as determined earlier. The second set of forces is much greater, more than 7.0 times the forces used in design. However, considering that an R factor of 6.0 was used in the

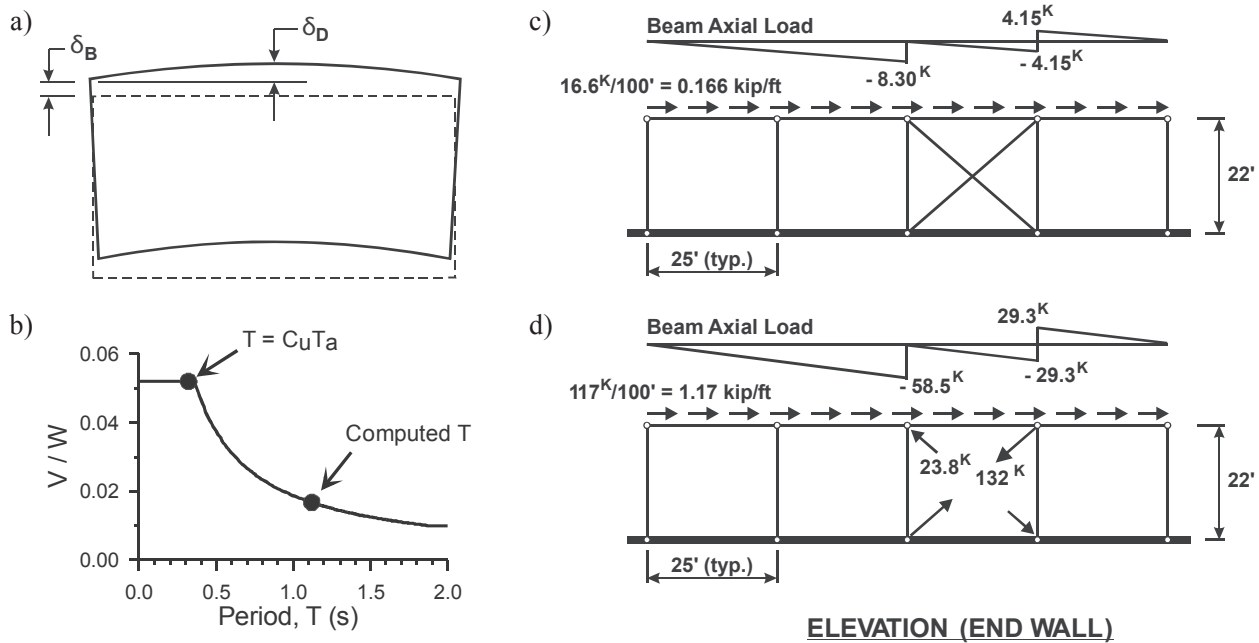


Fig. 4. (a) Bracing bent and roof diaphragm deformations, (b) variation of the seismic load with the period, (c) axial loads in edge beams acting as collector elements along the short walls under $V = 30.8$ kips, and (d) axial loads in edge beams acting as collector elements along the short walls upon brace yielding.

Table 1. Summary of the Design Parameters for the Building Examples				
Parameters	Boston area $S_s = 0.30, S_1 = 0.07, T_L = 6.0$ s SDC B $W = 593$ kips		Los Angeles area $S_s = 1.70, S_1 = 0.60, T_L = 12.0$ s SDC D $W = 453$ kips	
	SLRS	SCBF	OCBF	SCBF
R	6.0	3.25	6.0	3.25
$C_u T_a$ (s)	0.32	0.32	0.28	0.28
V (kips)	30.8	56.9	85.6	158
ρ	1.0	1.0	1.0	1.3
Brace design	T/C	T/O	T/C	T/O
Brace section	HSS 3×3×3/16	L2½×2×5/16	HSS 4×4×¼	2L3×3×7/16
T_{exp} (kips)	132	71.3	236	262
P_{exp} (kips)	23.8	—	75.1	37.5
S_u (kip/ft)	0.166	0.307	0.462	1.11
Deck sheets	22 ga.	22 ga.	22 ga.	16 ga.
Frame fasteners	36/3	36/4	36/4	36/4
Screws/joist spacing	2	3	2	11
G' (kips/in.)	12.4 (F)	22.8 (R)	25.1 (F)	102 (R)
T from Eq. 4 (s)	1.12	1.11	0.71	0.56
δ/h_s (%)	0.49	0.53	1.67	1.43
Note: (F) = flexible diaphragm, (R) = rigid diaphragm				

calculation of the design seismic load V , it is unlikely that such a high force demand will develop during the design earthquake. The resistance of the foundation to overturning uplift can also limit the forces delivered to the bracing bent. AISC (2006) provides an example illustrating how foundation uplift can be included in this calculation. Nevertheless, it is highly probable that forces in excess of the capacity of the perimeter beams and the diaphragm as designed will be reached in future earthquakes, which may cause severe damage and, possibly, failure of the diaphragm structure and collapse of the roof gravity system that it laterally supports. Caution should therefore be exercised by designers in the selection of the diaphragm and its chords and collectors to ensure that proper response will be achieved.

As mentioned, the 2005 NBCC in Canada states that diaphragms must be designed not to yield. They must therefore be provided with sufficient strength to match the expected strength (actual capacity) of the vertical system. The design forces need not exceed, however, the forces corresponding to elastic response, i.e., forces determined with the seismic response modification coefficients equal to 1.0. Had this concept been applied to the example building, the required shear strength for the roof diaphragm would have been $S_u = (6.0)(16.6 \text{ kips})/100 \text{ ft} = 1.0 \text{ kip/ft}$. In this case, the diaphragm design would call for a much stronger configuration such as 0.0474-in.-thick (18 ga.) deck panels connected

along the side-lap with eight screws per joist spacing and pins arranged in a 36/5 pattern.

The example building could have been designed using tension-only (T/O) bracing of the OCBF category. The main differences between the SCBF and OCBF design solutions are summarized in Table 1. An R factor of 3.25 would have been considered for the OCBF design, leading to a base shear force $V = 56.9$ kips. For this system, L2×2½×5/16 single-angle braces made of ASTM A36 steel ($A = 1.32 \text{ in.}^2$, $F_y = 36 \text{ ksi}$) would have represented an acceptable solution [$\phi T_n = 42.8 \text{ kips} > 40.9 \text{ kips} = (0.54)(56.9/\cos(41.3^\circ))$]. The required shear resistance for the diaphragm, without consideration of capacity design, would have been equal to 0.307 kip/ft [(0.54)(56.9)/100]. Deck panels 0.0295-in.-thick (22 ga.) are found adequate with three side-lap screws per joist span and pins installed on a 36/4 pattern (12 in. on center). Such a diaphragm has a factored shear resistance $\phi_d S_n = 0.315 \text{ kip/ft}$ and a shear stiffness, G' , of 22.8 kip/in. For angles, $R_y = 1.5$ in AISC *Seismic Provisions* and the expected brace tensile strength $T_{exp} = 71.3$ kips. Had capacity design principles been adopted, the design force for the diaphragm would have been equal to 0.535 kip/ft, as governed by tension yielding of the braces. This value is nearly half that required for the more ductile SCBF system. This difference is attributed to the fact that tension/compression bracing is required for SCBFs. The size of the braces is governed by

the compression capacity requirement; since the braces are generally long and slender due to the height of single-story structures they possess significant overstrength resulting from the large difference between tension and compression capacities. When applying capacity design principles, this large overstrength impacts on the forces that will be delivered to the components in the SLRS, which need to remain essentially elastic.

Building Design Example (Los Angeles)

The example building is designed for the Los Angeles area assuming the same site class (D), Occupancy Category (II) and importance factor ($I = 1.0$). Table 1 gives the key design parameters for the SCBF and OCBF designs. At this site, $F_a = 1.0$ and $F_v = 1.5$, which result in design spectral accelerations $S_{DS} = 1.13$ g and $S_{D1} = 0.60$ g. In view of these higher design spectral accelerations, the building must be assigned to a more severe Seismic Design Category D. The C_u factor for the period is also limited to 1.4, giving a design period $C_u T_a = 0.28$ s. There is no roof snow load in Los Angeles, thus the seismic weight W reduces to 453 kips. The base shear for the SCBF and OCBF categories are, respectively, equal to 85.6 kips and 158 kips. For the SCBF system, tension/compression brace design is selected and a redundancy factor $\rho = 1.0$ can be used despite the more critical SDC because removal of one brace results in less than a 33% reduction in lateral strength, and an extreme torsional irregularity condition does not exist. This is not the case when a tension-only bracing system is adopted for the OCBF example; $\rho = 1.3$ must be used for this design.

Rigid diaphragm behavior is assumed for the distribution of the lateral loads, and $0.54 V$ is considered to be resisted along the bracing bent. The selected braces and brace expected tensile and compressive strengths are given in Table 1. The design shear flow for the diaphragm and the properties of the selected roof deck system are also given in Table 1. For the SCBF system ($R = 6.0$), the S_u value is 0.456 kip/ft [(0.54)(85.6) kips/100 ft] and a 22 ga. (0.0295 in.) deck design with 36/4 frame fastener pattern and eight side-lap screws per joist span is selected: $\phi_d S_n = 0.489$ kip/ft and $G' = 25.1$ kips/in. For this structure, a shear flow of 2.34 kips/ft is associated with the braces reaching their expected tensile and compressive strengths. This is 5.1 times the design value, indicating that the system may not perform as intended when the building is subjected to strong seismic ground shaking. For the OCBF system ($R = 3.25$), $S_u = 1.11$ kips/ft [(1.3)(0.54) (158) kips/100 ft]. This higher force demand requires much heavier diaphragm design: 16 ga. (0.0598 in.) deck sheets with closely spaced side-lap fasteners. In this OCBF design, back-to-back angles were selected for the braces. Even if tension-only braces are assumed in design, this type of brace still possesses compressive strength that should be

considered in capacity design ($P_{exp} = 37.5$ kips with $KL/r = 221$). The expected shear flow when the braces reach their tensile and compressive strengths is therefore equal to 2.25 kips/ft, approximately twice the design value according to the current seismic provisions. Although less pronounced than the building designs for the Boston area, both the SCBF and OCBF systems in Los Angeles have computed fundamental periods longer than the values assumed in design.

EFFECT OF DIAPHRAGM FLEXIBILITY ON BUILDING PERIOD OF VIBRATION

In theory, accounting for the in-plane flexibility of the roof diaphragm may lead to more economical design solutions for single-story steel buildings, as was illustrated in the design example. However, recent ambient vibration studies on buildings of this type at the University of British Columbia and the University of Sherbrooke have shown that the period of vibration may be shorter than that predicted by analytical means (Paultre et al., 2004; Lamarche, 2005). The possible stiffening effect of non-structural roofing components diminishes to some extent the period lengthening effect of the roof deck diaphragm (Yang, 2003; Mastrogiuseppe et al., 2008), but this stiffening effect was found to be limited and not large enough to explain the differences between field measurements and analytical predictions. One drawback to the previous ambient vibration tests is that the building periods were obtained from the measurements of small building movement caused by relatively calm wind conditions. It is believed that roof diaphragms exhibit a stiffer response under such low amplitude loading because of the inherent friction resistance of the deck connections and the partial prevention of shear deformations from warping of the deck sheets at their ends due to the overlapping of the adjoining sheets. This represents a stiffer condition compared to the single sheet case that was considered in the development of the Steel Deck Institute (SDI) stiffness equations (Luttrell, 2004), which could also contribute to the observed differences between field tests and predictions (Figure 5). In this figure, the periods computed using Equation 4 are compared to those obtained from an empirical expression proposed by Lamarche (2005) based on field test data. The values $0.05h_n$ and $0.025h_n$ (where h_n = building height in m) are the predictor equations for the period of vibration of a concentrically braced frame based on the 2005 NBCC.

A more recent investigation that compared the results of ambient vibration measurements of a 74,100 ft² (approximately 23 ft in height, 300 ft by 234 ft in plan) single-story commercial building located in Magog, Quebec, with a 3D SAP 2000 building model (Figure 6a) showed that to obtain the measured periods (Figure 6b) a rigidly connected frame structure with infinitely stiff braces and continuous diaphragm panels would need to be assumed instead of the more common pin

connections and standard three- to four-span deck panels as would normally be used (Tremblay et al., 2008a, 2008a b). Analysis of the building accounting for the in-plane flexibility of the diaphragm and using assumptions commonly made in practice regarding member end fixity, brace stiffness and panel lengths led to a period of vibration of 1.11 s, significantly longer than the 0.39 s that was measured. In comparison, the NBCC would require that the period T_a be a maximum of 0.35 s, i.e. $T_a \leq 0.05 h_n$, which is in line with the ambient vibration result. A question remains as to whether this NBCC defined period should be allowed to be increased based on dynamic analyses of building models.

Preliminary large-scale dynamic tests were carried out at École Polytechnique of Montreal in the summer of 2007 on three diaphragm test specimens approximately 24 ft by 69 ft in plan (Figure 7). The test specimens were constructed using the popular 0.0295-in.-thick (22 ga.) 1½-in.-deep wide-rib deck profile with flutes spaced 6 in. on center. Nail frame connections and screw side-lap connections were used throughout. The test specimens represent a large portion of a building’s roof, including the roof structure and roof

mass. The frame was mounted on rockers and two 220-kip high-performance dynamic actuators were used to apply the load along both edges of the supporting steel frame, thus representing the ground motion forces being transmitted to the roof by the vertical braces or the walls at the diaphragm ends. The intent was to vibrate the diaphragm at increasing amplitudes to identify whether a decrease of the in-plane shear stiffness would occur and if so by what extent. Information of this nature could be used to determine whether the period expressions defined in model building codes could be modified to account for diaphragm behavior under earthquake induced vibrations. Furthermore, the impact of end panel overlaps on the in-plane stiffness was investigated by testing diaphragm specimens both with and without end-laps. A variety of dynamic tests ranging from low amplitude basic white noise vibrations and harmonic signals to inelastic loading signals were used. In the tests, the influence of the loading amplitude on the period was assessed through all of the above dynamic loading protocols (Tremblay et al. 2008b). The inelastic response of the different diaphragm designs was also examined.

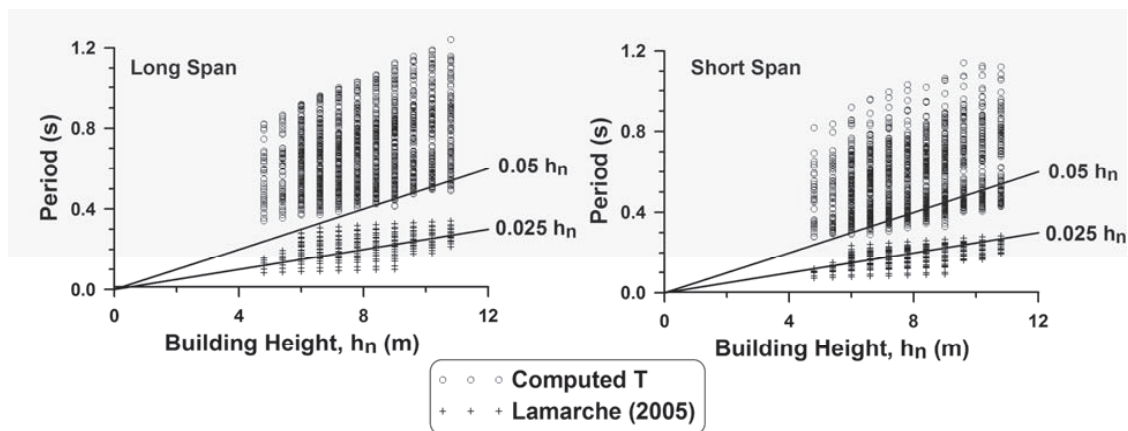


Fig. 5. Analytically computed periods and periods predicted using the empirical expression based on field test measurements (Tremblay and Rogers, 2005).

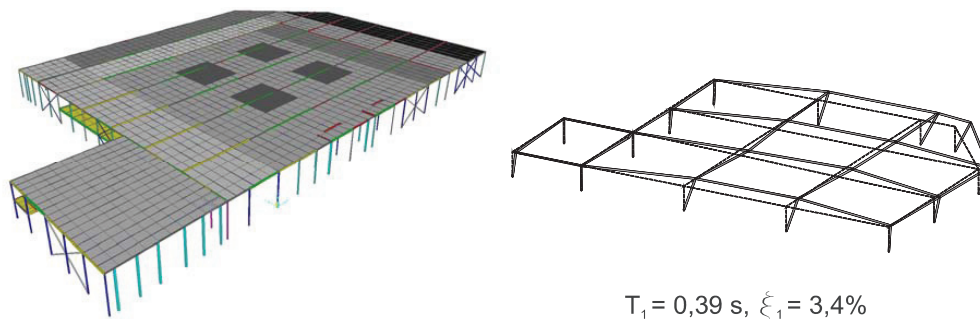


Fig. 6. (a) 3-D model of the structure and (b) measured fundamental mode and natural frequency (Tremblay et al., 2008a).

Figure 8 shows the variation of the fundamental period of vibration of a steel diaphragm specimen with the amplitude of dynamic excitation in terms of absolute acceleration at mid-span. Several white noise (random vibration signal with flat power spectral density used to obtain the frequency response) tests for which the displacement amplitude of the cycles was systematically increased were used to produce this figure. The plot shows that the period rapidly lengthens (flexibility increases) as the acceleration level exceeds that observed in field ambient vibration tests (typically less than 0.002 g). The higher initial stiffness is attributed to the lack of slip at the side-lap and deck-to-frame connections under low amplitude loading. Similarly, specimens submitted to a sine sweep protocol at increasing amplitudes showed that the resonant frequency of the diaphragm did not remain constant; rather the specimen became less stiff (resonant

frequency decreased) as larger amplitude cycles were applied. The results of the two loading protocols illustrate that the stiffness and natural frequency of a diaphragm are dependent on the level of deformation demand.

DUCTILE DIAPHRAGM DESIGN AND BUILDING ANALYSES

It may also be possible to rely on the inelastic behavior of the diaphragm in design; that is, specify the roof deck diaphragm to be the fuse element in the SLRS instead of the vertical braces (Figure 1b). The shear capacity of the diaphragm can be adjusted by changing the connector spacing and panel thickness, thus leading to a capacity force that is only marginally higher than the code calculated seismic force. This could lead to a less expensive seismic load

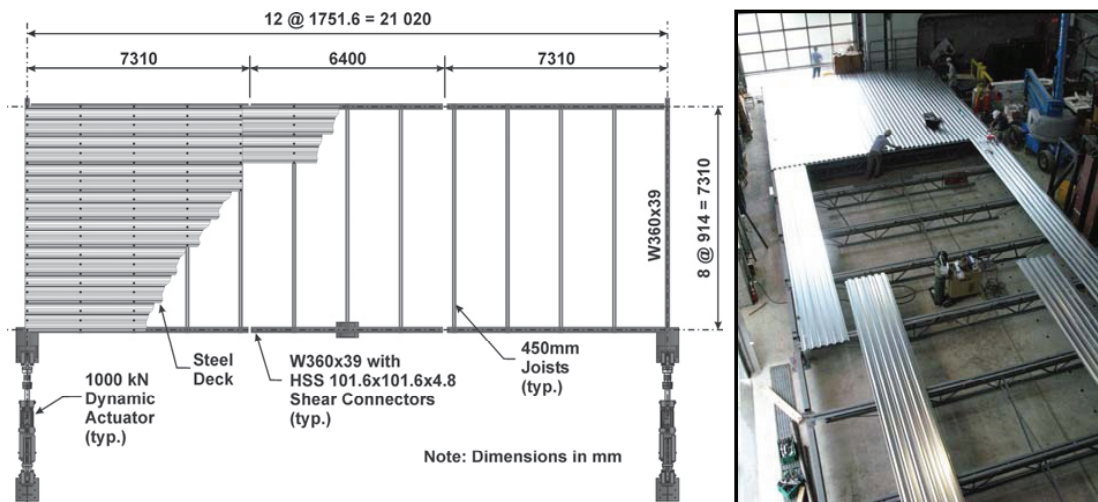


Fig. 7. Large-scale dynamic diaphragm test setup: (a) plan view and (b) during construction.

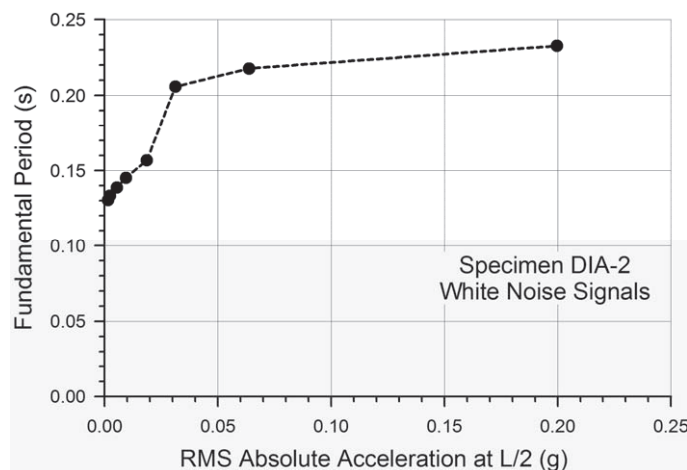


Fig. 8. Change in diaphragm period with white noise loading amplitude (adapted from Tremblay et al., 2008b).

resisting system and simpler detailing requirements for the braces and their connections because they would be expected to remain in the elastic range (Tremblay and Rogers, 2005). Experimental and analytical studies of the inelastic performance of diaphragms are summarized in the work of Tremblay et al. (2004) and Essa et al. (2003) (Figures 9 and 10). It was shown by means of testing that steel deck made of 0.0295-in.-thick (22 ga.) and 0.0358-in.-thick (20 ga.) sheets and connected with mechanical fasteners could undergo some limited cyclic inelastic deformations. It was noted, however, that relying on this inelastic behavior in the design of actual roof diaphragms could result in concentrations of large amplitude inelastic deformations in localized regions of the roofs, i.e., along braced wall lines, which could lead to undesirable diaphragm failures. This aspect could not be addressed in the past test programs due to the limited size of the diaphragm specimens (12 ft by 20 ft) and the type of displacement controlled loading that was used. Tests under dynamically applied loading on larger diaphragms were needed to properly assess the shear stiffness, distribution

of forces and inelastic deformations in metal roof deck diaphragms under actual seismic conditions, which lead to the tests illustrated in Figure 7.

The impact of capacity design provisions and period limitations on the seismic design of low-rise steel buildings was investigated (Tremblay and Rogers, 2005). Several design strategies were examined, including design without a capacity-based approach, capacity design with ductile bracing components, and capacity design assuming the cold-formed steel roof diaphragm acts as the main energy dissipation element in the SLRS. The effects of relaxing the period limitations and the capacity design forces for the roof diaphragm were also considered. A parametric study was carried out to evaluate the impact of the different strategies on the cost of the seismic load resisting systems (Figure 11). The building geometry, the seismic hazard level, the bracing configuration and the level of ductility were varied in this study. The results show that capacity design provisions have a significant impact on the structure, especially when tension-compression bracing is used. Substantial savings

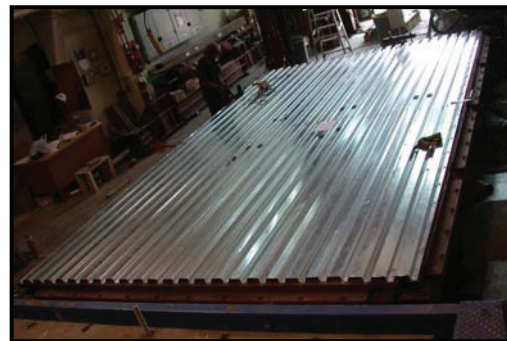
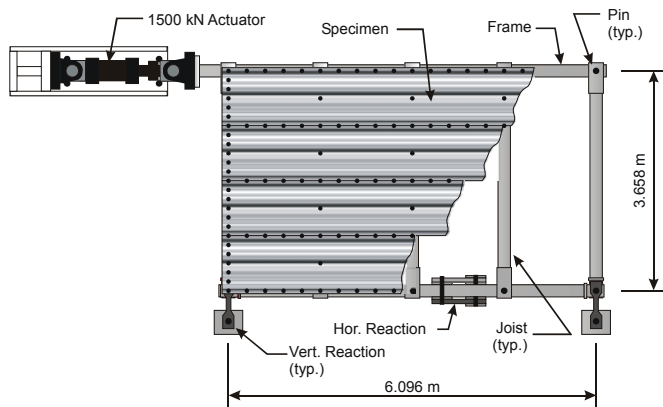


Fig. 9. Quasi-static diaphragm test specimen setup (Essa et al., 2003; Tremblay et al., 2004).

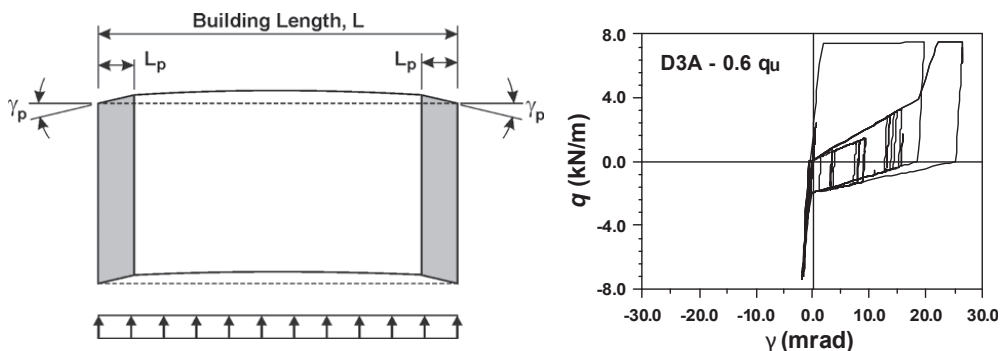


Fig. 10. Weak diaphragm design—concentration of inelastic design (adapted from Tremblay et al., 2004; Tremblay and Rogers, 2005).

could be realized with the use of a period obtained from methods of mechanics that incorporate diaphragm flexibility. Additional solutions for decreasing the cost of the structure also include relaxation of the capacity design provisions by reducing the upper limit on diaphragm forces or selecting the diaphragm as the main energy dissipating system. Nonlinear dynamic analyses of a limited number of these structures (Figure 12) were carried out using the RUAUMOKO (Carr, 2004) computer program. The roof diaphragm was modeled as a deep horizontal plane truss. A Stewart hysteretic model was selected for the diagonal roof truss members in order to reproduce the cyclic inelastic response measured for the screwed-nailed diaphragm system as described by Tremblay et al. (2004). The software and hysteretic model did not allow for the simulation of the strength degradation, which was observed during testing. The response of the example building was examined under one record from the 1994

Northridge earthquake scaled to match the design spectrum for Vancouver, Canada.

The time history response of the drift due to brace deformation (δ_B) and total building deformation ($\delta_B + \delta_D$) for three design scenarios is provided in Figure 13: (a) protected diaphragm (brace fuse), where $T_a = 0.05 h_n$; (b) weak (fuse) diaphragm, where $T_a = 0.05 h_n$; and (c) weak (fuse) diaphragm, where $T_a = T$ of the building accounting for the full diaphragm flexibility. Note: a protected diaphragm is selected so that its shear and flexural strength exceed the forces that correspond to the expected strength of the brace (fuse) elements; a weak diaphragm is selected to act as the inelastic fuse and thus has a strength that only needs to meet the building code seismic force. In all cases, the building experienced a maximum roof deformation that is below the prescribed limit of $2.5\% h_n$. A large portion of the overall story drift occurred in the bracing members due to

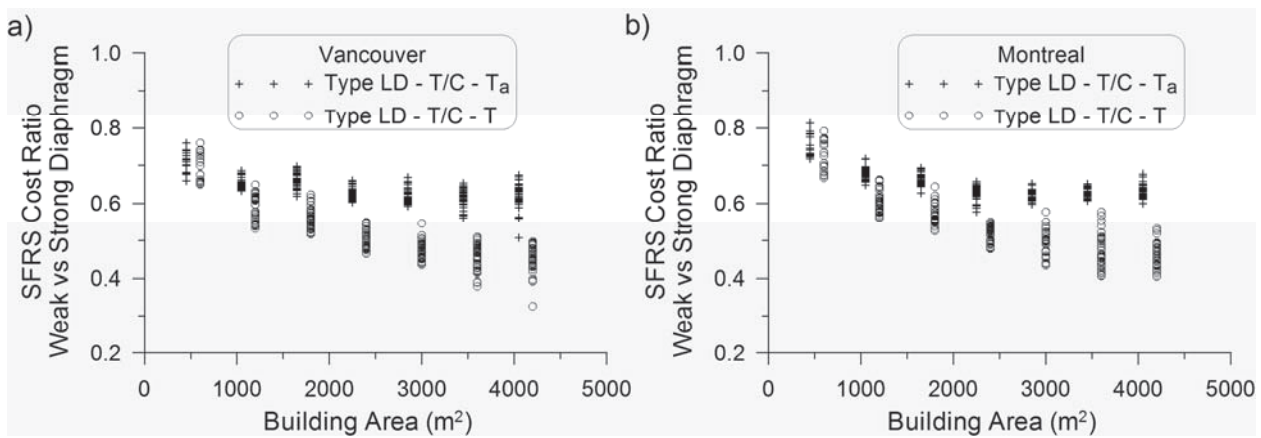


Fig. 11. SLRS cost ratios for (a) Vancouver and (b) Montreal (adapted from Tremblay & Rogers, 2005).

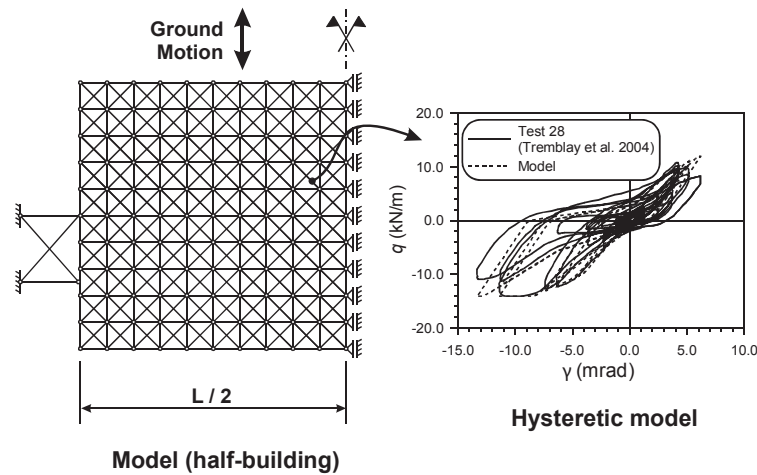


Fig. 12. Building model and Stewart hysteretic element (Tremblay and Rogers, 2005).

yielding; the in-plane diaphragm displacements were much less because this structural element was protected from entering into the inelastic range through implementation of the capacity design approach. After the strong motion segment of the record which ended at 14 s, significant deformations still developed in the bracing bents because the bracing members had been permanently elongated and were not able to offer any lateral resistance near the zero deformation position. As also expected from the design assumptions, plastic deformation was not observed in the roof diaphragm. In contrast, for the buildings in which the diaphragm was designed to be the fuse element, the peak roof displacement remained nearly the same but the inelastic demand switched from the bracing members to the roof diaphragm. The peak plastic demand in the roof, γ_p , is in accordance with the recommended permissible value of 10 mrad ($= 10 \times 10^{-3}$ rad) of shear deformation for nailed-screwed decks (Essa et al., 2003).

It must be realized that this is a single example building subjected to only one ground motion and that the performance can vary significantly with ground motions and building dimensions. In particular, inelastic demand can be very sensitive to design and modeling assumptions, as well as loading conditions. In addition, this study was limited to uniform rectangular structures and it is expected that higher ductility demand can be induced in structures with irregularities or a non-symmetric footprint, as often encountered in practice. Nonetheless, the

results show that allowing the inelastic response of the structure to take place in the roof diaphragm made of thin steel sheets can result in an acceptable overall seismic performance. However, variation in strength and localized demand may result in excessive plastic deformations of the diaphragm, and further studies are needed before this design approach can be adopted.

CONCLUSIONS

Seismic provisions of modern building codes now rely on capacity design procedures to provide a desired hierarchy of material yielding in the SLRS and better control of the inelastic response of a structure. For single-story steel buildings with concentrically braced steel frames, inelastic response is typically concentrated in the diagonal bracing members of the braced bays. Other components along the lateral load path, such as the roof diaphragm, including its chords and collectors, must be designed to resist the forces that will develop upon yielding in the vertical components of the seismic load resisting system. Current seismic provisions in the U.S. for buildings with $R > 3$ do not result in entirely consistent design between the steel framing and the roof diaphragm. If full capacity design principles were required, much higher design forces would need to be applied to the diaphragm. For simple metal roof deck design, an SCBF example studied herein for the Boston area showed that the roof deck would need to be increased from a thickness of 0.0295 in. to 0.0474 in. (22 ga. to 18 ga.) with a more closely spaced fastener arrangement. Similar results were obtained for the other cases that were studied. Alternative design approaches that reduce the force demand on the diaphragm are being evaluated. The designer could possibly take advantage of the in-plane flexibility of the roof diaphragm, as this is currently permitted in ASCE 41 for the seismic retrofit of existing structures. Parametric studies performed for Canadian seismic conditions have shown that there is a significant potential for savings if the period from dynamic analysis is used in design. However, field ambient vibration test data seem not to support this approach and caution must be exercised before using the period prediction that accounts for roof diaphragm flexibility in seismic design. It may also be possible to allow for inelastic deformation in the roof diaphragm, instead of the diagonal bracing members. For thin deck sheets, these deformations can develop in the form of bearing or tearing in the vicinity of the deck fasteners. Deformation capacity is however limited and means must be taken to ensure that it will be properly distributed over the diaphragm area so that no concentration will develop that can lead to failure of the diaphragm system, i.e., a loss in the ability to transfer lateral forces to the bracing bents and a possible decrease in the effectiveness of the deck panels to laterally brace the supporting joist and beam structure. Research projects have been undertaken to examine the potential use of these two alternative design strategies.

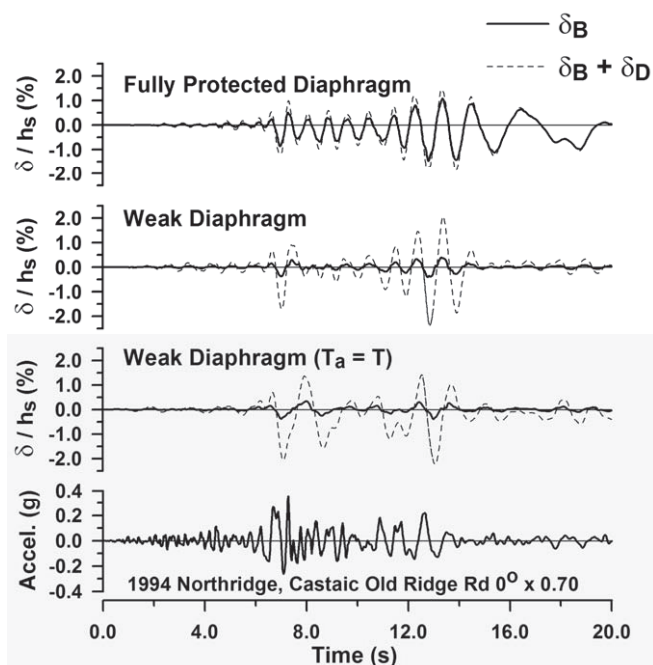


Fig. 13. Time histories of the story drifts for various design scenarios under a site-representative earthquake ground motion (adapted from Tremblay and Rogers, 2005).

ACKNOWLEDGMENTS

The authors would like to acknowledge the support provided by the Canada Foundation for Innovation, the Canadian Sheet Steel Building Institute, the Canam Group Inc., WSB Consulting Structural Engineers, RJC Consulting Engineers, the Vancouver Steel Deck Diaphragm Committee, the Steel Deck Institute and Hilti Limited. Additional funding for this research was provided by the Natural Sciences and Engineering Research Council of Canada and the Funds for Research in Nature and Technologies of the Province of Quebec. The authors thank research assistants Camelia Nedisan, Charles-Philippe Lamarche, John Franquet and Robert Massarelli, as well as Patrice Belanger, technician at École Polytechnique, for their valuable assistance during the large-scale diaphragm test program.

REFERENCES

- AISC (2005a), *Seismic Provisions for Structural Steel Buildings*, ANSI/AISC 341-05, American Institute of Steel Construction Inc., Chicago, IL.
- AISC (2005b), *Specification for Structural Steel Buildings*, ANSI/AISC 360-05, American Institute of Steel Construction Inc., Chicago, IL.
- AISC (2006), *Seismic Design Manual*, American Institute of Steel Construction Inc. and The Structural Steel Educational Council, Chicago, IL.
- ASCE 7 (2005), *Minimum Design Loads for Buildings and other Structures*, including Supplements Nos. 1 and 2, ASCE/SEI 7-05, American Society of Civil Engineers, Reston, VA.
- ASCE 41 (2006), *Seismic Rehabilitation of Existing Buildings*, American Society of Civil Engineers, Reston, VA.
- AISI (2004), *Supplement 2004 to the North American Specification for the Design of Cold-Formed Steel Structural Members*, 2001 ed., American Iron and Steel Institute, Washington, DC.
- Carr, A.J. (2004), RUAUMOKO, Inelastic Dynamic Analysis Program, Dept. of Civil Engineering, University of Canterbury, New Zealand.
- CSA (2005), *Supplement No. 1 to CAN/CSA-S16-01 Limit States Design of Steel Structures*, CSA-S16s1-05, Canadian Standard Association, Toronto, ON, Canada.
- Dubina, D., Zaharia, R. and Georgescu, M. (1997), "Stress Skin Design of Single-Story Steel Buildings in Seismic Areas," *Proceedings of the STESSA 97 Conference on the Behaviour of Steel Structures in Seismic Areas*, Kyoto, Japan, 1997, pp. 426–433.
- Essa, H.S., Tremblay, R. and Rogers, C.A. (2003), "Behavior of Roof Deck Diaphragms under Quasistatic Cyclic Loading," *Journal of Structural Engineering*, ASCE, Vol. 129, No. 12, pp. 1658–1666.
- Lamarche, C.-P. (2005), "Étude expérimentale du comportement dynamique des bâtiments de faible hauteur en acier," M.Sc.A. Thesis, Department of Civil Engineering, University of Sherbrooke, Sherbrooke, QC, Canada.
- Luttrell, L. (2004), *Diaphragm Design Manual*, 3rd ed., including Appendix VI Addendum November 2006, Publication No. DDMO3, Steel Deck Institute, Fox River Grove, IL.
- Mastrogiuseppe, S., Rogers, C.A., Nedisan, C.D. and Tremblay, R. (2008), "Influence of Non-structural Components on Roof Diaphragm Stiffness and Fundamental Periods of Single-Storey Steel Buildings," *Journal of Constructional Steel Research*, Vol. 64, No. 2, pp. 214–227.
- Medhekar, M.S. (1997), "Seismic Evaluation of Steel Buildings with Concentrically Braced Frames," Ph.D. Thesis, Department of Civil and Environmental Engineering, University of Alberta, Edmonton, AB, Canada.
- Naman, S.K. and Goodno, B.J. (1986), "Seismic Evaluation of a Low-Rise Steel Building," *Engineering Structures*, Vol. 8, No. 1, pp. 9–16.
- NRCC (2005), *National Building Code of Canada*, 12th ed., National Research Council of Canada, Ottawa, ON, Canada.
- Paultre, P., Proulx, J., Ventura, C., Tremblay, R., Rogers, C., Lamarche, C.-P. and Turek, M. (2004), "Experimental Investigation of Low-Rise Steel Buildings for Efficient Seismic Design," *Proceedings of the 13th World Conference on Earthquake Engineering*, Vancouver, BC, Canada, Paper No. 2919.
- Tena-Colunga, A. and Abrams, D.P. (1996), "Seismic Behavior of Structures with Flexible Diaphragms," *Journal of Structural Engineering*, ASCE, Vol. 122, pp. 439–445.
- Tremblay, R. (2005), "Canadian Seismic Design Provisions for Steel Structures," *Proceedings of the 2005 North American Steel Construction Conference*, Montreal, QC, Canada, AISC, Chicago, IL, 12 pp.
- Tremblay, R. and Stiemer, S.F. (1996), "Seismic Behavior of Single-Storey Steel Structures with Flexible Diaphragm," *Canadian Journal of Civil Engineering*, Vol. 23, pp. 49–62.
- Tremblay, R. and Bérair, T. (1999), "Shake Table Testing of Low-Rise Steel Buildings with Flexible Roof Diaphragms," *Proceedings of the 8th Canadian Conference on Earthquake Engineering*, Vancouver, BC, Canada, pp. 585–590.

- Tremblay, R., Bérair, T. and Filiatrault, A. (2000), "Experimental Behaviour of Low-Rise Steel Buildings with Flexible Roof Diaphragms," *Proceedings of the 12th World Conference on Earthquake Engineering*, Auckland, New Zealand, Paper No. 2567.
- Tremblay, R. and Rogers, C.A. (2005), "Impact of Capacity Design Provisions and Period Limitations on the Seismic Design of Low-Rise Steel Buildings," *International Journal of Steel Structures*, Vol. 5, No. 1, pp. 1–22.
- Tremblay, R., Rogers, C.A. and Nedisan, C. (2002), "Use of Uniform Hazard Spectrum and Computed Period in the Seismic Design of Single-Storey Steel Structures," 7th U.S. National Conference on Earthquake Engineering, Boston, MA, Paper No. 195.
- Tremblay, R., Rogers, C., Martin, É. and Yang, W. (2004), "Analysis, Testing and Design of Steel Roof Deck Diaphragms for Ductile Earthquake Resistance," *Journal of Earthquake Engineering*, Vol. 8, No. 5, pp. 775–816.
- Tremblay, R., Nedisan, C., Lamarche, C.-P. and Rogers, C.A. (2008a), "Periods of Vibration of a Low-Rise Building with a Flexible Steel Roof Deck Diaphragm," 5th International Conference on Thin-Walled Structures, Brisbane, Australia, pp. 615–622.
- Tremblay, R., Rogers, C.A., Lamarche, C.-P., Nedisan, C.D., Franquet, J., Massarelli, R. and Shrestha, K.M. (2008b), "Dynamic Seismic Testing of Large Size Steel Deck Diaphragms for Low-Rise Building Applications," 14th World Conference on Earthquake Engineering, Beijing, China, Paper No. 05-05-0066.
- Yang, W. (2003), "Inelastic Seismic Response of Steel Roof Deck Diaphragms Including Effects of Non-Structural Components and End Laps," M.A.Sc. Thesis, Department of Civil, Geological and Mining Engineering, École Polytechnique, Montreal, QC, Canada.

Notes on the Impact of Hole Reduction on the Flexural Strength of Rolled Beams

LOUIS F. GESCHWINDNER

ABSTRACT

The use of $\phi = 0.9$ and $\Omega = 1.67$ with the provisions in Section F13.1 of AISC 360-05 (AISC, 2005) to account for the reduction in flexural strength for a beam with holes in the tension flange has been questioned several times since the publication of the *Specification for Structural Steel Buildings* in 2005. The intent of this paper is to review and provide justification for the use of the resistance/safety factors within the 2005 *Specification* provisions for the impact on flexural strength of holes in the tension flange.

Keywords: bolt holes, tension flange, resistance factors, safety factors.

INTRODUCTION

The use of $\phi = 0.9$ and $\Omega = 1.67$ with the provisions in Section F13.1 of AISC 360-05 (AISC, 2005) to account for the reduction in flexural strength for a beam with holes in the tension flange has been questioned several times since the publication of the *Specification for Structural Steel Buildings* in 2005. The research basis for the 2005 provisions originated from a report by Dexter et al. (2002). Their report includes a proposed formulation for the limits on when the impact of the holes must be considered and how the strength should be determined in those cases; however, the report does not address the appropriate resistance or safety factors to be used. The intent of this paper is to review and provide justification for the use of the resistance/safety factors within the 2005 *Specification* provisions for the impact on flexural strength of holes in the tension flange.

THEORY

AISC 360-05 Equation F13-1 is intended to present a simple yet reasonable approach to account for holes in the tension flange of beams. Although not presented this way in the *Specification*, Equation F13-1 can be rewritten in terms of critical stress, always less than F_y , times the full elastic section modulus as illustrated by the following two equations:

$$M_n = F_{cr} S_x \quad (1)$$

$$F_{cr} = \left[\frac{F_u A_{fn}}{Y_t F_y A_{fg}} \right] F_y \quad (2)$$

Because ASTM A36 and A992 steels meet the limit given in Section F13 for $Y_t = 1.0$, and the term

$$\left[\frac{F_u A_{fn}}{F_y A_{fg}} \right]$$

in Equation 2 is always less than 1.0 if this check is applicable, the critical stress is always less than the yield stress. Therefore, use of the resistance/safety factors associated with yielding (i.e., $\phi = 0.9$, $\Omega = 1.67$) appears to be warranted.

To examine this interpretation more closely, three models are developed for determining flexural strength when holes are present in the tension flange of W-shapes.

Model 1

For ease of calculation, the W-shape is modeled with holes in both the tension and compression flanges. The flange forces are taken as the rupture force and the web is assumed to be yielding throughout. Thus,

$$M_n = F_u A_{fn} (d - t_f) + F_y \left[Z_x - A_{fg} (d - t_f) \right] \quad (3)$$

If the ratio of flange-rupture strength to flange-yield strength, which is always less than 1.0, is taken as

$$\Psi = \frac{F_u A_{fn}}{F_y A_{fg}} \quad (4)$$

Equation 3 can be stated as

$$M_n = F_y Z_x - (1 - \Psi) (F_y A_{fg}) (d - t_f) \quad (5)$$

Louis F. Geschwindner, Ph.D., P.E., Vice President, American Institute of Steel Construction, 1 E. Wacker Drive, Suite 700, Chicago, IL, 60601. E-mail: geschwindner@aisc.org

Since this equation represents a rupture failure mode, the resistance factor, $\phi = 0.75$, and safety factor, $\Omega = 2.00$, are used to determine the available strength.

When there is no reduction for the presence of holes, $\Psi = 1.0$, Equation 5 reduces to $M_n = F_y Z_x$. Thus, the design strength is $\phi M_n = 0.75 F_y Z_x$ and the allowable strength is $M_n / \Omega = 0.5 F_y Z_x$. Similarly, the provisions of Section F13, as represented by Equations 1 and 2, reduce to $M_n = F_y S_x$. Thus, the design strength, using $\phi = 0.9$, becomes $\phi M_n = 0.9 F_y S_x$ and the allowable strength, using $\Omega = 1.67$, becomes $M_n / \Omega = 0.6 F_y S_x$. In all cases where the shape factor, Z_x / S_x , is greater than or equal to 1.2 ($0.9/0.75 = 1.2$ or $2.00/1.67 = 1.2$), the *Specification* approach gives a lower or equal available strength when compared to this model. But, if the shape factor is less than 1.2, this model, which was initially thought to be conservative, gives a lower value than the *Specification* approach.

Model 2

A second model is investigated to see if this underprediction can be reversed by eliminating the holes at the compression flange which were included for convenience only.

For this model, only the holes in the tension flange are accounted for and the compression flange is not reduced. It takes a bit more calculation effort to determine the nominal strength with this approach, but it is expected to yield a more accurate representation of the true behavior. In this case, provided the plastic neutral axis remains in the web,

$$M_n = F_y Z_x - (1 - \Psi) \left(F_y A_{fg} \right) \left(\frac{d - t_f}{2} \right) - \frac{\left[(1 - \Psi) F_y A_{fg} \right]^2}{4 F_y t_w} \quad (6)$$

and the resistance/safety factor is again taken as $\phi = 0.75$ or $\Omega = 2.00$ since the strength calculation considered rupture of the tension flange. This model yields higher available flexural strength for most of the range of the ratio of flange-rupture strength to flange-yield strength. However, as the reduction for holes gets smaller—that is, as Ψ approaches 1.0, the nominal strength approaches $F_y Z_x$ and the same problem occurs as for Model 1, where the available strength predicted by this model is lower than that predicted by the *Specification* approach for *W*-shapes with a shape factor below 1.2.

Model 3

A third approach is developed with the goal of increasing the design strength for those cases where the reduction for holes is small.

Since the flange in tension is controlled by tension rupture and the remainder of the shape is controlled by yielding in Model 2, Model 3 simply applies two different resistance/safety factors, $\phi = 0.75$ or $\Omega = 2.00$, for the tension flange contribution and $\phi = 0.9$ or $\Omega = 1.67$, for the compression

flange and the web contributions. This multiple factor approach is similar to that used in connection design. For example, a bolted flange plate moment connection could have the tension flange plate controlled by rupture and the compression flange plate controlled by yielding. Thus, different resistance/safety factors would be applied in the design of each element yet they both participate in resisting the same connection moment. In the application here, using Equation 6, this approach yields directly the design strength as

$$\phi M_n = 0.9 F_y Z_x - (0.9 - 0.75 \Psi) \left(F_y A_{fg} \right) \left(\frac{d - t_f}{2} \right) - \frac{0.9 \left[(1 - \Psi) F_y A_{fg} \right]^2}{4 F_y t_w} \quad (7)$$

or the allowable strength as

$$\frac{M_n}{\Omega} = 0.6 F_y Z_x - (0.6 - 0.5 \Psi) \left(F_y A_{fg} \right) \left(\frac{d - t_f}{2} \right) - \frac{0.6 \left[(1 - \Psi) F_y A_{fg} \right]^2}{4 F_y t_w} \quad (8)$$

For this model, as Ψ approaches 1.0, the contribution of the tension flange is not fully restored to its yield strength since its contribution is always modified by the rupture resistance/safety factor when $\Psi = 1$. This amounts to a 15% reduction in the contribution of the tension flange to the design strength. For this model, the design strength and the allowable strength for all values of the ratio of flange-rupture strength to flange-yield strength results in available strengths greater than that obtained using Equation F13-1 from AISC 360-05.

SUMMARY

Figure 1 illustrates the LRFD results for the three models discussed earlier compared to the *Specification* equation for a *W*8×24. This particular shape was chosen because it is compact and has a shape factor close to the lowest of all *W*-shapes, 1.105. It can be seen that Model 3 predicts design strengths greater than those predicted by *Specification* Equation F13-1. Identical comparisons would result if ASD had been used for the figure.

The intent of this study was to confirm that Equation F13-1 with $\phi = 0.9$ or $\Omega = 1.67$ provides a prediction of flexural strength that is conservative. Models 1 and 2 show that for all *W*-shapes with a shape factor of 1.2 or greater, the prediction by the *Specification* equation is conservative. However, a more accurate model was needed for *W*-shapes with a shape factor less than 1.2. Model 3 is a reasonable analytical approach that can be considered conservative. Since Model 3 always provides an available flexural strength greater than that obtained using the *Specification* provisions, it is considered acceptable to use Equation F13-1 with $\phi = 0.9$ or $\Omega = 1.67$.

NOTATION

The notation used in this paper is consistent with that used in ANSI/AISC 360-05 with one symbol added, Ψ .

A_{fg} = gross flange area, in.² (mm²)

A_{fn} = net flange area, in.² (mm²)

F_{cr} = critical stress, ksi (MPa)

F_u = specified minimum tensile strength, ksi (MPa)

F_y = specified minimum yield stress, ksi (MPa)

M_n = nominal flexural strength, kip-in. (N-mm)

S_x = elastic section modulus about the x -axis, in.³ (mm³)

Y_t = hole reduction coefficient

Z_x = plastic section modulus about the x -axis, in.³ (mm³)

d = depth of section, in. (mm)

t_f = thickness of flange, in. (mm)

t_w = thickness of web, in. (mm)

ϕ = resistance factor

Ω = safety factor

Ψ = flange rupture to yield strength ratio

REFERENCES

AISC (2005), *Specification for Structural Steel Buildings*, ANSI/AISC 360, American Institute of Steel Construction, Chicago, IL.

Dexter, R.J., Altstadt, S.A. and Gardner, C.A. (2002), *Strength and Ductility of HPS70W Tension Members and Tension Flanges with Holes*, University of Minnesota, Minneapolis, MN, March 2002.

APPENDIX

Derivations for the equations presented in this paper follow.

Model 1

In this case, both flanges are assumed to have the same reduction for the presence of holes. The nominal plastic moment strength is given by $F_y Z_x$ when no holes are present. To account for the reduced strength of the flanges, the yield contribution of both flanges is deducted and replaced by the tension rupture contribution. This is clearly a conservative approach for determining the nominal flexural strength since it ignores the actual contribution of the compression flange. Thus,

$$M_n = F_y Z_x - 2F_y A_{fg} \left(\frac{d}{2} - \frac{t_f}{2} \right) + 2F_u A_{fn} \left(\frac{d}{2} - \frac{t_f}{2} \right) \quad (a)$$

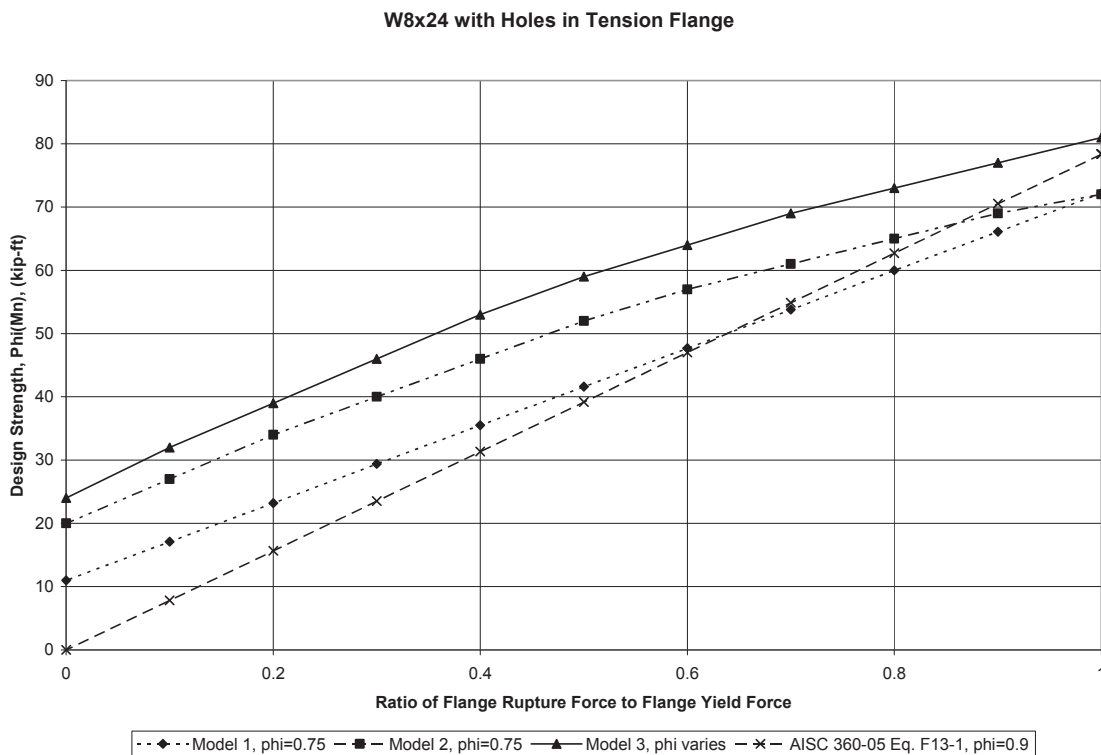


Fig. 1. Design strength for a W8x24 with holes in the tension flange.

Combining terms and multiplying the second term by $\left(\frac{F_y A_g}{F_y A_g}\right)$ yields

$$M_n = F_y Z_x + \frac{(F_u A_{fn} - F_y A_{fg})}{F_y A_{fg}} (d - t_f) (F_y A_{fg}) \quad (b)$$

Defining $\Psi = \frac{F_u A_{fn}}{F_y A_{fg}}$ and substituting into Equation b gives

$$M_n = F_y Z_x - (1 - \Psi) (F_y A_{fg}) (d - t_f) \quad (5)$$

Model 2

For this model, only the holes in the tension flange are considered. First, the contribution of the web is determined by deducting the flanges from the nominal plastic moment strength of the W-shape.

$$M_{n1} = F_y Z_x - 2 (F_y A_{fg}) \left(\frac{d}{2} - \frac{t_f}{2} \right) \quad (c)$$

Then the tension flange rupture and compression flange yield contributions are added.

$$M_{n2} = F_y Z_x - 2 (F_y A_{fg}) \left(\frac{d}{2} - \frac{t_f}{2} \right) + F_u A_{fn} \left(\frac{d}{2} - \frac{t_f}{2} \right) + F_y A_{fg} \left(\frac{d}{2} - \frac{t_f}{2} \right) \quad (d)$$

Finally, the last factor to consider is the impact of the shift in the plastic neutral axis into the compression zone of the web, defined as distance x from the centroid of the gross area. This results in a moment reduction based on the removal of some compression force and the addition of an equal tension force, captured through the multiplication by 2 in the last term. These forces are half of the difference between the flange yield force and flange rupture force. Thus,

$$M_{n3} = F_y Z_x - 2 (F_y A_{fg}) \left(\frac{d}{2} - \frac{t_f}{2} \right) + F_u A_{fn} \left(\frac{d}{2} - \frac{t_f}{2} \right) + F_y A_{fg} \left(\frac{d}{2} - \frac{t_f}{2} \right) - 2 \left[F_y t_w \left(\frac{x^2}{2} \right) \right] \quad (e)$$

and the distance that the plastic neutral axis moves up into the compression zone, x , is

$$x = \frac{F_y A_{fg} - F_u A_{fn}}{2 F_y t_w} \quad (f)$$

Substituting for x yields

$$M_{n3} = F_y Z_x - 2 (F_y A_{fg}) \left(\frac{d}{2} - \frac{t_f}{2} \right) + F_u A_{fn} \left(\frac{d}{2} - \frac{t_f}{2} \right) + F_y A_{fg} \left(\frac{d}{2} - \frac{t_f}{2} \right) - \frac{(F_y A_{fg} - F_u A_{fn})^2}{4 F_y t_w} \quad (g)$$

Combining terms and substituting $\Psi = \frac{F_u A_{fn}}{F_y A_{fg}}$ yields

$$M_n = F_y Z_x - (1 - \Psi) (F_y A_{fg}) \left(\frac{d - t_f}{2} \right) - \frac{[(1 - \Psi) F_y A_{fg}]^2}{4 F_y t_w} \quad (6)$$

Model 3

The only difference between Model 3 and Model 2 is the application of the yielding and rupture resistance/safety factors. Based on Equation g, for LRFD the design strength becomes

$$\phi M_n = \phi_y F_y Z_x - \phi_y 2 (F_y A_{fg}) \left(\frac{d}{2} - \frac{t_f}{2} \right) + \phi_r F_u A_{fn} \left(\frac{d}{2} - \frac{t_f}{2} \right) + \phi_y F_y A_{fg} \left(\frac{d}{2} - \frac{t_f}{2} \right) - \frac{\phi_y (F_y A_{fg} - F_u A_{fn})^2}{4 F_y t_w} \quad (h)$$

where ϕ_y is the resistance factor for yielding and ϕ_r is the resistance factor for rupture.

Combining terms and substituting $\Psi = \frac{F_u A_{fn}}{F_y A_{fg}}$, $\phi_y = 0.9$, and $\phi_r = 0.75$ yields

$$\phi M_n = 0.9 F_y Z_x - (0.9 - 0.75 \Psi) (F_y A_{fg}) \left(\frac{d - t_f}{2} \right) - \frac{0.9 [(1 - \Psi) F_y A_{fg}]^2}{4 F_y t_w} \quad (7)$$

For ASD the safety factors are applied to Equation g, yielding

$$\frac{M_n}{\Omega} = \frac{F_y Z_x}{\Omega_y} - 2 \frac{(F_y A_{fg})}{\Omega_y} \left(\frac{d}{2} - \frac{t_f}{2} \right) + \frac{F_u A_{fn}}{\Omega_r} \left(\frac{d}{2} - \frac{t_f}{2} \right) + \frac{F_y A_{fg}}{\Omega_y} \left(\frac{d}{2} - \frac{t_f}{2} \right) - \frac{(F_y A_{fg} - F_u A_{fn})^2}{\Omega_y (4 F_y t_w)} \quad (i)$$

where Ω_y is the safety factor for yielding and Ω_r is the safety factor for rupture.

Combining terms and substituting $\Psi = \frac{F_u A_{fn}}{F_y A_{fg}}$, $\Omega_y = 1.67$, and $\Omega_r = 2.00$ yields

$$\frac{M_n}{\Omega} = 0.6 F_y Z_x - (0.6 - 0.5 \Psi) (F_y A_{fg}) \left(\frac{d - t_f}{2} \right) - \frac{0.6 [(1 - \Psi) F_y A_{fg}]^2}{4 F_y t_w} \quad (8)$$

A Case for a Single Stiffness Reduction Factor in the 2010 AISC Specification

LOUIS F. GESCHWINDNER

ABSTRACT

The 2005 AISC *Specification for Structural Steel Buildings* includes a stiffness reduction factor, τ_b , in Appendix 7 to be used in the direct analysis method to account for the presence of residual stresses and their influence on the second-order effects of frame behavior. The 2005 Commentary includes a stiffness reduction factor, τ_a , to be used along with the effective length nomograph to account for the influence of column inelasticity due to residual stresses on effective length. These two stiffness reduction factors are intended to account for the same effect yet they are different. This paper provides the background for these two factors, and it will demonstrate that τ_b is the more correct stiffness reduction factor. The 2010 AISC *Specification* will recommend its use with both the direct analysis method and the effective length nomograph.

Keywords: stiffness reduction factor, direct analysis method, effective length nomograph, column inelasticity, residual stresses.

INTRODUCTION

Appendix 7 of the *Specification for Structural Buildings* (AISC, 2005) includes a stiffness reduction factor, τ_b , to be used in the direct analysis method to account for the presence of residual stresses and their influence on the second-order effects of frame behavior. The 2005 Commentary includes a stiffness reduction factor, τ_a , to be used along with the effective length nomograph to account for the influence of column inelasticity due to residual stresses on effective length. These two stiffness reduction factors are intended to account for the same effect, yet they are different. This paper provides the background for these two factors and the first stiffness reduction factor introduced in the literature in the early 1970s. It will demonstrate that τ_b is the more correct stiffness reduction factor and it should be used with both the direct analysis method and the effective length nomograph.

STIFFNESS REDUCTION FACTOR FOR DETERMINATION OF INELASTIC K -FACTOR

The requirement to use an effective length factor, K , in the determination of column strength was introduced with the 1963 AISC *Specification*. At about the same time, two nomographs were published to assist in determining these effective length factors. One of the assumptions used in the

derivation of the equations upon which the nomographs are based was that all members in the frame behave elastically. Since it was known at the time that columns behaved inelastically if they had sufficiently low slenderness ratios, there was a need to address the influence of inelastic column behavior on K . This was accomplished by using a stiffness reduction factor.

The first introduction of a stiffness reduction factor to be used in conjunction with the nomograph is found in the 1971 paper by Yura (1971). He shows that the joint stiffness ratio, G , used with the nomograph included the modulus of elasticity, E , in the numerator and denominator so that

$$G = \frac{\text{Column stiffness}}{\text{Beam stiffness}} = \frac{\Sigma(EI/L)_{col}}{\Sigma(EI/L)_{beam}} \quad (1)$$
$$= \frac{\Sigma(I/L)_{col}}{\Sigma(I/L)_{beam}} = G_{elastic}$$

However, if the columns behaved inelastically, E for the columns should be replaced by the tangent modulus, E_T , and the joint stiffness ratio became

$$G_{inelastic} = \frac{\Sigma(E_T I/L)_{col}}{\Sigma(EI/L)_{beam}} = \frac{E_T}{E} G_{elastic} \quad (2)$$

Yura pointed out that the difficulty would be in determining E_T/E . He went on to say that this could be accomplished in a reasonably accurate manner by noting that for a given Kl/r ,

$$\frac{E_T}{E} = \frac{F_{cr(inelastic)}}{F_e} \quad (3)$$

Louis F. Geschwindner, Ph.D., P.E., Vice President, American Institute of Steel Construction, 1 E. Wacker Drive, Suite 700, Chicago, IL, 60601. E-mail: geschwindner@aisc.org

where $F_{cr(inelastic)}$ is the critical stress in the inelastic region and

$$F_e = \frac{\pi^2 E}{\left(\frac{Kl}{r}\right)^2}$$

By using the stress equations from the AISC *Specification*, an approximate relationship could be established as

$$\frac{E_T}{E} = \frac{F_{cr(inelastic)}}{F_e} \approx \frac{F_a}{F'_e} \quad (4)$$

where F_a is the allowable stress given by the *Specification* and

$$F'_e = \frac{12\pi^2 E}{23 \left(\frac{Kl}{r}\right)^2}$$

Yura also noted that F_a and F'_e use different factors of safety, but that this could be ignored as a minor factor in the development.

Equation 4 is the basis for the stiffness reduction factors used with the Allowable Stress Design (ASD) specifications from 1969 through 1978, while Equation 3 is the basis for τ_a presented in the 2005 AISC *Specification*. Although these stiffness reduction factors are all based on the same relationship, Equation 3, the actual value of the stiffness reduction factor has gone through some variation as the column strength equations have changed through subsequent editions of the specification.

USE OF ACTUAL STRESS RATHER THAN ALLOWABLE STRESS

The use of the stiffness reduction factor as originally presented by Yura (1971) was an iterative process. First, the stiffness reduction factor was assumed to be 1.0 and K was determined. With this K , the allowable stress was determined and a new stiffness reduction factor was found. This stiffness reduction factor lead to a new, reduced K , which led to a new allowable stress and another new reduced K . This process eventually converged and, in the example presented by Yura, the column actually ended up having $K = 1.0$.

In order to eliminate the need to iterate in the determination of the stiffness reduction factor, Disque (1973) recommended using the actual stress rather than the allowable stress. He also suggested that an even more conservative approach would be to use the maximum possible allowable stress, $0.6F_y$, and he provided tables in his paper for that approach. The 8th edition *Steel Construction Manual* included a stiffness reduction factor table based on the actual stress.

1969 AISC SPECIFICATION

From the 1969 AISC *Specification*, column allowable stresses are given:

$$\text{for } \frac{Kl}{r} \leq C_c = \sqrt{\frac{2\pi^2 E}{F_y}} \text{ (inelastic behavior)}$$

$$F_a = \frac{\left[1 - \frac{(Kl/r)^2}{2C_c^2}\right] F_y}{\frac{5}{3} + \frac{3(Kl/r)}{8C_c} - \frac{(Kl/r)^3}{8C_c^3}} \quad (5)$$

$$\text{and for } \frac{Kl}{r} > C_c = \sqrt{\frac{2\pi^2 E}{F_y}} \text{ (elastic behavior)}$$

$$F_a = \frac{12\pi^2 E}{23(Kl/r)^2} \quad (6)$$

while

$$F'_e = \frac{12\pi^2 E}{23(Kl/r)^2} \quad (7)$$

Equations 5, 6, and 7 include the effects of both residual stresses and initial out of straightness (Johnson, 1966). Thus, the ratio of F_a/F'_e is not the ratio of E_T/E but an approximation, as already indicated by Yura.

Substituting Equations 5 and 7 into Equation 4 and defining the stiffness reduction factor as SRF_{1969} yields

$$SRF_{1969} = \frac{F_a}{F'_e} = \frac{\frac{23}{12} \left(1 - \frac{F_y}{4F_e}\right) \frac{F_y}{F_e}}{\left(\frac{5}{3} + \frac{3(Kl/r)}{8C_c} - \frac{(Kl/r)^3}{8C_c^3}\right)} \quad (8)$$

The factor 23/12 in the numerator is the safety factor for elastic buckling while the three-term denominator is the safety factor for inelastic buckling. In the inelastic region, for $Kl/r = 0$ the safety factor is 5/3 while for $Kl/r = C_c$, the safety factor is 23/12. For design according to the 1969 AISC *Specification*, the safety factors account for the influence of initial out of straightness while inelasticity is accounted for through the basic equations.

It should be noted that in the elastic buckling region, when $Kl/r > C_c$, the ratio of F_a/F'_e is 1.0 and there is no inelastic stiffness reduction factor, as would be expected.

1986 AISC LRFD SPECIFICATION

With the introduction of the 1986 AISC LRFD (Load and Resistance Factor Design) *Specification*, column behavior was defined at the critical stress level, without the use of factors of safety. In addition, the column strength equation in the inelastic region was changed. Thus,

$$\text{for } \lambda_c = \frac{KL}{r\pi} \sqrt{\frac{F_y}{E}} \leq 1.5 \text{ (inelastic behavior)}$$

$$F_{cr} = \left(0.658^{\lambda_c^2}\right) F_y \quad (9)$$

and for $\lambda_c > 1.5$ (elastic behavior)

$$F_{cr} = \left(\frac{0.877}{\lambda_c^2}\right) F_y \quad (10)$$

These equations also include the influence of initial out of straightness and residual stresses. In the elastic buckling region, Equation 10, the primary factor influencing column strength is the initial out of straightness. Thus, the 0.877 factor can be thought of as accounting for initial out of straightness. In the inelastic region, Equation 9, the separate influences of residual stresses and initial out of straightness can not be clearly distinguished. This is the same situation that was seen when using the 1969 ASD equations.

The stiffness reduction factor based on Eq. 3 and the LRFD column strength equations then becomes, for columns with $\lambda_c \leq 1.5$

$$SRF_{1986} = \frac{E_T}{E} = \frac{F_{cr(inelastic)}}{F_{cr(elastic)}} = \frac{\left(0.658^{\lambda_c^2}\right) F_y}{\left(\frac{0.877}{\lambda_c^2}\right) F_y} \quad (11)$$

2005 AISC SPECIFICATION

The column strength equations found in the 2005 AISC *Specification* are essentially the same as those from the 1986 AISC LRFD *Specification*. The only change is how the division between elastic and inelastic behavior is defined and the format of the actual terms in the equations. For the 2005 *Specification*, Eq. 11 becomes

$$\tau_a = \frac{E_T}{E} = \frac{\left(0.658^{\frac{F_y}{F_c}}\right) F_y}{0.877 F_c} \quad (12)$$

The 2005 Commentary gives τ_a in the format developed by the ASCE Task Committee on Effective Length (ASCE, 1997) as

$$\tau_a = -2.724 \left(\frac{P_n}{P_y}\right) \ln\left(\frac{P_n}{P_y}\right) \quad (13)$$

Where $P_n = F_{cr} A_s$ and F_{cr} is determined through Equation 9. Equations 11, 12 and 13 provide the same results.

A new stiffness reduction factor, τ_b , to be used in the Direct Analysis Method was introduced in the 2005 AISC *Specification*. It is based on column strength curves proposed by the Column Research Council in 1960 (Johnson, 1960; Galambos, 1998), where

$$\text{for } \lambda = \frac{KL}{r\pi} \sqrt{\frac{F_y}{E}} \leq \sqrt{2} \text{ (inelastic behavior)}$$

$$\frac{F_{cr}}{F_y} = \left(1 - \frac{\lambda^2}{4}\right) \quad (14)$$

and for $\lambda > \sqrt{2}$ (elastic behavior)

$$\frac{F_{cr}}{F_y} = \frac{1}{\lambda^2} \quad (15)$$

The slenderness parameter, λ , is the same as λ_c introduced in the 1986 AISC LRFD *Specification*. Equations 14 and 15 include the effects of residual stresses but do not include the effects of out of straightness (Johnson, 1960). With the substitution of λ , Equation 15 reduces to the Euler buckling stress equation,

$$F_{cr} = F_e = \frac{\pi^2 E}{\left(\frac{KL}{r}\right)^2} \quad (16)$$

and Equation 14 reduces to

$$F_{cr} = \left(1 - \frac{F_y}{4F_e}\right) F_y \quad (17)$$

The 2005 Commentary says that τ_b is similar to the inelastic stiffness reduction factor. For use with the nomograph, the stiffness reduction factor defined by Equation 3, using Equations 16 and 17, yields

$$\tau_b = \frac{E_T}{E} = \left(1 - \frac{F_y}{4F_e}\right) \frac{F_y}{F_e} \quad (18)$$

COMPARISON OF STIFFNESS REDUCTION FACTORS BASED ON SLENDERNESS RATIOS

The three stiffness reduction factors given in Equations 8, 12 and 18 are each a function of Kl/r , directly and through F_e . Figure 1 presents these three equations as a function of λ , which itself is a function of Kl/r , for $F_y = 50$ ksi. Table 1 gives values for Equations 8, 12, and 18 for $\lambda = 0$ to 1.5 ($Kl/r = 0$ to 113.5). It is seen from these results that the three equations for determining the stiffness reduction factor provide essentially the same results when presented as a function of slenderness. This confirms the claim of Yura

(1971) that the variation in safety factor was a minor factor. It also shows that the use of strength equations that include initial out of straightness and residual stresses (Equations 8 and 12), rather than just residual stresses (Equation 18) is also a minor factor in determining the stiffness reduction factor. Since the stiffness reduction factor was initially developed to assist in the proper use of the nomographs, which are of course based on Kl/r , it is clear that any of these three approaches would be reasonable for this purpose.

STIFFNESS REDUCTION FACTOR FOR USE IN THE DIRECT ANALYSIS METHOD

The stiffness reduction factor to be used with the direct analysis method is defined as τ_b as discussed above and is given directly as an unnumbered equation in Appendix 7 of the 2005 AISC Specification.

For $P_r/P_y \leq 0.5$

$$\tau_b = 1.0 \quad (19)$$

and for $P_r/P_y > 0.5$

$$\tau_b = 4 \left[\frac{\alpha P_r}{P_y} \left(1 - \frac{\alpha P_r}{P_y} \right) \right] \quad (20)$$

In Equation 20, $\alpha = 1.0$ for LRFD and $\alpha = 1.6$ for ASD. This factor is used to insure that the calculation is performed at an ultimate strength level.

This relationship was developed from the CRC column strength equations presented above as Equations 14 and 15.

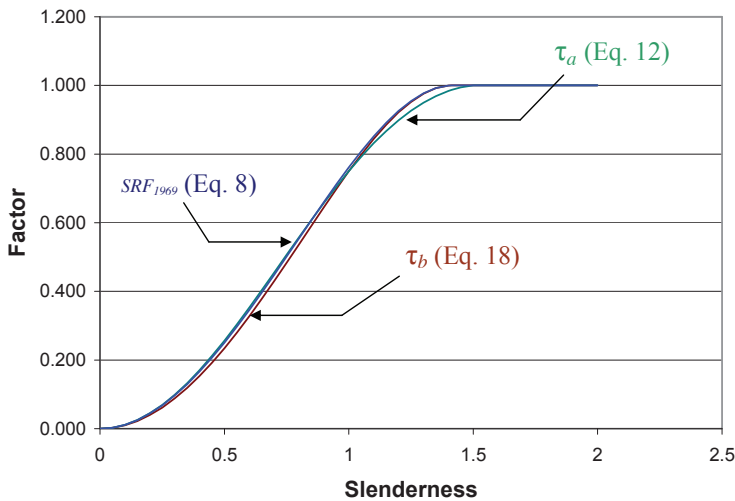


Fig. 1. Comparison of the three approaches to determining the stiffness reduction factor as a function of slenderness parameter, λ , for use with the nomograph.

λ	SRF_{1969} Eq. 8	τ_a Eq. 12	τ_b Eq. 18
0	0.000	0.000	0.000
0.05	0.003	0.003	0.002
0.10	0.011	0.011	0.010
0.15	0.025	0.025	0.022
0.20	0.044	0.045	0.040
0.25	0.068	0.069	0.062
0.30	0.097	0.099	0.088
0.35	0.129	0.133	0.119
0.40	0.166	0.171	0.154
0.45	0.207	0.212	0.192
0.50	0.250	0.257	0.234
0.55	0.297	0.304	0.280
0.60	0.346	0.353	0.328
0.65	0.396	0.404	0.378
0.70	0.449	0.455	0.430
0.75	0.502	0.507	0.483
0.80	0.555	0.558	0.538
0.85	0.608	0.609	0.592
0.90	0.661	0.658	0.646
0.95	0.712	0.705	0.699
1.00	0.762	0.750	0.750
1.05	0.808	0.792	0.799
1.10	0.852	0.831	0.844
1.15	0.891	0.867	0.885
1.20	0.926	0.899	0.922
1.25	0.955	0.926	0.952
1.30	0.977	0.950	0.976
1.35	0.993	0.969	0.992
1.40	1.000	0.984	1.000
1.45	1.000	0.994	1.000
1.50	1.000	1.000	1.000

If the inelastic critical stress is taken as τ_b times the elastic critical stress, then from Equation 15

$$F_{cr} = \tau_b \left(\frac{1}{\lambda^2} \right) F_y \quad (21)$$

This is simply a restatement of the Equation 3 and applies for both elastic and inelastic behavior when using Equations

19 and 20 for τ_b . If Equation 21 is solved for λ^2 and the result substituted into Equation 14,

$$\frac{F_{cr}}{F_y} = \left[1 - \frac{1}{4} \left(\frac{\tau_b F_y}{F_{cr}} \right) \right] \quad (22)$$

Equation 22 can then be solved for τ_b , which yields

$$\tau_b = 4 \left[\frac{F_{cr}}{F_y} \left(1 - \frac{F_{cr}}{F_y} \right) \right] \quad (23)$$

which can be written in terms of strength as

$$\tau_b = 4 \left[\frac{P_n}{P_y} \left(1 - \frac{P_n}{P_y} \right) \right] \quad (24)$$

Equations 20 and 24 are the same except that one is written in terms of αP_n , the amplified required strength, and one in terms of P_n , the nominal strength. This difference is similar to the two approaches presented by Disque (1973) and Yura (1971).

To allow for additional comparisons, the stiffness reduction factor using the 1969 AISC *Specification*, SRF_{1969} , can be linked to nominal strength. To accomplish this, F_a/F_y is increased by 5/3, removing a uniform factor of safety and increasing the allowable stress at $Kl/r = 0$ to F_y and the stresses at other values of Kl/r to a comparable critical stress level. This links Equation 8 to F_{cr}/F_y or P_n/P_y .

Figure 2 shows the three stiffness reduction factors as a function of P_n/P_y and Table 2 gives values for P_n/P_y from 1 to 0.39. It is clear from these results that the three approaches no longer can be viewed as giving essentially the same

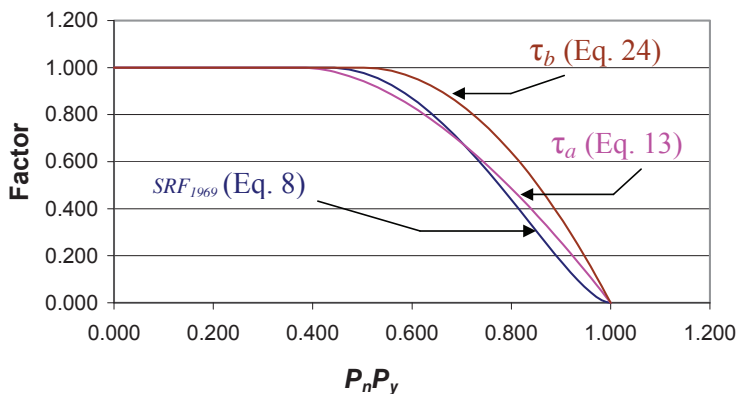


Fig. 2. Comparison of three stiffness reduction factors as a function of the nominal strength to yield strength ratio.

Table 2. Stiffness Reduction Factors Based on P_n/P_y

P_n/P_y	SRF_{1969} Eq.8	τ_a Eq. 13	τ_b Eq. 24
1.000	0.000	0.000	0.000
0.991	0.003	0.023	0.034
0.982	0.011	0.049	0.071
0.971	0.025	0.077	0.112
0.960	0.044	0.108	0.155
0.947	0.068	0.140	0.200
0.934	0.097	0.175	0.248
0.919	0.129	0.211	0.297
0.904	0.166	0.249	0.347
0.888	0.207	0.287	0.398
0.871	0.250	0.327	0.449
0.853	0.297	0.368	0.500
0.835	0.346	0.410	0.551
0.816	0.396	0.452	0.601
0.796	0.449	0.495	0.649
0.776	0.502	0.537	0.696
0.754	0.555	0.579	0.741
0.732	0.608	0.622	0.784
0.710	0.661	0.663	0.824
0.686	0.712	0.704	0.861
0.662	0.762	0.744	0.895
0.637	0.808	0.782	0.924
0.612	0.852	0.819	0.950
0.586	0.891	0.853	0.971
0.559	0.926	0.886	0.986
0.531	0.955	0.915	0.996
0.503	0.977	0.942	1.000
0.474	0.993	0.964	1.000
0.443	1.000	0.982	1.000
0.435	1.000	0.986	1.000
0.414	1.000	0.995	1.000
0.390	1.000	1.000	1.000

answer. The differences between the factors can be attributed to the inelastic column strength equations used. A detailed comparison of Equations 5 and 14 would show that the 1969 ASD equation is the CRC equation with a variable safety factor. The LRFD strength equation, Equation 9, is quite different when compared to both of the others.

A SINGLE STIFFNESS REDUCTION FACTOR

There are three stiffness reduction factors available for use with the nomograph as discussed earlier: Equations 8, 12 and 18. If the intent is only to use the stiffness reduction factor to modify the column end stiffness ratios, G , for use with the nomograph, it has been shown that any of these approaches will provide satisfactory results.

The SRF_{1969} and τ_a are based on strength equations that include initial out of straightness and residual stresses while τ_b is based on column strength equations that include only the effects of residual stresses. A comparison of these three approaches, Equations 8, 13 and 24, as a function of P_n/P_y , shows that they do not give similar results. Since the intent of the stiffness reduction factor, in all cases, is to include only the influence of inelastic behavior due to residual stresses, clearly τ_b should be used. Thus, the stiffness reduction factor for both the nomograph and the direct analysis method should be taken as τ_b .

Equations 19 and 20 for τ_b will be included in the 2010 AISC *Specification* as Equations C2-2a and C2-2b for use with the direct analysis method. The effective length method is covered in Appendix 7 of the 2010 *Specification*, and Commentary Section A7.2 indicates that the same equations used for stiffness reduction with the direct analysis method should be used with the effective length method.

REFERENCES

- AISC (2005), *Specification for Structural Steel Buildings*, ANSI/AISC 360, American Institute of Steel Construction, Chicago, IL.
- ASCE Task Committee on Effective Length (1997), *Effective Length and Notional Load Approaches for Assessing Frame Stability: Implications for American Steel Design*, American Society of Civil Engineers, New York, NY.
- Disque, R. O. (1973), "Inelastic K-factor for Column Design," *Engineering Journal*, AISC, Vol. 10, No. 2, pp. 33–35.
- Galambos, T.V. (ed.) (1998), *Guide to Stability Design Criteria for Metal Structures*, *Structural Stability Research Council*, 5th edition, John Wiley and Sons, New York, NY.
- Johnson, B.G., (ed.) (1960), *Guide to Design Criteria for Metal Compression Members*, *Column Research Council*, 1st edition, John Wiley and Sons, New York, NY.
- Johnson, B.G., (ed.) (1966), *Guide to Design Criteria for Metal Compression Members*, *Column Research Council*, 2nd edition, John Wiley and Sons, New York, NY.
- Yura, J. A. (1971), "The Effective Length of Columns in Unbraced Frames," *Engineering Journal*, AISC, Vol. 8, No. 2, pp. 37–42.

Bolt Shear Design Considerations

RAYMOND H.R. TIDE

Abstract

In this paper, bolt shear capacities are reviewed using the Load and Resistance Factor Design (LRFD) philosophy. Only bolt-shear limit states are addressed, although one aspect of slip critical limit states is addressed incidentally. This paper does not consider bolt bearing limit states. Test data used to justify the adoption of ASTM A325 and A490 high-strength bolts was obtained from previous research programs. The data also included various types of rivets and Huck bolts for general comparison. First, the test data are used to evaluate the current American Institute of Steel Construction (AISC, 2005) and Research Council on Structural Connections (RCSC, 2004) bolt shear provisions and to determine the current reliability, β , which is found to be conservative when based on a resistance factor, ϕ , of 0.75. The appropriateness of the ϕ -factor for bolt shear is addressed. Canadian (CSA S16-01) and Eurocode (EN 1993) provisions are also evaluated and shown not to be compatible with the test results. Two design equations are developed—one linear, one a step function—that result in a β value slightly greater than 3.0, appropriate for a manufactured product. The single-step function (with a step at 38 in.) is recommended for inclusion in updated design specifications. This design provision increases the design strength by 12.5% for short connections and by 17.2% for long connections. The test data indicate that there is no need for a bolt strength reduction due to the length of the connection, provided that the connection material gross and net section areas exceed certain ratios. That ratio is a function of the connection material yield and tensile strength, the total bolt shear area and the bolt tensile strength.

Keywords: bolt shear, reliability, resistance factor, connection length factor.

BACKGROUND

The current shear strength of a high strength bolt may be expressed by the following equation:

$$P_n = P_u A_b R_1 R_2 R_3 R_4 \quad (1)$$

where

P_u = ultimate tensile strength of bolt, ksi

R_1 = 0.625, shear-to-tension ratio

R_2 = 0.80, connection length reduction factor for
 $L \leq 50$ in.

R_3 = 1.00 if threads are excluded from the shear plane
= 0.80 if threads are included in the shear plane

R_4 = 0.80, additional connection length reduction factor
for $L > 50$ in.

L = connection length, in.

A_b = nominal unthreaded body area of bolt, in.²

The design shear values for ASTM A325 and A490 bolts are given in RCSC Specification Table 5.1 (RCSC, 2004). The design values, for other fasteners, such as ASTM A307 bolts and threaded material, are given in AISC *Specification for Structural Steel Buildings* (hereafter AISC *Specification*, 2005) Table J3.2. In Load Resistance and Factor Design (LRFD) terms, the design shear strength of a bolt is ϕR_n , with $\phi = 0.75$ and $R_n = P_n$.

The design values are based on an extensive research program conducted by the steel industry at the Fritz Engineering Laboratory at Lehigh University from the 1950s through the early 1970s. As was the custom at the time, the high-strength bolts were fully pretensioned. Bolt threads were excluded from the shear plane. In addition, an earlier research investigation at the University of Illinois and at University of California by Davis et al. (1940) was reviewed concerning riveted connections for the San Francisco–Oakland Bay Bridge. All of the data was summarized in the *Guide to Design Criteria of Bolted and Riveted Joints* (the *Guide*) by Kulak et al. (1987). The roles of 12 basic variable groups resulted in approximately 45 test variables that are described in the *Guide* and will not be repeated in this paper. However, three of the basic variable groups will be subsequently examined and used to develop a proposed design procedure.

The types of connections tested were the basic lap splice, the butt splice, the open shingle splice, and the closed shingle splice, as shown in Figure 1. A review of the literature revealed that the data from each test series were not uniformly reported. As a result, the original research reports were used to augment the background data. The connection length for a lap splice is the distance between the centerlines of the extreme end bolts. The connection length for a butt splice is the distance from the centerline of the bolt at one end of the connection to the centerline of the bolt closest to the overall connection centerline. Fortunately, large quantities of bolts were obtained from production lots, so essentially identical bolts were used in several test programs. Each lot of bolts was tested to determine both the tensile and shear strength.

Raymond H.R. Tide, D.Sc., S.E., P.E., Principal, Wiss, Janney, Elstner Associates, Inc., 330 Pflingsten Rd., Northbrook, IL 60062. E-mail: rtide@wje.com.

A literature search identified 11 papers and reports in addition to several supporting reports that resulted in data from 119 tests. Because of incomplete background information, the 40 tests from Davis et al. (1940) were not used other than to document its test results. Of the remaining 79 tests, the breakdown is as follows: 54 used ASTM A325 bolts, 18 used ASTM A490 bolts, 5 used rivets, and 2 used Huck bolts.

The CSA S16-01 standard, as supplemented in 2005, adopted the 2003 Eurocode EN 1993, Clause 3.8, which is shown as Equation 2, converted to U.S. customary units:

$$V_R = 0.60\phi F_u A_b \quad (2)$$

where

$\phi = 0.80$, resistance factor

$F_u =$ nominal bolt tensile stress, ksi

$A_b =$ bolt area, in.²

The R_1 factor of 0.60 represents the shear-to-tension ratio used in the CSA S16 document. When the threads are included in the shear plane, an R_3 factor of 0.70 is used. Of greater significance, V_R is valid up to a connection length, L , of $15d$, where d is the bolt diameter in inches. When the connection length exceeds $15d$, V_R is reduced by the factor $(1.075 - 0.005L/d)$ but is not taken as less than 0.75 times the original value given in Equation 2.

TEST DATA

As previously indicated, test data were obtained from 11 papers and reports: Bendigo et al. (1963), Davis et al. (1940), Fisher et al. (1963), Fisher and Kulak (1968), Fisher and Yoshida (1970), Foreman and Rumpf (1961), Kulak and Fisher (1968), Power and Fisher (1972), Rivera and Fisher (1970), and Sterling and Fisher (1965, 1966). Because of the various reporting formats and test parameters, it was not possible to directly compare the results. The published test ultimate shear strength of each connection was reduced to an average ultimate shear strength, P_{TEST} , of a single connector, bolt or rivet, loaded on two shear planes (double shear). The predicted ultimate shear strength of the same connector was computed using the reported appropriate single shear connector test data times two, P_{PRED} , for each lot of bolts or rivets.

The ratio P_{TEST}/P_{PRED} was then computed to compare the results, with connection length as the only independent variable. All of the reconfigured test data are given in Table 1 and plotted in Figure 2. The solid line represents the current step function for the length reduction factor. The dotted line represents the same equation multiplied by the current AISC ϕ for bolts, 0.75. The plotted data are in a non-dimensional form, eliminating the independent variables of bolt diameter, material type and connection configuration. Although this

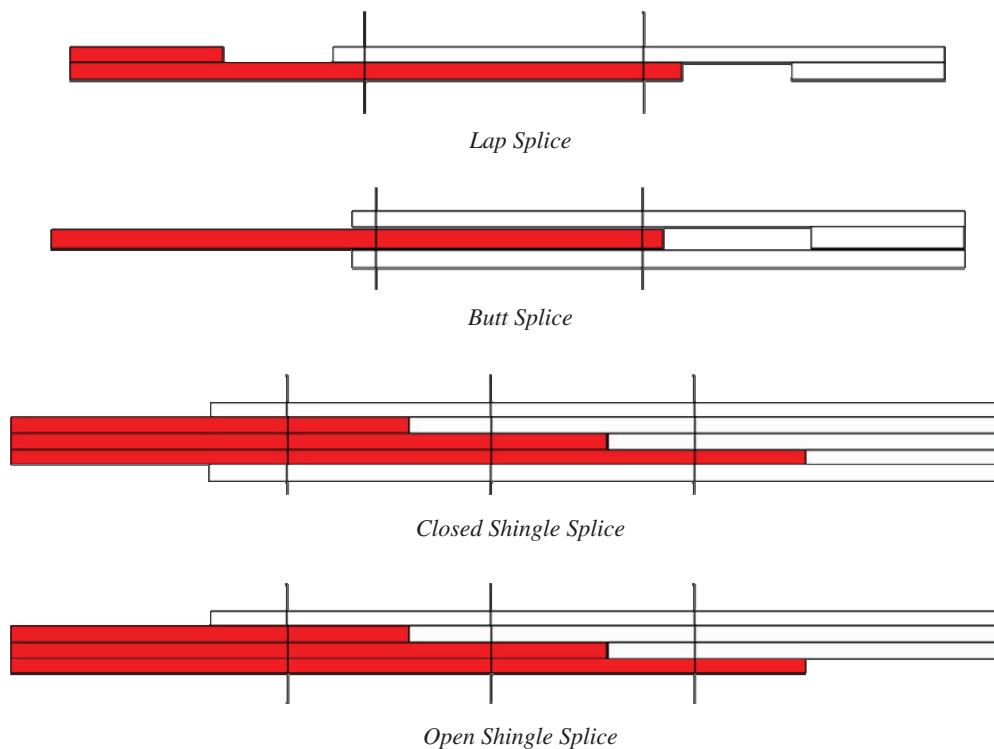


Fig. 1. Four types of connections.

Table 1. Connection Test and Computation Data

No.	ID	Dia. (in.)	Type	Bolts in Line	L (in.)	P_{TEST} (kip)	P_{PREL} (kip)	$\frac{P_{TEST}}{P_{PREL}}$	F_{yp} (ksi)	F_{up} (ksi)	F_v (ksi)	A_s (in. ²)	$\frac{A_n}{A_s}$	A_g (in. ²)	$\frac{0.90 A_s F_v}{F_{yp}}$ (in. ²)	A_n (in. ²)	$\frac{0.90 A_s F_v}{F_{up}}$ (in. ²)	(1) R_2	(2) Mat.	Ref. No.
1	F42b	1½	A325	4	10.5	131.5	131.4	1.001	114.0	121.4	66.1	15.9	0.51	13.0	8.3	8.07	7.8	0.90C	A514	4
2	F42c	1½	A325	4	10.5	133.0	131.4	1.012	114.0	121.4	66.1	15.9	0.56	13.8	8.3	8.9	7.8	0.90C	A514	4
3	F42d	1½	A325	4	10.5	132.0	131.4	1.005	114.0	121.4	66.1	15.9	0.61	14.5	8.3	9.66	7.8	0.90C	A514	4
4	F42e	1½	A325	4	10.5	132.8	131.4	1.01	114.0	121.4	66.1	15.9	0.66	15.4	8.3	10.5	7.8	0.90C	A514	4
5	F42g	1½	A325	4	10.5	134.3	131.4	1.022	114.0	121.4	66.1	15.9	0.72	16.3	8.3	11.4	7.8	0.90C	A514	4
6	F111	1½	A325	11	35.0	167.8	131.4	1.036	114.0	119.8	81.5	21.8	0.74	18.9	14.0	15.5	13.3	0.90C	A514	4
7a	HJ131	¾	A325	13	42.0	85.7	113.0	0.758	36.5	66.1	94.0	15.6	1.13	21.1	36.2	17.6	20.0	0.75S	A36M	4
7b									44.1	76.3	94.0	15.6	0.91	16.9	29.9	14.1	17.3	0.75S	A440L	4
8A	HJ132	¾	A325	13	42.0	69.8	113.0	0.618	36.5	66.1	94.0	15.6	0.89	16.3	36.2	13.9	20.0	0.75S	A36M	4
8b									44.1	76.3	94.0	15.6	0.71	13.0	29.9	11.1	17.3	0.75S	A440L	4
9a	HJ133	¾	A490	13	42.0	116.8	115.3	1.013	44.1	76.3	95.9	15.6	1.92	33.6	30.5	29.8	17.6	0.90C	A440M	4
9b									114.0	121.4	95.9	15.6	0.90	15.8	11.8	14.0	11.1	0.90C	A514L	4
10a	HJ135	¾	A325	13	42.0	95.7	96.9	0.988	44.1	76.3	80.6	15.6	1.68	29.8	25.7	26.1	14.8	0.90C	A440M	4
10b									114.0	121.4	80.6	15.6	0.79	14.1	9.9	12.3	9.3	0.90C	A514L	4
11	J42a	1	A490	4	10.5	154.8	151.7	1.020	114.0	121.4	96.6	12.6	0.76	13.9	9.6	9.58	9.0	0.90C	A514	7
12	J42b	1	A490	4	10.5	153.5	151.7	1.012	114.0	121.4	96.6	12.6	0.82	14.6	9.6	10.3	9.0	0.90C	A514	7
13	J42c	1	A490	4	10.5	150.8	151.7	0.994	114.0	121.4	96.6	12.6	0.86	15.2	9.6	10.9	9.0	0.90C	A514	7
14	J42d	1	A490	4	10.5	152.5	151.7	1.006	114.0	121.4	96.6	12.6	0.92	16.0	9.6	11.6	9.0	0.90C	A514	7
15	J072	¾	A490	7	21.0	121.4	116.6	1.041	101.6	111.9	97.0	8.41	0.91	9.58	7.2	7.66	6.6	0.90C	A514	7
16	J132	1½	A490	13	42.0	201.2	191.8	1.049	101.6	111.9	96.5	25.8	0.91	28.6	22.1	23.7	20.0	0.90C	A514	7
17	J172	¾	A490	17	56.0	118.5	119.8	1.016	101.6	111.9	97.0	20.4	0.90	20.4	17.5	18.5	15.9	0.90C	A514	7
18	J251	¾	A490	25	84.0	109.4	119.8	0.913	101.6	111.9	99.7	30.1	0.82	28.4	26.6	24.6	24.1	0.90C	A514	7
19	J252	¾	A490	25	84.0	124.0	119.8	1.035	101.6	111.9	99.7	30.1	1.12	37.6	26.6	33.7	24.1	0.90C	A514	7
20	D71	¾	A325	7	21.0	80.4	102.5	0.784	28.2	60.0	85.3	16.8	1.08	21.9	45.7	18.2	21.5	0.75S	A7	1
21	D81	¾	A325	8	24.5	80.1	102.5	0.782	28.2	60.0	85.3	19.2	1.09	24.7	52.3	21.0	24.6	0.75S	A7	1
22	D91	¾	A325	9	28.0	75.4	102.5	0.736	28.2	60.0	85.3	21.6	1.10	27.5	58.8	23.7	27.6	0.75S	A7	1
23	D101	¾	A325	10	31.5	75.3	102.5	0.734	28.2	60.0	85.3	24.0	1.08	29.8	65.3	26.1	30.7	0.75S	A7	1
24	D701	¾	A325	7	21.0	86.6	112.0	0.773	33.6	64.3	93.2	16.8	1.14	23.8	41.9	19.3	21.9	0.75S	A7	1

Notes:

(1) 0.90 indicates data represented by a circle (C) in Figure 3;

(2) 0.75 indicates data represented by a square (S) in Figure 3;

(3) 0.75* indicates data represented by a triangle (T) in Figure 3.

(4) L and M refer to lap plates and main member plates in hybrid connections.

Table 1. Connection Test and Computation Data (Cont.)

No.	ID	Dia. (in.)	Type	Bolts in Line	L (in.)	P_{TEST} (kip)	P_{PRED} (kip)	$\frac{P_{TEST}}{P_{PRED}}$	F_{yp} (ksi)	F_{up} (ksi)	F_v (ksi)	A_s (in. ²)	$\frac{A_n}{A_s}$	A_g (in. ²)	$\frac{F_{yp}}{A_n}$ (in. ²)	$\frac{0.90 A_s F_v}{F_{up}}$ (in. ²)	A_n (in. ²)	$\frac{0.90 A_s F_v}{F_{up}}$ (in. ²)	(1) R_2	(2) Mat.	Ref. No.
25	D801	7/8	A325	8	24.5	82.1	112.0	0.733	33.6	64.3	93.2	19.2	1.10	26.0	47.9	25.0	21.1	25.0	0.75S	A7	1
26	D901	7/8	A325	9	28.0	83.2	112.0	0.742	33.6	64.3	93.2	21.6	1.12	30.0	53.9	28.2	24.3	28.2	0.75S	A7	1
27	D1001	7/8	A325	10	31.5	83.4	112.0	0.744	33.6	64.3	93.2	24.0	1.12	33.1	59.9	31.3	26.8	31.3	0.75S	A7	1
28	D10	7/8	A325	10	31.5	77.2	109.0	0.708	28.2	60.0	90.7	24.0	1.09	33.7	69.5	32.7	26.2	32.7	0.75S	A7	1
29	D13A	7/8	A325	13	31.5	76.5	109.0	0.701	28.2	60.0	90.7	31.3	1.09	41.7	90.6	42.6	34.2	42.6	0.75S	A7	1
30	D13	7/8	A325	13	42.0	71.3	109.0	0.654	28.2	60.0	90.7	31.3	1.09	41.7	90.6	42.6	34.2	42.6	0.75S	A7	1
31	D16	7/8	A325	16	52.5	65.2	109.0	0.598	28.2	60.0	90.7	38.5	1.09	49.4	111.4	52.4	41.9	52.4	0.75S	A7	1
32	L2	7/8	A325	2	3.5	98.5	100.2	0.983	28.2	60.0	83.4	2.40	1.65	5.76	6.4	3.0	3.96	3.0	0.75*T	A7	1
33	L5	7/8	A325	5	14.0	89.2	100.2	0.89	28.2	60.0	83.4	6.01	1.32	9.63	16.0	7.5	7.92	7.5	0.75*T	A7	1
34	L7	7/8	A325	7	21.0	91.4	100.2	0.912	28.2	60.0	83.4	8.41	1.57	14.9	22.4	10.5	13.2	10.5	0.75*T	A7	1
35	L10	7/8	A325	10	31.5	74.8	100.2	0.746	28.2	60.0	83.4	12.0	1.10	14.9	31.9	15.0	13.2	15.0	0.75S	A7	1
36	DR71	7/8	A141R	7	21.0	52.7	66.5	0.793	28.2	60.0	55.3	16.8	0.785	16.9	29.7	13.9	13.2	13.9	0.75S	A7	1
37	DR101	7/8	A141R	10	31.5	47.1	66.5	0.709	28.2	60.0	55.3	24.0	0.769	22.2	42.4	19.9	18.5	19.9	0.75S	A7	1
38	DR131	7/8	A141R	13	42.0	46.8	66.5	0.704	28.2	60.0	55.3	31.3	0.762	27.5	55.2	26.0	23.8	26.0	0.75S	A7	1
39	B3	7/8	A325	4	10.5	87.5	96.2	0.910	36.6	65.5	80.0	24.0	1.11	36.0	47.2	26.4	26.6	26.4	0.75*T	A7	6
40	B6	7/8	A325	3	7.0	86.1	96.2	0.896	36.6	65.5	80.0	21.6	1.15	36.0	42.5	23.7	24.8	23.7	0.75*T	A7	6
41	BR2	7/8	A141R	5	14.0	52.0	60.0	0.867	36.6	65.5	49.9	30.0	0.887	36.0	36.8	20.6	26.6	20.6	0.75*T	A7	6
42	A3	1	A325	4	12.0	113.8	125.6	0.906	36.6	65.5	80.0	25.1	1.10	36.0	49.4	27.6	27.5	27.6	0.75S	A7	6
43	G1	1 1/8	A325	3	8.0	149.8	167.0	0.897	36.6	65.5	84.0	23.9	1.11	36.0	49.4	27.6	26.5	27.6	0.75S	A7	6
44	B5	1 1/8	A325	5	14.0	84.0	96.2	0.874	36.6	65.5	80.0	24.0	1.11	36.0	47.2	26.4	26.6	26.4	0.75*T	A7	6
45	K42a	7/8	A490	4	10.5	122.5	124.4	0.985	43.0	76.0	103.5	9.62	1.22	15.5	20.8	11.8	11.7	11.8	0.75S	A440	10
46	K42b	7/8	A490	4	10.5	122.5	124.4	0.985	43.0	76.0	103.5	9.62	1.27	16.0	20.8	11.8	12.2	11.8	0.75*T	A440	10
47	K42c	7/8	A490	4	10.5	124.5	124.4	1.001	43.0	76.0	103.5	9.62	1.31	16.4	20.8	11.8	12.6	11.8	0.75*T	A440	10
48	K42d	7/8	A490	4	10.5	125.5	124.4	1.009	43.0	76.0	103.5	9.62	1.37	17.0	20.8	11.8	13.2	11.8	0.75*T	A440	10
49	K131	7/8	A490	13	31.6	109.6	121.5	0.902	43.0	76.0	101.1	15.6	1.30	24.2	33.0	18.7	20.4	18.7	0.75*T	A440	10
50	K132	7/8	A490	13	63.0	100.9	121.5	0.830	43.0	76.0	101.1	15.6	1.30	24.1	33.0	18.7	20.3	18.7	0.75*T	A440	10
51	K133	7/8	A490	13	63.0	127.7	121.5	1.051	43.0	76.0	101.1	15.6	1.92	33.8	33.0	18.7	30.0	18.7	0.90C	A440	10
52	K191	7/8	A490	19	63.0	94.4	121.5	0.777	43.0	76.0	101.1	22.8	1.30	33.4	48.2	27.3	29.7	27.3	0.75*T	A440	10

Notes:

(1) 0.90 indicates data represented by a circle (C) in Figure 3;

0.75 indicates data represented by a square (S) in Figure 3;

0.75* indicates data represented by a triangle (T) in Figure 3.

(2) L and M refer to lap plates and main member plates in hybrid connections.

Table 1. Connection Test and Computation Data (Cont.)

No.	ID	Dia. (in.)	Type	Bolts in Line	L (in.)	P_{TEST} (kip)	P_{PREL} (kip)	$\frac{P_{TEST}}{P_{PREL}}$	F_{yp} (ksi)	F_{up} (ksi)	F_v (ksi)	A_s (in. ²)	$\frac{A_g}{A_s}$	A_n (in. ²)	$\frac{0.90 A_s F_v}{F_{up}}$ (in. ²)	(1) R_2	(2) Mat.	Ref. No.
53	E41b	7/8	A325	4	10.5	94.3	101.4	0.929	45.3	75.8	84.4	9.62	0.947	9.11	16.1	0.75S	A440	3
54	E41c	7/8	A325	4	10.5	96.3	101.4	0.949	45.3	75.8	84.4	9.62	0.981	9.49	16.1	0.75S	A440	3
55	E41e	7/8	A325	4	10.5	97.8	101.4	0.964	45.3	75.8	84.4	9.62	1.11	10.7	16.1	0.75*T	A440	3
56	E41f	7/8	A325	4	10.5	90.9	92.4	0.983	45.3	75.8	76.9	9.62	0.996	9.58	14.7	0.75*T	A440	3
57	E41g	7/8	A325	4	10.5	95.9	98.6	0.973	45.3	75.8	82.0	9.62	1.00	9.66	15.7	0.75*T	A440	3
58	E41	7/8	A325	4	10.5	91.0	92.4	0.985	45.3	75.8	76.9	9.62	1.01	9.70	14.7	0.75*T	A440	3
59	E71	7/8	A325	7	21.0	84.9	92.4	0.918	45.3	75.8	76.9	16.8	0.999	16.8	25.7	0.75*T	A440	3
60	E101	7/8	A325	10	31.5	80.5	92.4	0.871	45.3	75.8	76.9	24.0	1.00	24.0	36.7	0.75*T	A440	3
61	E131	7/8	A325	13	42.0	81.7	95.2	0.859	45.3	75.8	79.2	31.3	0.994	31.1	49.3	0.75*T	A440	3
62	E161	7/8	A325	16	52.5	79.5	95.2	0.835	45.3	75.8	79.2	38.5	0.994	38.2	60.6	0.75*T	A440	3
63	E46	7/8	A325	4	10.5	90.8	92.4	0.983	45.3	75.8	76.9	28.9	1.01	29.2	44.2	0.75*T	A440	3
64	E74	7/8	A325	7	21.0	86.1	92.4	0.931	45.3	75.8	76.9	33.7	0.995	33.5	51.5	0.75*T	A440	3
65	E741	7/8	A325	7	21.0	80.4	92.4	0.869	45.3	75.8	76.9	33.7	1.00	33.7	51.5	0.75*T	A440	3
66	Rivet	7/8	A502 Gr 1	32	94.0	43.8	54.1	0.809	59.0	88.0	45.0	76.9	0.660	50.8	52.8	0.90C	A572	9
67	Bolt	7/8	A325	32	94.0	55.5	91.4	0.607	59.0	88.0	76.0	76.9	0.660	50.8	89.2	0.75S	A572	9
68	1	7/8	A325	18	52.0	67.2	105.9	0.635	49.0	79.0	88.1	14.4	0.750	10.9	23.3	0.75S	A572	8
69	2	7/8	Huck	12	34.0	81.8	110.0	0.744	49.0	79.0	91.5	10.8	1.00	10.9	18.2	0.75S	A572	8
70	3A	7/8	A325	12	33.5	85.8	105.9	0.810	49.0	79.0	88.1	10.8	1.00	10.9	17.5	0.75*T	A572	8
71	3B	7/8	Huck	12	33.5	87.0	110.0	0.791	49.0	79.0	91.5	10.8	1.00	10.9	18.2	0.75S	A572	8
72	5	7/8	A325	18	52.0	63.4	105.9	0.599	49.0	79.0	88.1	16.8	0.646	10.9	27.2	0.75S	A572	8
73	6	7/8	A325	12	33.0	95.8	107.6	0.891	49.0	79.0	89.5	14.4	1.13	16.3	23.7	0.75*T	A572	8
74	7	7/8	A325	32	94.0	30.1	47.0	0.640	49.0	79.0	78.2	25.2	0.322	8.13	36.2	0.75S	A572	8
75	8	7/8	A325	21	61.0	44.4	47.0	0.944	49.0	79.0	78.2	18.6	0.436	8.13	26.7	0.75S	A572	8
76	E721	7/8	A325	7	21.0	76.4	92.6	0.826	45.3	76.0	77.0	16.8	0.805	13.6	25.7	0.75*T	A440	11
77	E722	7/8	A325	7	21.0	90.7	92.6	0.980	45.3	76.0	77.0	16.8	1.21	20.4	25.7	0.90C	A440	11
78	E163	7/8	A325	16	52.5	68.1	95.0	0.717	45.3	76.0	79.0	38.5	0.805	31.0	60.4	0.75*T	A440	11
79	E164	7/8	A325	16	52.5	87.0	95.0	0.917	45.3	76.0	79.0	38.5	1.20	46.2	60.4	0.90C	A440	11

Notes:

(1) 0.90 indicates data represented by a circle (C) in Figure 3;

0.75 indicates data represented by a square (S) in Figure 3;

0.75* indicates data represented by a triangle (T) in Figure 3;

(2) L and M refer to lap plates and main member plates in hybrid connections.

Table 2. Test Data for San Francisco–Oakland Bay Bridge Connections

No.	ID	Dia. (in.)	Type*	Rivets in Line	L (in.)	P_{TEST} (kip)	P_{PRED} (kip)	$\frac{P_{TEST}}{P_{PRED}}$	F_v (ksi)	A_n/A_s	Ref. No.
80	CCC 7-1	1	R(c)	8	6	89.0	89.2	0.998	56.8	1.19	2
81	CCC 7-2	1	R(c)	8	6	90.0	89.2	1.009	56.8	1.19	2
82	DCC 7-1	1	R(c)	14	4	89.1	89.2	0.999	56.8	0.771	2
83	DCC 7-2	1	R(c)	14	4	88.9	89.2	0.997	56.8	0.771	2
84	ACM 12-1	1	R(m)	12	15.75	121.7	119.0	1.023	75.8	1.58	2
85	ACM 12-2	1	R(m)	12	15.75	116.5	119.0	0.979	75.8	1.58	2
86	ASM 12-1	1	R(m)	12	15.75	113.3	119.0	0.952	75.8	1.22	2
87	ASM 12-2	1	R(m)	12	15.75	113.8	119.0	0.956	75.8	1.22	2
88	ACC 18-1	1	R(c)	18	24.50	87.0	89.2	0.975	56.8	1.06	2
89	ACC 18-2	1	R(c)	18	24.50	87.8	89.2	0.984	56.8	1.06	2
90	ACC 36-1	1	R(c)	36	24.50	79.5	89.2	0.891	56.8	0.528	2
91	ACC 36-2	1	R(c)	36	24.50	81.1	89.2	0.909	56.8	0.528	2
92	ACC 54-1	1	R(c)	54	40.75	77.1	89.2	0.864	56.8	0.352	2
93	ACC 54-2	1	R(c)	54	40.75	79.9	89.2	0.896	56.8	0.352	2
94	ASC 18-1	1	R(m)	18	19.5	86.7	119.0	0.728	75.8	0.812	2
95	ASC 18-2	1	R(m)	18	19.5	85.4	119.0	0.718	75.8	0.812	2
96	ASC 36-1	1	R(m)	36	24.5	84.9	119.0	0.714	75.8	0.406	2
97	ASC 36-2	1	R(m)	36	24.5	84.4	119.0	0.710	75.8	0.406	2
98	ASC 54-1	1	R(m)	54	31.25	80.3	119.0	0.675	75.8	0.271	2
99	ASC 54-2	1	R(m)	54	31.25	80.1	119.0	0.673	75.8	0.271	2
100	ACM 24-1	1	R(m)	24	35	119.8	119.0	1.006	75.8	0.791	2
101	ACM 24-2	1	R(m)	24	35	123.6	119.0	1.039	75.8	0.791	2
102	ACM 36-1	1	R(m)	36	54.25	108.2	119.0	0.909	75.8	0.528	2
103	ACM 36-2	1	R(m)	36	54.25	115.8	119.0	0.973	75.8	0.528	2
104	ASM 24-1	1	R(m)	24	35	118.1	119.0	0.992	75.8	0.609	2
105	ASM 24-2	1	R(m)	24	35	126.8	119.0	1.066	75.8	0.609	2
106	ASM 36-1	1	R(m)	36	54.25	115.3	119.0	0.969	75.8	0.406	2
107	ASM 36-2	1	R(m)	36	54.25	112.9	119.0	0.949	75.8	0.406	2
108	ANM 12-1	1	R(m)	12	15.75	118.8	119.0	0.999	75.8	1.053	2
109	ANM 12-2	1	R(m)	12	15.75	115.8	119.0	0.973	75.8	1.053	2
110	ANM 24-1	1	R(m)	24	35	124.8	119.0	1.049	75.8	0.526	2
111	ANM 24-2	1	R(m)	24	35	119.2	119.0	1.001	75.8	0.526	2
112	ANM 36-1	1	R(m)	36	54.25	118.1	119.0	0.992	75.8	0.351	2
113	ANM 36-2	1	R(m)	36	54.25	119.7	119.0	1.006	75.8	0.351	2
114	BCC 20a-1	1	R(c)	22	15	86.6	89.2	0.971	56.8	1.031	2
115	BCC 20a-2	1	R(c)	22	15	86.6	89.2	0.971	56.8	1.031	2
116	BCC 20b-1	1	R(c)	22	22.5	91.2	89.2	1.022	56.8	1.031	2
117	BCC 20b-2	1	R(c)	22	22.5	93.0	89.2	1.043	56.8	1.031	2
118	BCC 20c-1	1	R(c)	22	30	90.6	89.2	1.016	56.8	1.031	2
119	BCC 20c-2	1	R(c)	22	30	89.0	89.2	0.998	56.8	1.031	2

Notes:
* R(c) = Carbon rivet; R(m) = Manganese rivet

did not completely eliminate the bending effect of the lap-and open-shingle splice, the quantity of these tests is small compared to the quantity of butt-splice connection tests, so that their overall effect is very limited. The available data for the 40 tests conducted by Davis et al. (1940) are in Table 2. As expected, there are a few data points that are randomly scattered throughout the plot. Because 22 data points are concentrated at 10.5 in., they have been distributed to 9.5 in., 10.5 in. and 11.5 in. for clarity. The bottom of the vertical scale is also truncated to spread out the data.

Figure 3 shows a plot of the test data, where the test data are identified relative to the connection's strength and quasi-stiffness characteristics (developed later in this paper). A review of Figure 3 indicates that the test results fall into groupings that suggest different design criteria for different connection lengths—as indicated by the earlier AISC and RCSC step function, which is shown in Figure 2. It appears that there is a band of data above the $0.90P_{TEST}/P_{PRED}$ level that extends across the full range of connection lengths. However, there is another group of data that slopes downwards between approximately 15 in. and approximately 40 in. After 40 in., the boundary line is a minimum of approximately $0.60P_{TEST}/P_{PRED}$.

The earlier research identified the connection net section, A_n , as a significant variable. Similarly, the total area, A_s , of all the bolt shear planes was also found significant. A ratio of

A_n/A_s in some form was reported in each document. The test results, as clearly reported in the *Guide*, demonstrated that as A_n/A_s increased, the connection performance P_{TEST}/P_{PRED} also improved.

Recently, Moore et al. (2008) reported results that included tests on 1,533 high-strength bolts. The program included ASTM A325, A490, F1852 and F2280 bolts. The latter two are nominally referred to as tension control bolts and are comparable to A325 and A490 bolts, respectively. The program reported on both threads included in the shear plane as well as threads excluded from the shear plane. Tension tests were also performed to calibrate the various lots of bolts. Compared to the earlier Lehigh tests (e.g., Fisher et al., 1963), these bolts were tested in the snug-tight condition and not fully pretensioned. The results indicate that manufactured bolts have reasonably uniform properties as compared to an assembled connection and therefore warrant consideration of a lower target reliability, β .

Based on the data for bolt shear with threads excluded, a β of 4.0 was obtained by Moore et al. (2008) for a live to dead load ratio of 3.0. A resistance factor, ϕ , of 0.85 was obtained for the same condition. Thus, the current AISC/RCSC ϕ of 0.75 appears to be conservative. This observation was considered, along with other factors, when proposed revisions to the AISC and RCSC provisions were developed.

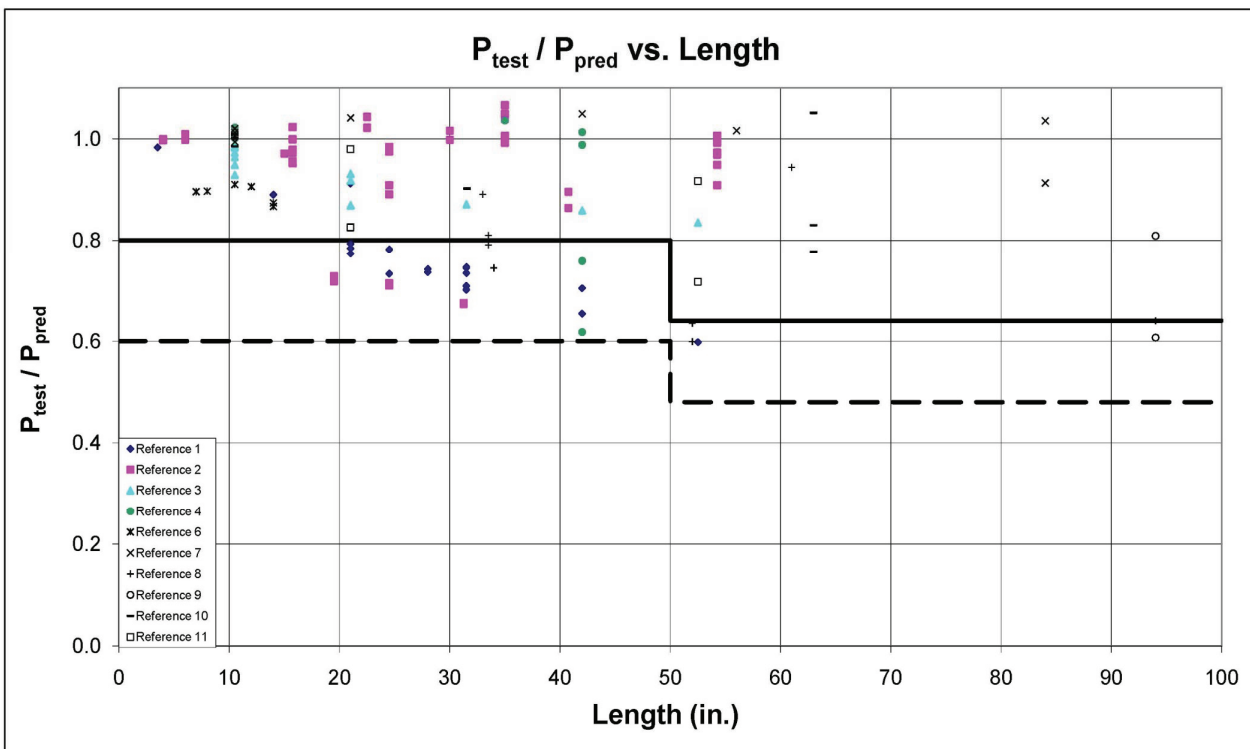


Fig. 2. Results of 119 connection tests with current design criteria superimposed.

DESIGN CRITERIA

The test data that are plotted above the $0.90P_{TEST}/P_{PRED}$ level, in Figure 3, indicate that under certain conditions there is no reduction in connection capacity regardless of the connection length. As previously noted, early research showed that as the ratio A_n/A_s increased, connection capacity also increased. A review of the test data indicated that there was a better correlation when the following ratios were compared to the P_{TEST}/P_{PRED} ratio:

$$\frac{A_n F_{up}}{A_s F_v} = N_1 \quad (3)$$

and

$$\frac{A_g F_{yp}}{A_s F_v} = N_2 \quad (4)$$

where

- A_g = gross area of connection material, in.²
- A_n = net area of connection material, in.²
- A_s = total bolt area in shear plane, in.²
- F_{up} = nominal tensile strength of connection material, ksi
- F_{yp} = yield stress of connection material, ksi
- F_v = ultimate shear strength of the bolt, ksi
- N_1, N_2 = target ratios, selected considering test data or specification criteria

Equation 3 represents, in non-dimensional form, the net section of a connection, and Equation 4 represents, in non-dimensional form, the gross section of the connection. Equation 3 can be considered to represent a strength relationship. Similarly, Equation 4 can be considered to represent a quasi-stiffness concept, because as the ratio increases, the plates essentially remain elastic as the ultimate shear strength of the bolt is reached. These are not unfamiliar concepts, because checking the net and gross sections of a connection has been part of AISC specifications for years. The numerical values of N_1 and N_2 must be chosen to satisfy both the test data and Chapter D of the AISC *Specification*.

For design purposes, it is more appropriate to rearrange Equations 3 and 4, substituting nominal values for ultimate values, e.g., replacing F_v with $R_1 F_u$, taking R_1 as 0.625. The procedure is shown in Appendix A, which evaluates the net and gross section requirements of Chapter D of the AISC *Specification*, taking the length reduction factor, R_2 , as 0.90. The computed values for N_1 and N_2 are determined to be 0.56 and 0.47, respectively. Coincidentally, the 0.56 value for N_1 is equivalent to a P_{TEST}/P_{PRED} ratio of 0.90 (shown by the horizontal line in Figure 3).

The general forms of the design equations in Appendix A follow as Equations 5 and 6. Because of the uncertainties associated with bolt installation (pretensioned versus snug-tight), second-order effects, and the dictated resistance

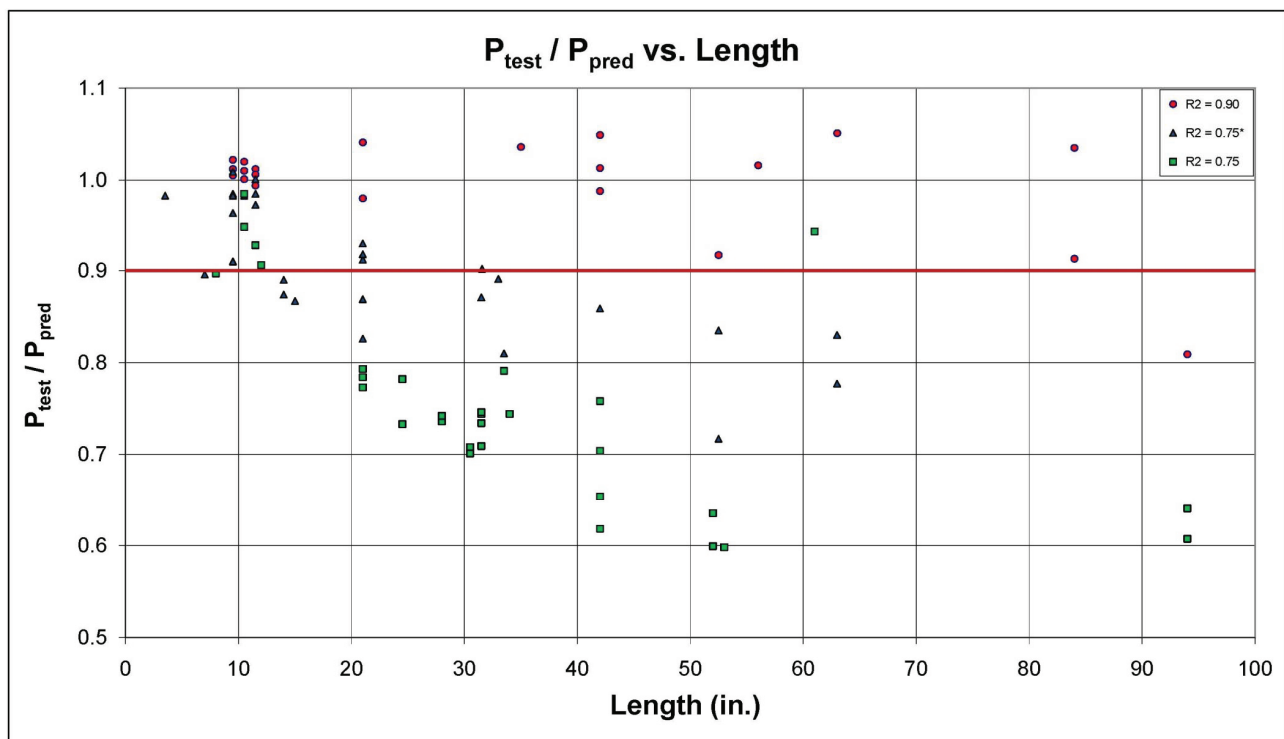


Fig. 3. Test results (79) identified by strength and quasi-stiffness criteria.

factors, N_2 was set equal to N_1 at a common value of 0.56. Solving for the net and gross areas so that the predicted P_{TEST}/P_{PRED} ratio will exceed 0.90 yields:

$$A_n \geq 0.56A_s F_u / F_{up} \quad (5)$$

and

$$A_g \geq 0.56A_s F_u / F_{yp} \quad (6)$$

where F_u is the nominal tensile strength of the bolt in ksi. The 0.56 factor results from the product of 0.625 and 0.90 ($R_1 \times R_2$) rounded to two significant figures.

The values for A_n and A_g , as well as the computed values for Equations 5 and 6, are shown in Table 1 for the test data. Because the shear strength of the bolts was established in the research reports, there was no need to convert the bolt tensile strength to the bolt shear strength. When the data were tabulated, three conditions were identified. The first condition was when both net and gross area, A_n and A_g , exceeded the respective inequalities shown in Equations 5 or 6, respectively. These P_{TEST}/P_{PRED} data are shown as circles in Figure 3. The second condition was when only one of the two inequalities was exceeded. Typically it was the net area, A_n , and these are shown with triangles in Figure 3. The third condition was when neither inequality was satisfied, and these are shown as squares in Figure 3. The letters C, T and S are used in to R_2 column and footnote of Table 1 to identify the shape of the data point in Figure 3.

With the exception of the one test at 94 in., all of the test results out of the 21 shown as circles satisfied both inequalities and had P_{TEST}/P_{PRED} ratios greater than 0.90. This one test, No. 66, with a P_{TEST}/P_{PRED} ratio of 0.809, was for an ASTM A502 Grade 1 rivet with ASTM A572 connection plates. The other 20 tests had P_{TEST}/P_{PRED} ratios that varied from 0.913 to 1.051.

The next group of bolts consists of 28 test results where only one inequality was satisfied, shown as triangles. Only 26 test data show up in Figure 3 because in two cases, both at a connection length of 10.5 in., the test results were essentially identical. Twenty-three of these data had connection lengths less than 38 in. and 14 were less than 14 in. For the short connection lengths the test data fall above or very close to the $0.90P_{TEST}/P_{PRED}$ line.

There are 30 test results shown as a square in Figure 3, where neither inequality was satisfied. Only 29 squares are evident because there is a duplicate at 31.5 in. The one test data at 61 in. for an enclosed shingle connection with a P_{TEST}/P_{PRED} ratio of 0.944 is an anomaly. A review of the original research data did not identify any obvious inconsistency. The square and triangular data indicate that between approximately 21 in. and 42 in. there is a transition in connection behavior depending on the material properties and plate area (A_g , A_n) proportions relative to the total bolt shear area, A_s .

DESIGN EQUATIONS

A practical approach must be chosen to satisfy the needs of design office, detailer and fabrication requirements. For shear connections with lengths less than approximately 15.5 in., a basic reduction factor R_2 of 0.90 is recommended to account for variability in connection behavior. This is an increase from the current basic reduction factor value of 0.80, resulting in a 12.5% increase in bolt capacity from current methods for “short” connections. The resistance factor, ϕ , of 0.75 is still appropriate.

The increase in R_2 is considered appropriate because all of the tests were uni-axial, whereas actual connections typically have a nominal bi-axial contribution. Finite element studies have demonstrated this effect for shear and bending at the end of both simply-supported and fixed-end beams. Similarly, the connections at the ends of diagonals in long span trusses, although designed with pin ends, actually have some bending due to transverse differential displacements at their ends as the truss deflects under load.

For connection lengths greater than 15.5 in. but less than 28.8 in., R_2 could be taken as a function of connection length as follows:

$$R_2 = 1.075 - 0.0113L \quad (7)$$

R_2 is limited to a minimum of 0.75. Beyond approximately 28.8 in. there is a constant strength reduction, R_2 , of 0.75. With the application of $\phi = 0.75$, the overall bolt design value is less than all of the test data considered, whether bolt, rivet or Huck connector. Connection lengths greater than 28.8 in. result in a nominal bolt strength increase of 17.2% compared to current practice, because the length reduction factor would increase from 0.64 to 0.75.

With the foregoing design criteria in mind, and observing the distribution of the test data in Figures 2 and 3, a simplified design criterion was chosen. An initial straight line with a constant R_2 of 0.90 extending to 38 in. was chosen. Next is a step function that drops to 0.75. Thereafter, R_2 remains constant at 0.75 for connection lengths greater than 38 in. These design equations are shown graphically in Figure 4, where they are superimposed on the data of Figure 2. In both cases ϕ remains at 0.75. The proposed design criteria are compatible with the theoretical results shown in Figure 5.18 of the *Guide* (Kulak et al., 1987).

The 38-in. length was arbitrarily chosen because it was not a multiple of any of the standard bolt gage spacings and was less than 42 in. The 42-in. length represents the beginning of the lower plateau for test results. Once again the resulting final design criterion is less than the least of the test data. Using the proposed criteria, a revision to the bolt shear portion of AISC *Specification* Table J3.2, is presented in Table 3. Similar revisions to RCSC Table 5.1 for ASTM A325 and ASTM A490 bolts are appropriate.

Table 3. Proposed Bolt Shear Revisions to AISC Table J3.2		
Nominal Shear Stress in Bearing-Type Connection, F_{nv} (ksi)		
Bolt Type	Less than 38 in.	38 in. and greater
A307	27	23
A325 threads included	54	45
A325 threads excluded	68	56
A490 threads included	68	56
A490 threads excluded	84	70
Threaded rods threads included	$0.45F_u$	$0.375F_u$
Threaded rods threads excluded	$0.563F_u$	$0.469F_u$

The historical tests were performed on fully tightened high-strength bolts with hardened washers using the turn-of-nut method. A high degree of slip resistance (friction) was achieved. The effect of pretensioned bolts is demonstrated by examining Figure 3. The eight test data identified by a circle with connection length greater than 38 in. and above the 0.90 horizontal line indicate that the shear strength of all bolts was reached. In Table 4 the ratio of connection net area divided by Equation 5 is greater than 1.0 with an

average value of 1.43 and a standard deviation of 0.24. Similar results for the less critical gross area represented by Equation 6 yield an average value of 1.32 and a standard deviation of 0.26. With a connection frictional component of approximately 30%, these relationships would indicate that all the bolt shear strength would be fully engaged at the connection's ultimate load.

With the use of snug-tight bolts there is effectively no frictional component to the connection capacity. Regardless, the

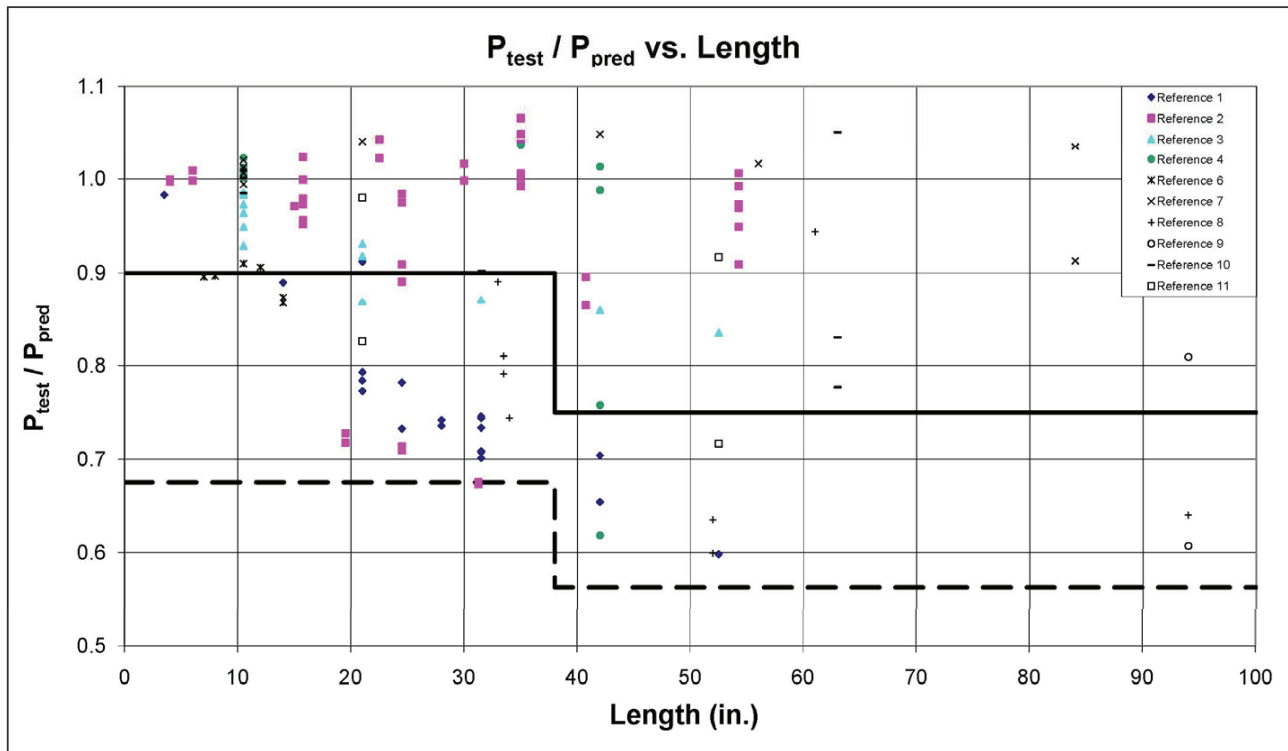


Fig. 4. Proposed design criteria superimposed on 119 connection test results.

Test No.	Length (in.)	$\frac{P_{TEST}}{P_{PRED}}$	A_g (in.)	Eq. 6 (in. ²)	$\frac{A_g}{Eq. 6}$	A_n (in. ²)	Eq. 5 (in. ²)	$\frac{A_n}{Eq. 5}$
9	42	1.013	33.6	30.5	1.10	29.8	17.6	1.69
10	42	0.988	29.8	25.7	1.16	26.1	14.8	1.76
16	42	1.049	28.6	19.7	1.45	23.7	18.5	1.28
79	52.5	0.917	107.4	60.4	1.78	46.2	36.0	1.28
17	56	0.989	20.4	16.1	1.27	18.5	15.1	1.23
51	63	1.051	33.8	33.0	1.02	30.0	18.7	1.60
18	84	0.913	28.4	23.7	1.20	24.6	22.2	1.11
19	84	1.035	37.6	23.7	1.59	33.7	22.2	1.52
Average					1.32			1.43
Standard Deviation					0.26			0.24

test results can still be used for snug-tight bolted connections because the frictional component is offset by using a reduced ϕ of 0.75 from 0.85 (Moore et al., 2008), a reduction of 13%; and by limiting the connection length reduction factor, R_2 , to 0.90 from 1.0 (the single-bolt connection case), a reduction of 11%. In addition, the coefficient N_2 in Equation 6 was increased from 0.47 to 0.56 (19%), reducing the stress on the plates and more uniformly distributing the force to the bolts. As reported in the literature (Fisher and Kulak, 1968), the bolts were ordered and supplied near the low end of the applicable ASTM standard. In comparison, it is likely that the average production bolt will have a slightly higher ultimate strength. All of these factors would justify not having a length reduction factor less than 0.90 for connections exceeding 38 in. The coefficients could be fine tuned by performing a limited number of tests. However, the proposed step function is conservative.

The proposed design criteria do not require any appreciable difference in design methodology from current methods. The only new item is that the total bolt shear area, A_s , has to be computed. Because A_s reflects the number of bolts in the connection times the shear area (a function of the bolts being in single or double shear, including or excluding the threads), it is a number that the connection designer already has available. The design equation is a modification of Equation 1 as follows:

$$P_n = P_u A_b R_1 R_2 R_3 \quad (8)$$

The value of R_2 is either 0.90 or 0.75 depending on the connection's strength and quasi-stiffness as well as whether the connection has a length greater than 38 in.

Bolt Shear Design Sequence

1. Determine design load, P .
2. Initially assume maximum bolt capacity and $L \leq 38$ in. Select ASTM A325 or A490 bolts, bolt diameter, thread condition (included or excluded), and single or double shear to obtain V_n .
3. Determine number of bolts by dividing P by V_n .
4. Calculate A_s , considering thread condition (included or excluded) and single or double shear.
5. Choose a bolt pattern and determine the connection length, L .
6. If $L \leq 38$ in., the design is complete for bolt shear. If $L > 38$ in., continue.
7. Compute A_g and A_n .
8. Check Equations 5 and 6 ($L > 38$ in.):
Equation 5: $A_n \geq 0.56A_s F_u / F_{up}$
Equation 6: $A_g \geq 0.56A_s F_u / F_{yp}$
9. If A_g and A_n criteria are not satisfied, revise bolt capacity for $L > 38$ in. criteria and recompute the number of bolts.
10. Size splice plates to satisfy main member requirements.

Connection Length (in.)	R_2	No. of Tests	Mean Value	Std. Dev.	Reliability (β)				Resistance (ϕ)			
					Live/Dead Load Ratio (L_n/D_n)				Live/Dead Load Ratio (L_n/D_n)			
					2	3	4	5	2	3	4	5
10.5	0.80	21	0.988	0.0293	5.5	5.1	5.0	4.8	0.933	0.949	0.958	0.963
21.0	0.80	9	0.893	0.0889	4.4	4.2	4.1	4.1	0.807	0.818	0.825	0.829
31.5	0.80	7	0.772	0.0804	3.7	3.6	3.5	3.4	0.731	0.738	0.743	0.746
42.0	0.80	7	0.848	0.176	3.2	3.1	3.1	3.1	0.714	0.718	0.721	0.723
52.3	0.64	7	0.756	0.159	3.5	3.5	3.4	3.4	0.757	0.762	0.766	0.768
62.0	0.64	4	0.901	0.122	5.1	4.9	4.8	4.7	0.897	0.912	0.921	0.928
94.0	0.64	2	0.624	0.0233	4.2	4.0	3.9	3.8	0.781	0.790	0.795	0.798

Notes:
* Rivet tests not included in these values
 $\phi_{average} = 0.814$

RELIABILITY

With the bolt shear strength design criteria established, it is now possible to evaluate the results in terms of LRFD concepts. The reliability, β , is determined using the equation:

$$\beta = \frac{\ln\left(\frac{\bar{R}}{\bar{Q}}\right)}{\sqrt{V_R^2 + V_Q^2}} \quad (9)$$

and the corresponding resistance factor, ϕ , is determined using the equation:

$$\phi = \left(\frac{R_m}{R_n}\right) e^{-0.55\beta V_R} \quad (10)$$

In Equation 10, ϕ is dependent on knowing β . Similarly, when the step-by-step-procedures are followed in Equation 9, ϕ is required to solve for β . This dilemma is resolved by using the current $\phi = 0.75$ from the AISC *Specification*. A step-by-step solution for these equations and explanation of terms is given in Appendix B using criteria established by Fisher et al. (1978).

There are two procedures that can be followed to determine β . One approach would be to establish a least-square determination of the P_{TEST}/P_{PRED} relationships relative to the overall connection length and solve for one β for the total database. The second approach would determine β at discrete connection lengths that have adequate test results. The first procedure has the advantage of using more test data in one computation; however, large amounts of data at one length can disproportionately mask other issues. The second procedure was used in this study to try to identify significant variables from the multitude that were identified in the testing programs.

The critical issue was the importance of connection strength and quasi-stiffness as the connection became longer. Once the connection strength and quasi-stiffness exceeded a predetermined amount, length was no longer a variable in the performance of the connection. As a result, the test data was examined for both cases: first, by examining the data from the test results above the $0.90P_{TEST}/P_{PRED}$ ratio, and then by examining the data excluding the test results above the $0.90P_{TEST}/P_{PRED}$ ratio.

The current design criteria were examined for all the applicable bolt test data for nominal live load (L_n) to dead load (D_n) ratios of 2.0 to 5.0. The results for β and ϕ are given in Table 5. Because of the scatter in test data, β is quite variable and ranges from 3.1 to 5.5. It is not surprising that short connections have a high β value because connection length is not really a variable, although a 0.75 reduction factor is mandated. A similar spread in ϕ was also obtained, ranging from 0.714 to 0.963, with a high average value of 0.814. This would suggest that the bolt shear design criteria could be increased.

A review of reliability, β , for the CSA S16 (CSA, 2001, 2005) and Eurocode EN 1933 (CEN, 2003) criteria shown in Table 6 will reinforce the understanding that increasing bolt strength with bolt diameter is not justified. For 1-in.-diameter bolts, the β values drop to approximately 2.0 for a live to dead load ratio of 5.0. When the β values are computed for 1½-in.-diameter bolts, the value drops to 1.9, an unacceptably low value. Although 1½-in.-diameter bolts were not tested, the computed β values are sufficiently accurate because the test data have been converted to a non-dimensional format. The ¾-in., 1-in. and 1½-in. bolt data indicate that the non-dimensional concept appears reasonable. The CSA S16 document uses a ϕ of 0.80.

Bolt Dia. (in.)	Connection Length (in.)	Live/Dead Load Ratio				ϕ Avg.
		2	3	4	5	
1	10.5	3.8	3.6	3.4	3.4	0.82
	21.0	3.1	2.9	2.9	2.8	0.74
	31.5	2.6	2.5	2.5	2.4	0.70
	42.0	2.6	2.5	2.5	2.5	0.72
	52.3	2.3	2.3	2.3	2.3	0.70
	62.0	3.9	3.7	3.6	3.6	0.85
1½	94.0	2.9	2.7	2.6	2.6	0.72
	10.5	3.8	3.6	3.4	3.4	0.82
	21.0	2.9	2.8	2.7	2.7	0.73
	31.5	2.4	2.3	2.2	2.2	0.67
	42.0	2.3	2.2	2.2	2.2	0.69
	52.3	2.0	2.0	2.0	1.9	0.66
	62.0	3.3	3.2	3.1	3.1	0.78
94.0	2.8	2.6	2.6	2.5	0.71	

* $\phi = 0.80$ in CSA-S16

Connection Length (in.)	R_2	No. of Tests	Mean Value	Std. Dev.	Reliability (β)				Resistance (ϕ)			
					Live/Dead Load Ratio (L_n/D_n)				Live/Dead Load Ratio (L_n/D_n)			
					2	3	4	5	2	3	4	5
10.5	0.90	21	0.988	0.0293	4.8	4.6	4.4	4.3	0.856	0.868	0.875	0.879
21.0	0.90	9	0.893	0.0889	3.9	3.7	3.6	3.6	0.747	0.755	0.760	0.763
31.5	0.90	7	0.772	0.0804	3.2	3.1	3.0	3.0	0.677	0.682	0.685	0.687
42.0	0.75	7	0.848	0.176	3.4	3.4	3.3	3.3	0.740	0.745	0.748	0.751
52.3	0.75	7	0.756	0.159	3.0	2.9	2.9	2.9	0.693	0.696	0.698	0.699
62.0	0.75	4	0.901	0.122	4.4	4.2	4.1	4.1	0.813	0.824	0.831	0.835
94.0	0.75	2	0.624	0.0233	3.4	3.2	3.1	3.1	0.696	0.701	0.704	0.707

Notes:
* Rivet tests not included in these values
 $\phi_{average} = 0.754$

The proposed AISC/RCSC design criteria, all the reported bolt test data, and the computed β and ϕ values are given in Table 7. The range in β values has been reduced to 2.9 to 4.8. The test data ratios of P_{TEST}/P_{PRED} that are still above 0.90 result in a large coefficient of variation resulting in the low values for the 52.3 in. connection length. As previously mentioned, high-strength bolts are a manufactured product, which suggests that a β of approximately 3.0 would be acceptable. The resistance factor, ϕ , has a similar variation in

value because of the test results. The magnitude of the values is centered, average 0.754, on the starting value of 0.75. This indicates that appropriate adjustments have been made to the current design criteria.

The final set of computations included only the test data that exhibited a change in performance with connection length. The test data with a P_{TEST}/P_{PRED} ratio above 0.90 were excluded. These β and ϕ results are shown in Table 8. Once the high P_{TEST}/P_{PRED} data are removed from the calculations, the

Table 8. Reliability (β) and Resistance (ϕ) Values with Limited P_{TEST}/P_{PRED} Data (< 0.90)*

Connection Length (in.)	R_2	No. of Tests	Mean Value	Std. Dev.	Reliability (β)				Resistance (ϕ)			
					Live/Dead Load Ratio (L_n/D_n)				Live/Dead Load Ratio (L_n/D_n)			
					2	3	4	5	2	3	4	5
10.5	0.90	0	—	—	—	—	—	—	—	—	—	—
21.0	0.90	4	0.813	0.0438	3.7	3.6	3.5	3.4	0.731	0.738	0.742	0.745
31.5	0.90	6	0.751	0.0618	3.2	3.1	3.0	2.9	0.676	0.681	0.684	0.686
42.0	0.75	4	0.722	0.108	3.3	3.2	3.2	3.1	0.701	0.706	0.710	0.712
52.3	0.75	5	0.677	0.101	3.0	3.0	2.9	2.9	0.675	0.679	0.682	0.684
62.0	0.75	2	0.804	0.0385	4.6	4.4	4.3	4.2	0.830	0.841	0.848	0.852
94.0	0.75	2	0.624	0.0233	3.4	3.2	3.1	3.1	0.696	0.701	0.704	0.707

Notes:
 * Rivet tests not included in these values
 $\phi_{average} = 0.726$

β values ranged from 2.9 to 4.6. The β of 2.9 does not change because at 52.3 in. there was no data above 0.90. As previously explained, for a manufactured product, a β of 2.9 is acceptably close to the target value of 3.0. This change is reflected in the resistance factor, ϕ , that on average (0.726) is below the starting value of 0.75. The difference is not significant.

SUMMARY AND CONCLUSIONS

A review of the historic research test data was made to determine bolt shear strength in terms of LRFD principles. A total of 119 connection tests were identified. Of these, 40 tests were with rivets associated with the design and construction of the San Francisco–Oakland Bay Bridge. Unfortunately, insufficient information was reported to allow full utilization of the test data. Of the remaining 79 connection tests, the connector distribution was 54 with ASTM A325 bolts, 18 with ASTM A490 bolts, 5 with rivets, and 2 with Huck bolts. The statistical analysis was performed using the ASTM A325 and A490 bolts. Subsequently, it was possible to show that the rivet and Huck bolt test data were compatible with the recommended design criteria.

Because of the many connection variables, the test data were reduced to a non-dimensional form to limit the significance of all the variables. As a result, the connection length remained as the desired and predominate independent variable. Recent tests sponsored by RCSC also indicated that the reliability, β , of the shear strength of bolts was similar to plates and shapes reported in earlier literature. Based on other anecdotal information there does not appear to be any justification to change the current resistance factor, ϕ .

In addition to the AISC/RCSC design criteria, the equivalent Canadian CSA and Eurocode provisions were examined.

The CSA S16 provision was identical to and transferred from the Eurocode document. The two key issues in these provisions are variable and decreasing bolt shear strength with increasing connection length and increasing bolt shear strength with increasing diameter. The reviewed test data indicate that the first issue is justified, although the benefit gained by having a sliding scale is probably not justified relative to the complexity. The second issue is the increasing bolt shear strength with increasing diameter, which is not justified by the test data and at large bolt diameters results in unacceptably low reliability, β .

The current LRFD principles have a target reliability, β , of approximately 4.0 for connections, which include slip-critical connections and bolt-bearing connections. In comparison, the target β for main members—a manufactured product—typically have β of approximately 3.0, or slightly lower. Because the bolt itself is a manufactured product, there is some leeway as to what β is acceptable for bolts. As a practical consideration, it is reasonable to use a common resistance factor, ϕ , value of 0.75 for slip critical connections, bolt bearing connections, and for this study of bolt shear strength.

The current AISC/RCSC design criteria result in variable β from 3.1, and in some cases, to a conservatively high value of 5.5. In comparison, the proposed design criteria β range from 2.9 to 4.8. When the P_{TEST}/P_{PRED} test data above 0.90 are excluded, the range for β becomes 2.9 to 4.6. The short connection values for β are going to be high because the test results are for axially loaded specimens and do not include the secondary forces associated with biaxial beam end reactions or adjacent truss-panel-point relative displacement. The effect of pretensioned bolts versus snug tight bolts has not been directly evaluated.

The proposed criteria have a step function at 38 in. to permit an initial length reduction factor, R_2 , increase from 0.80 to 0.90. This represents a 12.5% increase in bolt shear strength. Beyond 38 in., the length reduction factor is increased from 0.64 to 0.75, a 17.2% increase. As a result, the proposed design procedure is identical to the current requirements except with an increased bolt shear design value and a step function at 38 in. instead of 50 in.

An unexpected result of the study was the realization that under circumstances of sufficient connection strength, represented by the net area, A_n , and in conjunction with sufficient connection quasi-stiffness, represented by the connection gross area, A_g , in comparison to the total bolt shear area, A_s , there would be no need for a connection strength reduction less than 0.90 with increasing length. This condition exists when the inequalities expressed in Equations 5 and 6 are satisfied. Equation 6 is not exactly a stiffness criterion, but it indicates that the connection plates remain essentially elastic as the bolt ultimate shear strength is reached.

Because the historical tests were performed on fully tightened high strength bolts, the use of Equations 5 and 6 when snug-tight bolts are used has not been experimentally confirmed. However, the strength component attributed to friction has been offset by the reduced ϕ of 0.75 (13%), limiting the connection capacity ratio to 0.90 (11%) and increasing the gross area coefficient requirement in Equation 6 from 0.47 to 0.56 (19%). In addition, the statistical bolt strength will be somewhat higher than the research programs intentional use of low end bolt strength. Performing a few tests would quantify and refine the N_1 and N_2 coefficients.

The statistical study was based on ASTM A325 and A490 bolts; however, when the limited rivet and Huck bolt data were compared with the bolt results, no inconsistency was found. Similarly, the connection plate material varied from relatively low-strength ASTM A7 steel to high-strength ASTM A514 steel with intermediate-strength ASTM A440 and A572 steel in between, again with no inconsistencies. This would indicate that the data in a non-dimensional format did not have any apparent bias and indicates that the procedure is acceptable for all current grades of connectors, plates and shapes. In conclusion, the proposed design criteria are essentially identical to the current provisions except the bolt strengths are adjusted slightly upwards, resulting in a more uniform reliability, β , closer to the professionally accepted values. In addition, Equations 5 and 6 provide a means of proportioning a connection to gain optimum bolt shear strength.

ACKNOWLEDGMENTS

The author wishes to acknowledge several colleagues who assisted him in this bolted connection study: T.V. Galambos, who set up the reliability procedure that was used to calibrate β ; J.A. Yura, who made several meaningful

suggestions; D.D. Crampton, who performed all the spreadsheet iterations to locate the preferred design criteria; and finally, W.F. Baker, R.B. Johnson, M.V. Holland, L.S. Muir, and A. Vercellino, who provided examples of large connections.

REFERENCES

- AISC (2005), *Specification for Structural Steel Buildings*, American Institute of Steel Construction, Chicago, IL.
- Bendigo, R. A., Hansen, R.M. and Rumpf, J.L. (1963), "Long Bolted Joints," *Journal of the Structural Division*, ASCE, Vol. 89, No. ST6, Proc. Paper 3727, December. (Reference 1 in Figures 2 and 4.)
- CEN (2003), *Eurocode 3: Design of Steel Structures*, EN 1993, European Committee for Standardization, Brussels, Belgium.
- CSA (2001), *Limit States Design of Steel Structures*, CSA-S16-01, Canadian Standards Association, Rexdale, Ontario, Canada.
- CSA (2005), *Supplement 1 to CAN/CSA-S16-01, Limit States Design of Steel Structures*, CSA S16s1-05, Canadian Standards Association, Rexdale, Ontario, Canada.
- Davis, R. E., Woodruff, G.B. and Davis, H.E. (1940), "Tension Tests of Large Riveted Joints," *Transactions*, ASCE, Vol. 105, p. 1193. (Reference 2 in Figures 2 and 4.)
- Fisher, J.W., Galambos, T.V., Kulak, G.L. and Ravindra, M.K. (1978), "Load and Resistance Factor Design Criteria for Connectors," *Journal of the Structural Division*, ASCE, Vol. 104, No. ST9, September.
- Fisher, J.W., Ramseier, P.O. and Beedle, L.S. (1963), "Strength of A440 Steel Joints Fastened with A325 Bolts," *Publications*, IABSE, Vol. 23. (Reference 3 in Figures 2 and 4.)
- Fisher, J.W. and Kulak, G.L. (1968), "Tests of Bolted Butt Splices," *Journal of the Structural Division*, ASCE, Vol 94, ST11, November. (Reference 4 in Figures 2 and 4.)
- Fisher, J.W. and Yoshida, N. (1970), "Large Bolted and Riveted Shingle Splices," *Journal of the Structural Division*, ASCE, Vol 96, No. ST9, Proc. Paper 7534, Sept., pp. 1903-1918. (Reference 5 in Figures 2 and 4.)
- Foreman, R.T. and Rumpf, J.L. (1961), "Static Tension Tests of Compact Bolted Joints," *Transactions ASCE*, Vol. 126, p. 228. (Reference 6 in Figures 2 and 4.)
- Kulak, G.L. and Fisher, J.W. (1968), "A514 Steel Joints Fastened by A490 Bolts," *Journal of the Structural Division*, ASCE, Vol. 94, ST10, October. (Reference 7 in Figures 2 and 4.)
- Kulak, G.L., Fisher, J.W. and Struik, J.H.A. (1987), *Guide Design Criteria for Bolted and Riveted Joints*, 2nd edition, John Wiley and Sons, New York, NY.

Moore, A.M., Rassati, G.A. and Swanson, J.A. (2008), "Evaluation of the Current Resistance Factors for High Strength Bolts," Final report submitted to the Research Council on Structural Connections.

Power, E.H. and Fisher, J.W. (1972), "Behavior and Design of Shingle Joints," *Journal of the Structural Division*, ASCE, Vol. 98, No. ST9, September. (Reference 8 in Figures 2 and 4.)

RCSC (2004), *Specification for Structural Joints Using ASTM A325 or A490 Bolts*, Research Council on Structural Connections, Chicago, IL.

Rivera, U. and Fisher, J.W. (1970), "Load Partition and Ultimate Strength of Shingle Joints," *Fritz Laboratory Report 340.6*, Lehigh University. (Reference 9 in Figures 2 and 4.)

Sterling, G.H. and Fisher, J.W. (1965) "Tests of Long A440 Steel Bolted Butt Joints," *Fritz Engineering Laboratory Report No. 288.26*, Lehigh University. (Reference 11 in Figures 2 and 4.)

Sterling, G.H. and Fisher, J.W. (1966), "A440 Steel Joints Connected by A490 Bolts," *Journal of the Structural Division*, ASCE, Vol. 92, No. ST3, Proc. Paper 4845, June. (Reference 10 in Figures 2 and 4.)

APPENDIX A

AISC SPECIFICATION SECTION D2

Plate Yielding

Use Equation D2-1 from the 2005 AISC *Specification*:

$$P_n = F_y A_g$$

The design tensile strength of the plate is $\phi_t P_n$ and $\phi_t = 0.90$. Thus,

$$\phi_t P_n = \phi_t F_y A_g$$

For bolts, the design shear strength is $\phi_b P_n$, with $\phi_b = 0.75$. Also, $P_n = P_u R_1 R_2$, assuming threads excluded from the shear plane. We also know that $P_u = F_u A_s$. Substituting, we have:

$$\phi_b P_n = \phi_b (P_u R_1 R_2) = \phi_b (F_u A_s) R_1 R_2$$

R_1 has been established at 0.625. Take R_2 as 0.90 by assuming $L < 38$ in., avoiding reducing R_2 from 0.90 to 0.75 for $L > 38$ in.

Equating the bolt shear strength to the plate yield strength (with F_{yp} the yield stress of the plate):

$$\phi_b (F_u A_s) R_1 R_2 = \phi_t F_{yp} A_g$$

Solving for A_g ,

$$A_g = \frac{\phi_b F_u A_s R_1 R_2}{\phi_t F_{yp}} = \frac{0.75(F_u A_s)(0.625)(0.90)}{0.90 F_{yp}} = \frac{0.469 F_u A_s}{F_{yp}}$$

Bolt shear will control as long as:

$$A_g \geq \frac{0.469 F_u A_s}{F_{yp}}$$

Plate Fracture

Use Equation D2-2 from the 2005 AISC *Specification*:

$$P_n = F_u A_n$$

The design rupture strength of the plate is $\phi_t P_n$ and $\phi_t = 0.75$. Thus,

$$\phi_t P_n = \phi_t F_u A_n$$

Equating the bolt shear strength to the plate rupture strength (with F_{up} the rupture stress of the plate):

$$\phi_b (F_u A_s) R_1 R_2 = \phi_t F_{up} A_n$$

Solving for A_n and substituting as before, we obtain:

$$A_n \geq \frac{0.563 F_u A_s}{F_{up}}$$

Bolt shear will control over tensile rupture as long as this inequality is satisfied.

Notes:

1. A_s and F_u are bolt properties.
2. For design purposes, use a coefficient of 0.56 for both calculations (i.e., for N_1 and N_2) until further research quantifies pretensioning and second-order effects.

APPENDIX B

SAMPLE β CALCULATION FOR BOLT SHEAR

$$\beta = \frac{\ln\left(\frac{\bar{R}}{\bar{Q}}\right)}{\sqrt{V_R^2 + V_Q^2}}$$

where

- \bar{R} = mean resistance
- \bar{Q} = mean load effect
- V_R = coefficient of variation
- V_Q = coefficient of variation

$$\bar{R} = f\{\bar{R}_1, F_{UN}, R_p, R_M, R_F\}$$

where

- F_{UN} = nominal tensile strength of bolt
- \bar{R}_1 = ratio of shear to tensile strength = 0.625, $V_{\bar{R}_1} = 0.05$
- R_p = mean test value, V_{R_p} = ratio of standard deviation to mean test value
- R_M = fabricating factor = 1.20, $V_{R_M} = 0.07$
- R_F = fabricating factor = 1.00, $V_{R_F} = 0.02$

These data are from Fisher et al. (1978).

EXAMPLE

- $L = 42$ in., 7 tests
- $R_p = 0.848$, standard deviation = 0.1761

1. Mean Resistance

$$\begin{aligned} \bar{R} &= \bar{R}_1 R_p R_M R_F F_{UN} \\ \bar{R} &= (0.625)(0.848)(1.20)(1.00)F_{UN} = 0.6360F_{UN} \\ V_{R_p} &= 0.1761/0.848 = 0.2077 \\ V_R &= \sqrt{V_{\bar{R}_1}^2 + V_{R_p}^2 + V_{R_M}^2 + V_{R_F}^2} \\ V_R &= \sqrt{0.05^2 + 0.2077^2 + 0.07^2 + 0.02^2} = 0.2257 \end{aligned}$$

2. Mean Load Effect

$$\begin{aligned} D_N, L_N &= \text{nominal dead and live loads, respectively} \\ \bar{D} &= 1.05D_N, V_D = 0.10 \\ \bar{L} &= L_N, V_L = 0.25 \end{aligned}$$

For this example, assume $L_N/D_N = 3.0$

$$\begin{aligned} Q_N &= \text{nominal load effect} \\ &= 1.2D_N + 1.6L_N = D_N [1.2 + 1.6(L_N/D_N)] = 6.0D_N \\ \bar{Q} &= \text{mean load effect} \\ &= \bar{D} + \bar{L} \\ &= 1.05D_N + L_N = 1.05D_N + 3.0D_N = 4.05D_N \end{aligned}$$

$$\begin{aligned} V_Q &= \frac{\sqrt{(\bar{D}V_D)^2 + (\bar{L}V_L)^2}}{Q} \\ &= \frac{\sqrt{[(1.05D_N)(0.10)]^2 + [(3.00D_N)(0.25)]^2}}{4.05D_N} \\ &= 0.1870 \end{aligned}$$

3. Nominal Design Strength

In non-dimensional form, $R_N = \bar{R}_1 R_2 F_{UN}$, where R_2 is a design level criteria. The connection length is 42 in., which is greater than 38 in. Therefore, R_2 is taken as 0.75.

$$\begin{aligned} R_N &= (0.625)(0.75)F_{UN} \\ &= 0.4688F_{UN} \end{aligned}$$

Set ϕR_N equal to Q_N , with $\phi = 0.75$, and solve for D_N :

$$\begin{aligned} 0.75(0.4688F_{UN}) &= 6.0D_N \\ D_N &= 0.0586F_{UN} \end{aligned}$$

Now, calculate \bar{Q} :

$$\begin{aligned} \bar{Q} &= 4.05D_N \\ &= 4.05(0.0586F_{UN}) \\ &= 0.2373F_{UN} \end{aligned}$$

The reliability, β , may now be calculated:

$$\begin{aligned} \beta &= \frac{\ln\left(\frac{0.6360F_{UN}}{0.2373F_{UN}}\right)}{\sqrt{(0.2257)^2 + (0.1870)^2}} \\ &= \frac{0.9859}{0.2931} \\ &= 3.36 \end{aligned}$$

4. Resistance Factor, ϕ

$$\phi = \left(\frac{R_M}{R_N}\right) e^{-0.55\beta V_R}$$

- R_M = mean test value (R_p) from β calculations
- R_N = proposed design criteria, R_2
- β = from previous calculations (Step 3)
- V_R = coefficient of variation

$$\begin{aligned} \phi &= \left(\frac{0.848}{0.75}\right) e^{-[(0.55)(3.36)(0.2257)]} \\ &= (1.1307) e^{-0.417} \\ &= (1.1307)(0.659) \\ &= 0.745 \end{aligned}$$

Current Steel Structures Research

REIDAR BJORHOVDE

INTRODUCTION

Among the thorniest problems for researchers in general—and maybe for American structural engineering researchers in particular—is the subject of money, that is, research funding. This is especially acute for academic researchers under the current economic conditions, what with limited governmental and private research grants funding being further reduced or in many cases entirely eliminated. What many government leaders and business executives and accountants do not appear to understand is that when markets “turn south,” investment in research and marketing is more important than ever, for that is when the foundation is placed for rapid advances when business picks up again.

American university research and researchers are especially vulnerable, considering that funding must be obtained not just for graduate student support (commonly \$20,000 or more per year, to cover tuition and stipend), test specimens, equipment, and other legitimate expenses, but also to cover typically three months of income for the professor(s) as well as university overhead of 40% to 60% of the contract amounts. How many Americans know that university professors (like public school teachers) are paid only for nine months of the year and that the remainder of the annual income has to come from research funds or other sources? And if the researcher wants to advance in his or her academic career, research funding *must* be obtained to ensure that results, publications and recognition will be obtained for scientific achievement. In brief, an academic career without research and attendant evidence of scholarly success equals failure in most institutions, because teaching alone is simply not sufficient. You must demonstrate scholarly success, and that comes from successful research work.

The modus operandi is different for researchers and institutions in most other parts of the world, although there are some signs that universities in the U.K., for example, are looking at the American model as a means of reducing the demands on university budgets. In most of these other

locales, the research contract budgets do not need to cover the 25% of the professor’s annual salary, which means that the overall cost is reduced significantly. At the same time, the sheer size of the total American academic research undertaking dwarfs that of all other countries. So the rest of the world is working hard to catch up with the American research enterprise, which is still the most effective and powerful in the world. But the efforts within the European Union, for example, are notable and very impressive, as is the support offered in countries like China, Japan, Singapore and Australia. Therefore, unless American federal and state governments and industry are prepared to address the funding issue aggressively, the leading role of U.S. universities will be eroded—significantly. That will not be helpful to anyone, anywhere.

Many of the research studies presented here have been conducted in Europe, with financial support from various instances within the European Union. Some of these are typical of many current research projects in Europe, as they reflect collaboration between universities in different countries. For example, a study of the axial and flexural capacities of welded built-up box cross sections is a joint effort between institutions in Germany and Slovenia, and an examination of the buckling capacity of slender composite tubular columns has been a joint effort between schools in the U.K. and Lithuania. Certain bridge evaluations have been conducted in Denmark and the U.K., and an interesting assessment of structural strengthening using adhesives has been done jointly by researchers in Germany and Poland. The potential performance and use of girders with corrugated webs in building structures is conducted in Germany; this is an application that until now has only been seen in bridge construction. Finally, composite construction continues to be the subject of aggressive research work in Australia, as reported here, as is a major investigation of the steel storage racks that are so important for many industrial and other manufacturing operations. By all indications, these studies are typical of research institutions that conduct high quality research on subjects that are likely to attract attention in many engineering locales.

References are provided throughout the paper, whenever such are available in the public domain. However, much of the work is still in progress, and in many cases reports or publications have not yet been prepared for public dissemination.

Reidar BJORHOVDE, Ph.D., P.E., Research Editor for *Engineering Journal*, 5880 E. Territory Ave., Suite 202, Tucson, AZ, 85750-1803. E-mail: rbj@bjorhovde.com

PERFORMANCE OF STRUCTURAL MEMBERS

Slender Thin-Walled Box Columns: This study has been conducted at the University of Ljubljana in Ljubljana, Slovenia, and the University of Stuttgart in Stuttgart, Germany. Professors Darko Beg (Ljubljana) and Ulrike Kuhlmann (Stuttgart) have been the directors of the project.

Focusing on the use of thin-walled box cross section columns, the members were fabricated using hot-rolled plates as well as cold-formed elements. The usual material property tests were conducted, as were complete evaluations and measurements of residual stresses, member out-of-straightnesses and out-of-plumbs. Eight full-scale column tests were conducted, using concentric and eccentric axial loads, and the correlation between the analytical and the experimental results was found to be very good (Pavlovic et al., 2009). Figure 1 shows two of the column specimens during testing.

The residual stress magnitudes and distributions were determined using the well-known method of sectioning, as developed and used extensively at Lehigh University (Tebedge et al., 1973). There was very good agreement with the data provided by other investigations, for welded built-up as well as cold-formed members (Galambos, 1998).

The analytical computations were performed using the ABAQUS software. It predicted correct ultimate limit states and accurate failure loads for local as well as overall buckling limit states, with an accuracy of ± 6 percent. This is comparable to what was found in the classical column study of Bjorhovde and others, although the earlier investigations did not have access to such advanced software as ABAQUS (Bjorhovde, 1972; Galambos, 1998).

Plate Girders with Corrugated Webs for Building Applications: This project has been conducted at the Brandenburg University of Technology in Cottbus, Germany, in partnership with the Bochum University of Applied Science in Bochum, Germany. The project director has been Professor Hartmut Pasternak.

Plate girders with corrugated webs were originally developed for use in bridge structures. The depth and spans of the typical plate girders with flat-plate webs often required extensive transverse and even longitudinal stiffeners, with attendant stability problems as well as long-term cyclic load performance and difficulties in the form of fatigue cracking. The flat-plate web thickness also could be substantial, resulting in heavy girders.

The corrugated webs of the girders that have been studied by Professor Pasternak benefit from increased web buckling strength due to the shape of the web and its innate stability. As a result, these girders are now being used in building structures, due to their reduced self weight. Plate thicknesses in these girders are typically 1.5 to 3 mm ($\frac{1}{16}$ in. to $\frac{1}{8}$ in.), and the corrugations are sinusoidally shaped (Pasternak et al., 2009a). The sinusoidal fabrication process has been automated, with the result that corrugated web thicknesses up to 12 mm ($\frac{1}{2}$ in.) can be used. The girders have seen application in storage warehouses, as shown in Figure 2, and now also in short span bridges. Design criteria for the girders are provided by Eurocode 3, Section 1-5, Annex D, although the current requirements limit the web thickness to no more than 3 mm ($\frac{1}{8}$ in.) (CEN, 2005a).



Fig. 1. Slender box column specimen during different loading stages (Photos courtesy of Professors Darko Beg and Ulrike Kuhlmann).

The researchers are now developing formulations that can be used for larger web thicknesses, taking into account non-linear response characteristics, lateral-torsional buckling and patch loading. This effort is a joint project between the Brandenburg and Braunschweig technological universities in Germany (Pasternak et al., 2009a).

STRENGTH AND BEHAVIOR OF COMPOSITE ELEMENTS AND STRUCTURES

Behavior of Composite Beams with Deep Trapezoidal Slabs Containing Headed Stud Shear Connectors: This is a major project that has been conducted at the Centre for Infrastructure Engineering and Safety of the University of New South Wales in Sydney, Australia, with Professor Mark Bradford as the director. Funding and other support have been provided by the Australian Research Council and the Australian Steel Institute, as well as the Australian steel deck producer BlueScope Lysaght.

Composite beams using corrugated steel deck and headed stud shear connectors have been very common since an early research project was conducted at Lehigh University in the late 1960s (Fisher, 1970; Grant et al., 1977). For a number of years the types of steel deck exhibited various forms of trapezoidal and other corrugations, and the deck depths were mostly 1½ in., 2 in., and 3 in. These systems were eminently suitable for floor beams and girders in commercial and residential low- and high-rise building frames. The span of the concrete slab on top of the steel deck was commonly 8 ft to 12 ft, due to the limitations imposed by moment capacity of the slab, the shear stud length and capacity, and the deflections of the slab. Various deck types and geometric configurations have since been developed, with depths up to 6 in. to 8 in. (150 mm to 200 mm), but the shear connectors and the overall design criteria have not evolved accordingly. However, longer spans clearly would be very useful for many applications.



Fig. 2. Storage warehouse with corrugated web girders (Photo courtesy of Professor Hartmut Pasternak).

The project at the University of New South Wales developed a push-test to replace the push-out test that has been the traditional one to use to assess stud shear capacity, etc. (Ranzi et al., 2009). The push-out tests in many cases led to premature failures of a type that never occurred in full-scale beam tests, hence the need for the improved modeling and test as provided by the UNSW group. Figure 3 shows the push-test laboratory assembly, and Figure 4 shows the very favorable ductile load-slip response of the studs.

Two full-scale beam tests were run at the University of Sydney to verify and validate the results of the push-test that had been developed. With beam spans of 8 m (26 ft 8 in.), the beams performed very well, with ductile behavior as predicted by the push-test. The correlation with the analytical results was excellent. Figure 5 shows the test setup for the full-scale beams.

Additional work focuses on the development of serviceability criteria for these types of beams, including the warping effect of slab shrinkage and its interaction with the partial shear connection between the slab and the steel beam.



Fig. 3. Push-test for stud shear connector performance (Photo courtesy of Professor Mark Bradford).

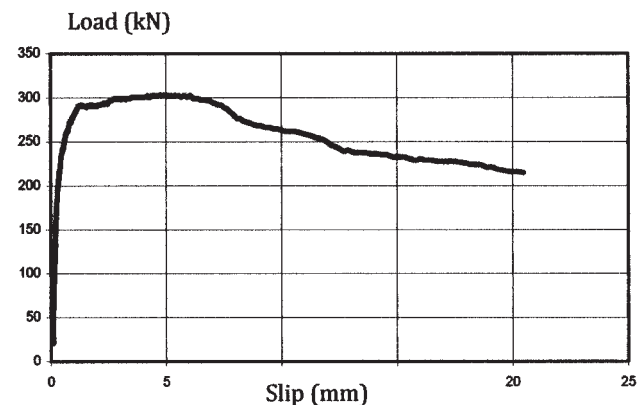


Fig. 4. Ductile load-slip performance of push-tested shear connector (Figure courtesy of Professor Mark Bradford).

Buckling of Slender Composite Concrete-Filled Steel Columns: This has been an international collaborative research project between the Vilnius Gediminas University in Vilnius, Lithuania and the University of Manchester in Manchester, England. Professors Audronis Kvedaras (Vilnius) and Cameron Goode (Manchester) have been the project directors.

The project has effected a major data collection and evaluation of test results for square and round tubular columns, to assess the design criteria that are specified in Eurocode 4 (Goode, 2008; CEN, 2005b). It has been found that Eurocode 4 tends to be conservative for circular tubular columns, and the criteria can be readily extended up to concrete cylinder strengths of 100 MPa (14 ksi), or significantly higher than the current limitation of 75 MPa (approximately 11 ksi). This does not extend to rectangular columns, for which the current limit is 50 MPa (7 ksi).

INDUSTRIAL STRUCTURES

Strength and Behavior of Steel Storage Racks: This has been a major, multi-year project at the University of Sydney in Sydney, Australia. Professor Kim Rasmussen is the project director for a study that has wide governmental and industrial support.

The study has focused on the performance of the storage racks when they are subjected to impact forces due to forklifts. This is a very common and sometimes disastrous occurrence. In addition to detailed three-dimensional strength and stability analyses of the racks, full-scale tests have also been conducted to ensure as realistic conditions as possible. Among other considerations, the tests include actual collisions of forklifts with rack columns (“uprights”), evaluating the dynamic response of the structure (Gilbert and Rasmussen, 2009). Progressive collapse scenarios are also assessed.

The pallet loading of the racks is a central issue, including what takes place when a pallet falls through several “stories” of a rack that may have experienced upright damage. The

full-scale tests that have been conducted demonstrate the response of the structures under gravity and lateral loads. One such test is illustrated in Figures 6 and 7, which show the rack before the test and the condition after a typical pallet loading case, as described earlier.

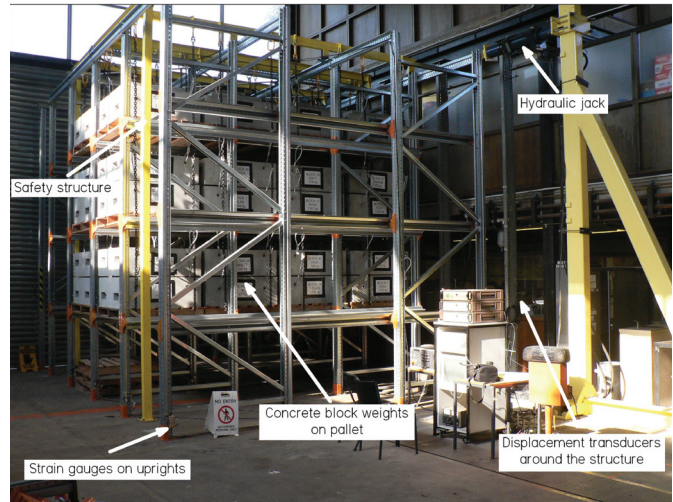


Fig. 6. Full-scale storage rack before testing (Photo courtesy of Professor Kim Rasmussen).

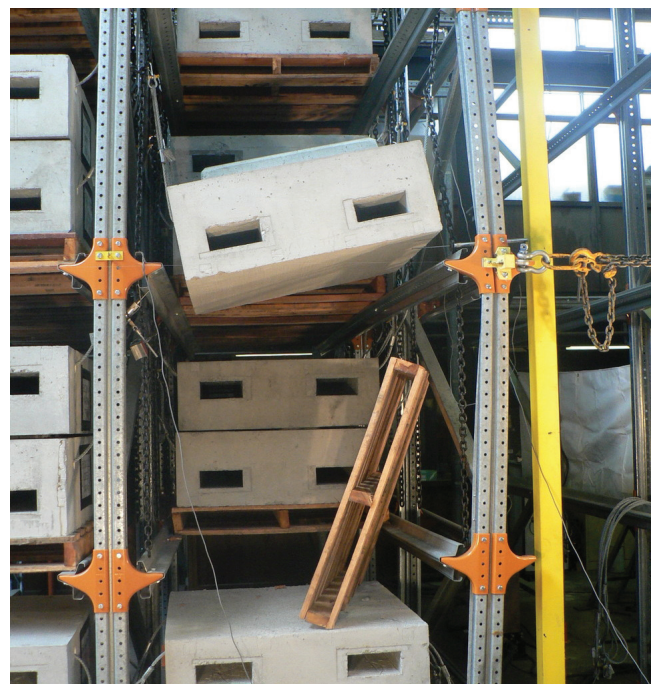


Fig. 7. Pallet-loading-induced failure of storage rack (notice the damaged upright on the right-hand side of the photograph) (Photo courtesy of Professor Kim Rasmussen).



Fig. 5. Full-scale composite beam test with deep trapezoidal steel deck (Photo courtesy of Professor Mark Bradford).

The project work includes assessments of component tests and other aspects of various international storage rack criteria, such as the American code by RMI (Rack Manufacturers Institute) and the relevant European code. Additional component tests are being developed, including one for the stiffness of base plates subjected to uplift.

BRIDGE STRUCTURES

Stability of Girders Using U-Frames: This study was conducted at City University of London, England, while the project director, Kuldeep S. Viridi, was a faculty member at that university. He is now at Aarhus University in Aarhus, Denmark.

Lateral-torsional buckling is a major consideration for beams and girders, and maybe especially for the long-span members often used in bridge construction. While actual bracing is the most common approach to increase the stability and strength of the girders, there are a number of cases where such is not suitable, especially for through-type bridges and where overhead bracing members are not practical. The so-called U-frame provides girder stability through connections between the floor beams and the girders, as shown in Figure 8, and the floor beams also support the roadway slab.

The study examined the influence of a range of girder and floor beam spacings to determine the buckling strength of the system (Viridi and Azzi, 2009). An example of the buckled shape for one of the U-frame configurations is shown in Figure 9.

A parametric analysis of the U-frame system was performed, using a bridge span of 18 m (60 ft), a bridge deck width of 6.3 m (21 ft), 1.8-m-deep (6 ft) girders, and 0.8-m-deep (30 in.) floor beams. The bridge deck was designed as composite with the floor beams. The U-frame spacing was varied from 2 m to 3 m (6 ft 8 in. to 10 ft), giving structures with eight to five U-frames.

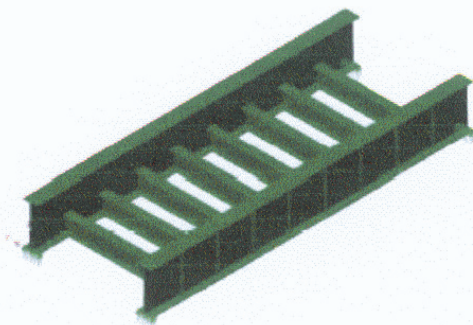


Fig. 8. Girders and floor beams constitute the U-frames of the bridge (Figure courtesy of Professor Kuldeep Viridi).

Figure 10 shows the variation of the effective length of the girders, as a function of the spacing of the U-frames and the buckling mode. For instance, mode 1 (top curve) is the usual single wave form, reflecting the lowest buckling load. Increasing the U-frame spacing from 2 m to 3 m increases the effective length by 20%, meaning that the buckling load is reduced by $(1.2)^2$ or 44%. This is as should be expected.

STRUCTURAL REPAIR AND RETROFIT

Use of Adhesives to Strengthen Steel Structures: This project has been a joint international effort between the Brandenburg University of Technology in Cottbus, Germany, and the Krakow University of Technology in Krakow, Poland. The project directors are Professors H. Pasternak (Brandenburg) and M. Piekarczyk (Krakow). The funding sources have not been identified, but they are likely to be major European Union programs.

Adhesives have actually been used in a number of construction projects in Germany, starting with several box girder bridges in the 1960s. These structures have continued to function properly, now after nearly 50 years of service. In the

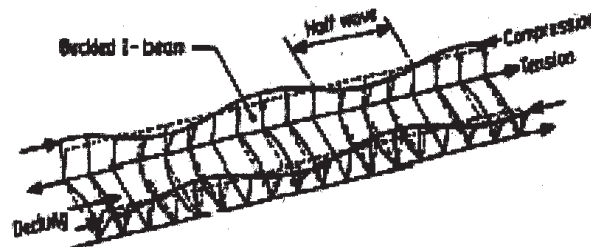


Fig. 9. One of the buckling shapes of a typical structure with U-frames (Figure courtesy of Professor Kuldeep Viridi).

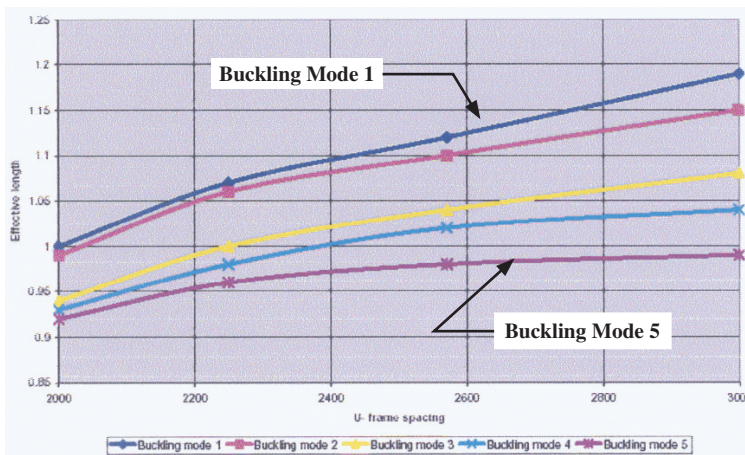


Fig. 10. Variation of girder effective length as a function of U-frame spacing (Figure courtesy of Professor Kuldeep Viridi).

current project, a box girder was tested at Krakow and knee joints were tested at Brandenburg, and ABAQUS analyses were conducted for all of the test specimens. There was good correlation between the tests and the analytical results.

For the knee joints it was found that it was better to use epoxy-glued plates on both sides of the joint; a single sided plate was sufficient when polyurethane glue was used. Similar results were found for the box girders. The increases in load-carrying capacity were substantial, including the fact that local buckling did not affect the ultimate limit states. It is clear that the use of various forms of adhesives can play an important strengthening role—it is still a question whether the organic stability of the glued joints and surfaces will suffice. However, the performance of the older German bridges speaks well for the method and the materials.

REFERENCES

- Bjorhovde, Reidar (1972), “Deterministic and Probabilistic Approaches to the Strength of Steel Columns,” Ph.D. Dissertation, Lehigh University, Bethlehem, PA.
- CEN (2005a), *Eurocode 3—Design of Steel Structures—EN 1993-1*, Comité Européen de Normalisation, Brussels, Belgium.
- CEN (2005b), *Eurocode 4—Design of Composite Steel and Concrete Structures—EN 1994-1*, Comité Européen de Normalisation, Brussels, Belgium.
- Fisher, J.W. (1970), “Design of Composite Beams with Formed Metal Deck,” *Engineering Journal*, AISC, Vol. 7, No. 3, pp. 88–96.
- Galambos, T.V., ed. (1998), *Guide to Stability Design Criteria for Metal Structures*, 5th edition, John Wiley & Sons, New York, NY.
- Gilbert, B.P. and Rasmussen, K.J.R. (2009), “Impact Tests and Parametric Impact Studies on Drive-In Steel Storage Racks,” International Conference on Advances in Steel Structures (ICASS’09), Hong Kong, December 16–18.
- Goode, C.D. (2008), “Composite Columns—1819 Tests on Concrete-Filled Steel Tube Columns Compared with Eurocode 4,” *The Structural Engineer*. Vol. 86, No. 16, pp. 33–38.
- Goode, C.D., Kuranovas, A. and Kvedaras, A.K. (2009), “Buckling of Slender Composite Concrete-Filled Steel Columns,” in *Stability and Ductility of Structures*, Audronis Kvedaras, ed., International Colloquium, Vilnius Gediminas Technical University, Vilnius, Lithuania.
- Grant, J.A., Fisher, J.W. and Slutter, R.G. (1977), “Composite Beams with Formed Steel Deck,” *Engineering Journal*, AISC, Vol. 14, No. 1, pp. 24–43.
- Pasternak, H., Kubieniec, G. and Robra, J. (2009a), “Plate Girders with Corrugated Webs,” in *Stability and Ductility of Structures*, Audronis Kvedaras, ed., International Colloquium, Vilnius Gediminas Technical University, Vilnius, Lithuania.
- Pasternak, H., Kubieniec, G. and Piekarczyk, M. (2009b), “Adhesives in Strengthening of Steel Structures,” in *Stability and Ductility of Structures*, Audronis Kvedaras, ed., International Colloquium, Vilnius Gediminas Technical University, Vilnius, Lithuania.
- Pavlovcic, L., Froschmeier, B., Kuhlmann, U. and Beg, D. (2009), “Slender Thin-Walled Box Columns Subjected to Compression and Bending,” in *Stability and Ductility of Structures*, Audronis Kvedaras, ed., International Colloquium, Vilnius Gediminas Technical University, Vilnius, Lithuania.
- Ranzi, G., Bradford, M.A., Ansourian, P., Filonov, A., Rasmussen, K.J.R., Hogan, T.J. and Uy, B. (2009), “Full-Scale Tests on Composite Steel-Concrete Beams with Trapezoidal Steel Decking,” *Journal of Constructional Steel Research*, Vol. 65, No. 7, pp. 1490–1506.
- Tebedge, N., Alpsten, G.A. and Tall, L. (1973), “Residual Stress Measurement by the Sectioning Method,” *Experimental Mechanics*, Vol. 13, pp. 88–96.
- Virdi, K. S. and Azzi, W. (2009), “Stability of Girders Using U-Frames,” in *Stability and Ductility of Structures*, Audronis Kvedaras, ed., International Colloquium, Vilnius Gediminas Technical University, Vilnius, Lithuania.

ACKNOWLEDGMENTS

Special thanks are due the following members of the International Structural Steel Research Advisors (ISSRA) who provided input to this paper:

- Darko Beg, University of Ljubljana, Ljubljana, Slovenia
- Mark Bradford, University of New South Wales, Sydney, Australia
- Ulrike Kuhlmann, University of Stuttgart, Stuttgart, Germany

Additional assistance has been provided by Audronis Kvedaras, Vilnius Gediminas Technical University, Vilnius, Lithuania; Hartmut Pasternak, Brandenburg University of Technology, Cottbus, Germany; Luka Pavlovcic, University of Ljubljana, Ljubljana, Slovenia; Kim Rasmussen, University of Sydney, Sydney, Australia; and Kuldeep Virdi, Aarhus University, Aarhus, Denmark.

GUIDE FOR AUTHORS

SCOPE: The ENGINEERING JOURNAL is dedicated to the improvement and advancement of steel construction. Its pages are open to all who wish to report on new developments or techniques in steel design, research, the design and/or construction of new projects, steel fabrication methods, or new products of significance to the uses of steel in construction. Only original papers should be submitted.

GENERAL: Papers intended for publication may be submitted by mail to the Editor, Keith Grubb, ENGINEERING JOURNAL, AMERICAN INSTITUTE OF STEEL CONSTRUCTION, One East Wacker Drive, Suite 700, Chicago, IL, 60601, or by email to grubb@aisc.org.

The articles published in the *Engineering Journal* undergo peer review before publication for (1) originality of contribution; (2) technical value to the steel construction community; (3) proper credit to others working in the same area; (4) prior publication of the material; and (5) justification of the conclusion based on the report.

All papers within the scope outlined above will be reviewed by engineers selected from among AISC, industry, design firms, and universities. The standard review process includes outside review by an average of three reviewers, who are experts in their respective technical area, and volunteers in the program. Papers not accepted will not be returned to the author. Published papers become the property of the American Institute of Steel Construction and are protected by appropriate copyrights. No proofs will be sent to authors. Each author receives three copies of the issue in which his contribution appears.

MANUSCRIPT PREPARATION: Manuscripts must be provided in Microsoft Word 2003 format. A laser-quality proof or high quality PDF must accompany your submittal. Download our complete author guidelines at www.aisc.org/ej.



There's always a solution in steel.

ENGINEERING JOURNAL
American Institute of Steel Construction
One East Wacker Drive, Suite 700
Chicago, IL 60601